ISOTOPIC STUDIES OF THE EARLY SOLAR SYSTEM OBJECTS IN METEORITES BY AN ION MICROPROBE

A THESIS SUBMITTED

TO

GUJARAT UNIVERSITY

FOR

THE DEGREE OF DOCTOR OF PHILOSOPHY
IN PHYSICS

By
Sandeep Sahijpal

PHYSICAL RESEARCH LABORATORY,
NAVARANGPURA,
AHMEDABAD – 380 009, INDIA

February, 1997

CERTIFICATE

I hereby declare that the work presented in this thesis is original and has not formed the basis for the award of any degree or diploma by any University or Institution.

Sandeep Sahijpal

(Author)

Certified by:

Prof. J.N. Goswami (Thesis Supervisor)

Physical Research Laboratory, Nagrangpura, Ahmedabad – 380 009, INDIA

To

Binu, Nitu and
Mummy, Papa

Contents

Acknowledgements

List of Figures

Chapter 1

Chapter 2

Chapter 3

sequence. Scale bar is 0.5 mm. (b) Optical photomicrograph of the [HAL] hibonite crystal studied in this work. The hibonite crystal is ~ 800 μm across.

Fig. 3.2. (a) Subophitic pyroxene (px) with concentric crystals (dashed lines) and plagioclase (pl) enclose spinel (black) in inclusion EGG3 of Allende meteorite. Stippled areas are alteration. (b) Optical photomicrograph of pyroxene analyzed for K isotopic composition.

Fig. 3.3. (a) Backscattered electron photomicrograph of Allende CAI, USNM 3529-42 (#2). Hibonites from two marked areas, namely, A and B were analyzed for K and Mg isotopic composition[s]. (b) Backscattered electron photomicrograph of hibonite laths in 3529-42 analyzed by ion microprobe. Scale bar is 40 μm.

Fig. 3.4. Backscattered electron photomicrograph of epoxy mounted hibonites (fig. a) and spinel-hibonite inclusions (fig. b) from Murchison meteorite. Scale bar is 40 μm.

Fig. 3.5. Backscattered electron photomicrographs of polished sections of the Efremovka CAIs, E40 (fig. a) and E44 (fig. b). The dominant mineral species (melilite: Mel; spinel: Sp; pyroxene: Fas and anorthite: An) are marked on the photomicrographs. Scale bar is 1 mm in each case.

Fig. 3.6. Optical photomicrograph of a polished hibonite-rich section of the Efremovka CAI E50 (fig. a). The hibonite has a lath like structure, the spinel grains present in this zone are interwoven with melilite. The backscattered electron image (fig. b) shows lath like hibonite crystals. Scale bar is 50 μm.

Fig. 3.7. (a) Optical photomicrograph of a section of Severnyi Kolchim (H3) meteorite. Inset shows an igneous inclusion (~ 800 μm) analyzed for Mg-Al isotopic systematics. (b), (c) Optical photomicrograph of a chromite chondrule and an inclusion (~ 200 μm across), respectively, from Raguli (H3) meteorite. The light portions in the chondrule and inclusion is chromite, whereas, dark portions represent plagioclase.

Chapter 4

Fig. 4.1. Decomposition to various components (Double plus, hydride, normal and excess) of count rates at mass 41 for various pyroxenes from Efremovka CAIs with Ca/K $> 10^6$. The total counts at mass 41 in each case is also shown. Data for terrestrial pyroxene and perovskite are also shown.

Fig. 4.2. K isotopic composition of different phases from Efremovka CAIs plotted as a function of their Ca/K ratios. The error bars are $2\sigma_m$. The dashed line represents normal terrestrial standard value for $^{41}K/^{39}K = 0.072$.

Fig. 4.3. $^{41}K/^{40}Ca$ vs. $^{39}K/^{40}Ca$ plot for Efremovka CAIs. The data yield an initial $^{41}K/^{39}K$ value of 0.0712 ± 0.0012 and $^{41}Ca/^{40}Ca$ of $(1.29 \pm 0.20) \times 10^{-8}$. The error

bars are $2\sigma_m$.

Chapter 5

values, respectively, were used for the calculations.

Chapter 6

List of Tables

Chapter 1

Chapter 2

Chapter 3

Chapter 4

Chapter 1

Introduction

The solar system formed about 4.56 billion years (Ga) ago due to the gravitational collapse of a fragment of interstellar molecular cloud composed of interstellar gas and dust. The elemental/isotopic composition of this cloud fragment (the proto-solar cloud) was established by input of material synthesized and ejected to interstellar medium by various stellar sources that include, AGB (asymptotic giant branch) and Wolf-Rayet stars, supernova, nova etc. The proto-solar cloud collapsed to form the solar nebula with the Sun at its center. As the nebula cooled down, micron-sized grains condensed from reprocessed nebular gas and dust. These grains coagulated to form millimeter to centimeter size objects as they spiral down to the mid plane of the nebula under the influence of gravitational field of the proto-sun. These objects in turn, coalesced to form meter-sized bodies whose accretion, triggered by gravitational perturbations, led to the formation of few kilometers to tens of kilometer-sized planetesimals, the building blocks of planets. Various models proposed for the evolution of the solar nebula and the formation of planetesimals are reviewed by Wood and Morfill (1988), Weidenshilling (1988). To get insight into these early stages of evolution of the solar system, it is necessary to understand the physico-chemical processes operating during the various stages of evolution and their associated time scales. Meteorites serve as a unique tool to understand some

of these aspects. Meteorites are mostly derived from asteroids because of recent (the last few tens of million years) collisions among these bodies. Unlike the Earth and the Moon, parent bodies of some meteorites, particularly, the primitive carbonaceous chondrites have not experienced any drastic reprocessing during their entire evolution that could have resulted in large scale thermal processing in them. Some of these primitive meteorites have very specific mineral phases with distinct chemical and isotopic compositions that reflect primordial signatures of some of the early solar system processes. In-depth study of these phases helps to unravel the early evolution of the solar system.

1.1 Isotopic Anomalies and Early Solar System Phases

Isotopic analyses of stable and short-lived nuclides in primitive meteoritic phases have played a vital role in understanding the early solar system processes. In addition, it has provided new information on distinct nucleosynthetic components that contributed to the initial mix of material representing the solar nebula (Woolum, 1988; Clayton, 1988; Lee, 1988; Podosek and Swindle, 1988). The basic approach in these studies is to measure isotopic composition of diagnostic elements in primitive meteorite phases, and look for departures from "normal" isotopic composition measured in "standard" samples. The standards usually considered are well-processed samples, e.g., terrestrial analog phases. Departures in isotopic compositions of meteorite phases from normal values are termed as isotopic anomalies and could result from several sources. The most prominent sources of isotopic anomalies are: (1) radiogenic (*in situ* decay of radionuclides), (2) cosmogenic (production by energetic particle interactions), (3) nuclear (residual signatures of specific nucleosynthetic component present in the solar nebular mix that got incorporated into the early solar system phases).

Table 1.1 Condensation sequence of refractory phases and their abundance (%) in CAIs

Condensation *T(^{o}K)	Minerals	CV[†] Meteorites Types			CM[‡] Meteorites	
		A	B	C	Hibonite rich	Spinel rich
1758	Corundum Al_2O_3	-	-	-	Trace	-
1748	Hibonite $CaAl_{12}O_{19}$	≤ 5	-	-	5-85	-
1647	Perovskite $CaTiO_3$	1-3	-	-	1-10	1-20
?	Fassaite $Ca(Mg,Al,Ti)(Si,Al)_2O_6$	low	30-60	18-34	0-5	-
1625	Melilite $Ca_2Al_2SiO_7$-$Ca_2MgSi_2O_7$	≥ 75	5-20	0-25	-	-
1513	Spinel $MgAl_2O_4$	5-20	15-30	2-12	10-80	60-90
1450	Diopside $CaMgSi_2O_6$	-	-	-	2-5	2-5
1360	Anorthite $CaAl_2Si_2O_8$	-	5-25	45-60	-	-

[*]From Grossman (1972) and Grossman and Clark (1973).
[†] Carbonaceous chondrites belonging to the Vigarona type.
[‡] Carbonaceous chondrites belonging to the Mighei type.

Most of the isotopic anomalies detected in primitive meteorites are found in certain refractory objects, the so-called Calcium-Aluminum Inclusion (CAI). The CAIs consist of oxides and silicates of refractory elements (e.g., Ca, Al, Ti, Mg), and occur in trace amounts in carbonaceous chondrites (MacPherson et al., 1988). These phases represent some of the earliest formed solar system solids. This can be inferred from their mineralogy and chemistry that resemble the thermodynamic model based predictions for the earliest solid phases that would condense in solar nebula with a high initial temperature ($\geq 1500^o$K). The expected condensation sequence of refractory minerals in the

solar nebula at 10^{-3} atmospheric pressure (Grossman, 1972) is shown in Table 1.1 along with the dominant mineral species observed in CAIs in carbonaceous chondrites. The primitive nature of CAIs could also be inferred from their radiogenic ages. For example, the Pb-Pb age of 4.566 ± 0.002 Ga for CAIs from the Allende meteorite (Manhès et al., 1988) make them the oldest dated material in the solar system. Detailed chemical and petrographic study of CAIs, however, show deviations in their mineral assemblage from the ideal condensation sequence. Presence of both high and low temperature phases within individual CAIs have also been found showing their complex formation history. Various processes like evaporation, condensation, melting, re-crystallization that could have been involved in CAI formation are suggested to explain these observations and/or their alteration in nebular environment. Because of such complex evolution, the signatures of the nebular processes incorporated into the CAIs might have got distorted. However, studies of appropriate CAIs that do not show signatures of secondary alterations can provide extremely useful information about early solar system processes.

The Ca-Al-rich refractory inclusions (CAIs) are host to a variety of stable isotopic anomalies (Lee, 1988). These range from enrichment of the neutron-rich isotopes of Ca, Ti and Cr (i.e., ^{48}Ca, ^{50}Ti and ^{54}Cr) to isotopic anomalies in Sm, Nd, Ba and Sr. While the enrichment of neutron-rich stable isotopes suggests the presence of a neutron-rich nucleosynthetic component in the solar nebula, the isotopic anomalies in the heavy elements could be due to the presence of supernova nucleosynthesis products. In addition, one of the most widespread stable isotope anomalies in meteorites is that of oxygen. A component enriched in ^{16}O, which has undergone mixing with normal and a ^{16}O poor component, has been found to be present in various meteorites (Clayton, 1993).

The presence of abundant stable isotopic anomalies in primitive meteoritic phases has offered a rare insight into various nucleosynthetic processes that contributed to the

initial solar nebula mix. It has also provided valuable information about the presolar environment of the molecular cloud from which the solar nebula evolved. The oxygen isotopic anomalies in different meteorite types have provided useful knowledge about early solar system processes. However, the study of stable isotopic anomalies does not give any insight into the time scale of processes starting with the collapse of the molecular cloud fragment, to the formation of planetesimals. The information regarding these time scales has come from the study of radiogenic isotopic anomalies in primitive meteorite phases that resulted from *in situ* decay of now-extinct short-lived nuclides, e.g., ^{26}Al ($\tau \sim 1$ Ma).

1.2 Short-lived Nuclides in the Early Solar System

The first short-lived, now extinct radionuclide, whose one time presence could be inferred in meteorites is ^{129}I (mean life, $\tau \sim 23$ Ma; Jeffery and Reynold, 1961). This was followed by the discovery of ^{244}Pu($\tau \sim 118$ Ma) in several meteorites (Rowe and Kuroda, 1965) and then of ^{26}Al ($\tau \sim 1$ Ma) in CAIs from carbonaceous chondrites (Lee et al., 1976). The one time presence of the short-lived nuclides in meteoritic phases is inferred on the basis of excess found in their daughter nuclide abundance over the normal value. For example, the presence of ^{26}Al in CAIs is inferred based on excess found in its daughter nuclide ^{26}Mg over its normal abundance. This excess is attributed to *in situ* decay of ^{26}Al in these phases if the observed excess also correlates with the concentration of the parent element (^{27}Al, here) in the analyzed phases. The radionuclide with shortest mean life whose presence in CAIs has been detected is ^{41}Ca ($\tau \sim 0.15$ Ma; Srinivasan et al., 1994, 1996). In Table 1.2, we show a list of short-lived nuclides whose presence in meteorites has been established. Studies of these short-lived nuclides have provided a wealth of information regarding the formation and early evolution of solar system, particularly, the time scale of processes that took place within the first few millions to few tens of

million years.

Table 1.2 Short-lived nuclides in the early solar system

Radionuclide	Mean life (τ) Million years	Daughter Nuclide	Initial Abundance $^\diamond$[References] Analyzed phases	Stellar† Production Site
^{41}Ca	0.15	^{41}K	^{41}Ca/^{40}Ca = 1.5 $\times$ 10^{-8} [1] **CAIs**	S A W
^{36}Cl	0.43	^{36}Ar	^{36}Cl/^{35}Cl = 1.4 $\times$ 10^{-6} [2] **CAI, Silicates**	S A
^{26}Al	1.07	^{26}Mg	^{26}Al/^{27}Al = 5 $\times$ 10^{-5} [3] **CAIs**	S A W
^{60}Fe	2.2	^{60}Ni	^{60}Fe/^{56}Fe = 0.4-3.9 $\times$ 10^{-9} [4] **Eucrites**	S A
^{53}Mn	5.3	^{53}Cr	^{53}Mn/^{55}Mn = 3.1-3.6 $\times$ 10^{-6} [5] **Eucrites** ^{53}Mn/^{55}Mn = 4.4 $\times$ 10^{-5} [6] **CAIs**	S
^{107}Pd	9.4	^{107}Ag	^{107}Pd/^{108}Pd = 2.0 $\times$ 10^{-5} [7] **Iron meteorites**	S A W
^{182}Hf	13	^{182}W	^{182}Hf/^{180}Hf = 8-80 $\times$ 10^{-6} [8] ^{182}Hf/^{180}Hf $\geq$ 2.4 $\times$ 10^{-4} [9] **Chondrite and Iron meteorites**	S A
^{129}I	23.1	^{129}Xe	^{129}I/^{127}I = 1.0 $\times$ 10^{-4} [10] **Bulk chondrite**	S
^{244}Pu	118	α, SF‡	^{244}Pu/^{238}U = 4-7 $\times$ 10^{-3} [11] **Bulk chondrite**	S

† S = Supernova; A = AGB star and W = Wolf-Rayet star
‡ SF : Spontaneous fission products
$^\diamond$**References:** [1] Srinivasan et al. (1994). [2] Murty et al. (1995, 1997).
[3] Lee et al. (1976). [4] Shukolyukov and Lugmair (1993a, b). [5] Lugmair et al. (1995).
[6] Birck and Allegre (1985). [7] Kelly and Wasserburg (1978). [8] Harper et al. (1991).
[9] Lee and Halliday (1996). [10] Jeffery and Reynold (1961). [11] Rowe and Kuroda (1965).

The primary emphasis of the present work is to study the records of the two shortest-lived, now extinct radionuclides, ^{41}Ca and ^{26}Al in early solar system phases. In the subsequent sections, the role of these two short-lived nuclides as chronometer of early solar system processes, and their plausible sources are discussed. In addition, the

plausibility of ^{26}Al as a heat source for thermal processing of meteorite parent bodies is considered.

1.3 ^{41}Ca and ^{26}Al as Chronometers of Early Solar System Processes

Until recently, ^{26}Al was known as the shortest-lived radionuclide ($\tau \sim 1$ Ma) whose widespread presence in CAIs has been established conclusively (Lee et al., 1976; Wasserburg, 1985; Podosek et al., 1991; Goswami et al., 1994; MacPherson et al., 1995). Although, the measured value of initial ^{26}Al/ ^{27}Al in CAIs varies over a wide range (0 to 5×10^{-5}; Fig. 1.1), an initial ^{26}Al/ ^{27}Al in the solar nebula at the time of formation of the CAIs is believed to be uniform with a value of 5×10^{-5}. The lower values for initial ^{26}Al/^{27}Al, found mostly in petrographically altered CAIs, are attributed to secondary alterations that resulted in exchange/redistribution of magnesium isotopes in these objects. If we assume a stellar source for the ^{26}Al present in the solar nebula and the theoretically calculated production ratios of ^{26}Al/^{27}Al in various nucleosynthetic sites, the time scale for the formation of CAIs can be estimated to be 3-10 Ma. This time scale refers to the duration between the last injection of ^{26}Al to the solar nebula from one of the various plausible nucleosynthetic sites, e.g., stars evolving through asymptotic giant branch (AGB) phase, novae, supernova or Wolf-Rayet stars, and the formation of CAIs. The spread in the deduced time scale reflects the variation in the production ratios of ^{26}Al/ ^{27}Al in these stellar sources, and also uncertainties in estimating the extent of dilution of the freshly synthesized material with pre-existing nebular material devoid of ^{26}Al. Obviously the most stringent constraint on this time scale will be placed by the shortest-lived nuclide and a search was on to look for nuclides with mean life shorter than ^{26}Al, e.g., ^{41}Ca ($\tau \sim 0.15$ Ma), ^{99}Tc ($\tau \sim 0.29$ Ma) and ^{36}Cl ($\tau \sim 0.43$ Ma). With the recent discovery of ^{41}Ca ($\tau \sim 0.15$ Ma) in Efremovka CAIs by Srinivasan et al.
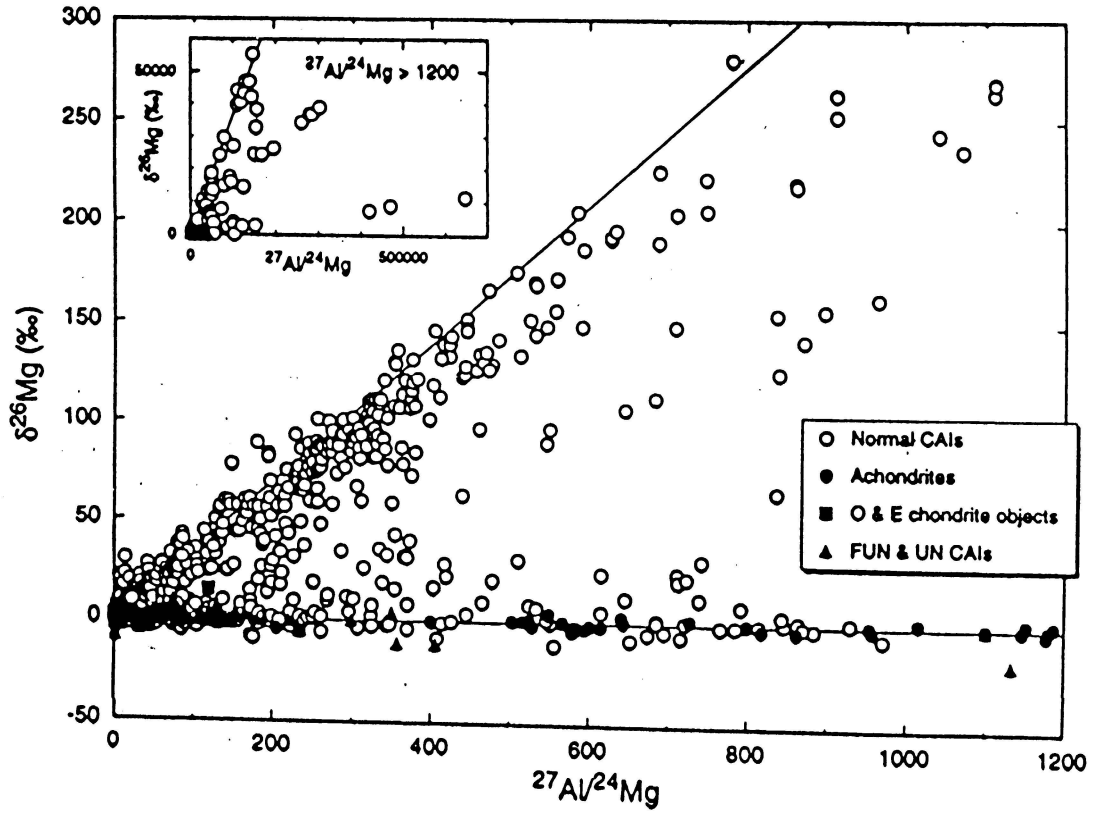
Figure 1.1: δ^{26}Mg vs. ^{27}Al/^{24}Mg ("isochron diagram") for all available meteoritic data. The two reference lines shown in the figure correspond to initial ^{26}Al/^{27}Al ratios of 0 and 5×10^{-5} (Figure taken from MacPherson et al., 1995).
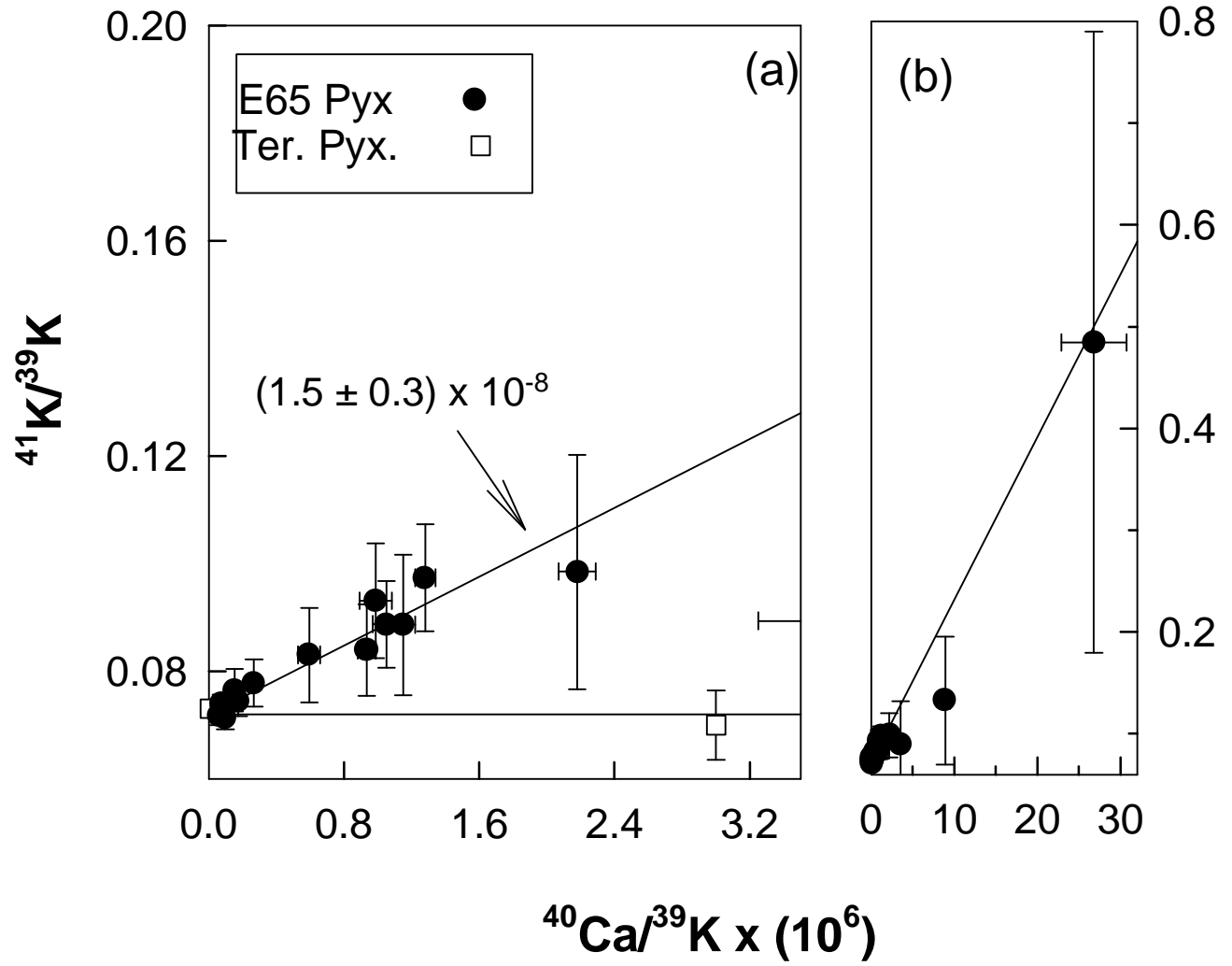
Figure 1.2: Potassium isotopic ratio (^{41}K/^{39}K plotted as function of ^{40}Ca/^{39}K for refractory pyroxene (Pyx) phases in Efremovka CAI. The data yield an initial value of $(1.5 \pm 0.3) \times 10^{-8}$ for ^{41}Ca/^{40}Ca (Figure taken from Srinivasan et al., 1994).

(1994), a new chapter in the study of short-lived nuclides has begun.

Several attempts have been made earlier to look for the one time presence of the short-lived nuclide, ^{41}Ca in Allende CAIs (Begemann and Stegmann, 1976; Huneke et al., 1981; Stegmann and Specht, 1983; Hutcheon et al., 1984). Most of these attempts were not successful, even though Hutcheon et al. (1984) suggested an upper limit of $(8 \pm 3) \times 10^{-9}$ for the initial ^{41}Ca/^{40}Ca at the time of formation of two Allende CAIs, namely, EGG3 and 3529Z. In recent studies conducted by Srinivasan et al. (1994), a clear excess in ^{41}K, that can be attributed to the decay of ^{41}Ca, was found in refractory phases of several CAIs from the carbonaceous chondrite, Efremovka. An initial ^{41}Ca/^{40}Ca value of $\sim 1.5 \times 10^{-8}$ at the time of formation of these phases was inferred from the data (Fig. 1.2). The presence of ^{41}Ca ($\tau \sim 0.15$ Ma) in Efremovka CAIs suggests that the time interval between the injection of freshly synthesized ^{41}Ca to the solar nebula and the formation of the CAIs could not have been more than 1 Ma. In the following section, I present a brief review of the various scenarios proposed for the production of short-lived nuclides present in the early solar system.

1.4   Source(s) of Short-lived Nuclides Present in the Early Solar System

To infer the time scale for the formation of some of the early solar system objects (e.g., CAIs), following the collapse of the proto-solar cloud, we need to know the initial concentration of the short-lived nuclides both in the proto-solar cloud and the CAIs. The presence of short-lived nuclides in the proto-solar cloud could be either due to injection of freshly synthesized material from specific stellar sources (e.g., AGB and Wolf-Rayet stars, nova, supernova, etc.) or due to energetic particle induced reactions in the molecular cloud complex of which proto-solar cloud fragment was a part. Stellar nucleosynthesis theories provide reasonable estimates of the expected initial amount of

these short-lived nuclides (Srinivasan et al., 1996 and references therein), and detailed calculations have been performed recently that provide estimate for energetic particle induced production of these nuclides in a molecular cloud complex (Ramaty et al., 1996). It is therefore possible to obtain the time scale for the formation of some of the early solar system phases from measurements that allow estimation of the initial concentrations of the short-lived nuclides in them. In fact studies of isotopes with mean lives > 2 Ma (e.g., ^{60}Fe, ^{53}Mn, ^{107}Pd, ^{129}I) in meteorites have also provided information on the time scales for the formation of the planetesimals (meteorite parent bodies) and their subsequent differentiation. There are however several factors that need careful considerations in this regard. One of them being the identification of the exact stellar source that is responsible for the injection of one or more short-lived nuclides present in the proto-solar cloud. Another is the dilution of the freshly synthesized stellar material with pre-existing material of normal isotopic composition present in the proto-solar cloud (Cameron, 1993; Wasserburg et al., 1994). In the case of energetic particle irradiation, the plausible sources of the energetic particles, their intensity, composition and spectral shapes are some parameters that are difficult to ascertain with confidence. Finally, in either of the scenario, we have to assume a uniform initial abundance of radionuclide in the solar nebula, at least in the region of meteorite (CAI) formation.

Although the role of short-lived nuclides as chronometer of early solar system processes is now widely accepted, it should be noted that there are alternate models that attempt to explain their presence without any chronological significance. The foremost among these is the "fossil" hypothesis proposed by Clayton in a series of papers (Clayton, 1977, 1982, 1986). In this model the decay of short-lived nuclides took place in interstellar grains that had preferentially incorporated such nuclides in their stellar formation sites. The possible presence of excess ^{41}K of "fossil" origin in refractory inclusions of primitive meteorites, which would enhance the ^{41}K/^{39}K ratio in these objects above the normal solar system value, was specifically noted by Clayton (1977). The

proposed scenario involves the formation of refractory condensates (stardust) in stellar environment (e.g., supernova envelope) that are enriched in their refractory element concentrations (e.g., Ca) compared to the volatile (e.g., K) and as such they will have high Ca/K ratio and also excess ^{41}K from ^{41}Ca decay. Since these stellar condensates are expected to be an important component of the solar nebula, they will find their way into the CAIs that can inherit excess ^{41}K from the stellar condensates. A similar argument can be made for the presence of excess ^{26}Mg in refractory inclusion that is due to decay of ^{26}Al. Obviously in this scenario the isotopic anomaly cannot provide any information on early solar system chronology. Another proposal that attempts to explain the presence of short-lived nuclides in early solar system phases, attributes their production to energetic particle irradiation of material in the solar nebula from an active early Sun. Several variations of this model have been proposed that include irradiation of the nebular gas as well as gas and dust, and the CAIs themselves (Heymann and Dziczkaniec, 1976; Heymann et al., 1978; Clayton et al., 1977; Lee, 1978; Kaiser and Wasserburg, 1983; Clayton and Jin, 1995; Shu et al., 1996). Obviously, in such a scenario it will be difficult to extract chronological information of early solar system processes. However, if true, it could provide us useful information on the activity of the early Sun.

In the present work, I am mainly concerned with the study of the records of the two short-lived nuclides, ^{41}Ca and ^{26}Al in CAIs and refractory phases from several primitive meteorites which may allow us to infer their most plausible source. In the following, a summary of various stellar sources and energetic particle irradiation scenarios that are proposed to be the sources of the short-lived nuclides in the early solar system is presented.

1.4.1 Nucleosynthetic origin of short-lived nuclides

In the nucleosynthesis scenario, short-lived nuclides found in early solar system phases, begin their journey from inside star(s) where they are produced by nuclear reactions during various stages of stellar evolution. During the final stages of the evolution of a star, it sheds away its mass and some of the freshly synthesized nuclides, injected into the interstellar medium can find their way into the proto-solar cloud. If this proto-solar cloud collapses to form the Sun and early solar system phases within a time scale comparable to the mean lives of these radionuclides, there is a chance that these radionuclides will be incorporated 'live' into the early-formed phases and will later manifest themselves in the form of observed excesses in their daughter nuclides abundances within these phases.

The plausible stellar sources that can synthesize short-lived nuclides, ^{41}Ca and ^{26}Al are: low mass (ZAMS $\sim$ 3 $M_\odot$, where ZAMS stands for Zero-Age Main Sequence and $M_\odot$ denotes one solar mass) stars evolving through the AGB phase, Wolf-Rayet stars (ZAMS $\geq$ 40 $M_\odot$), nova and supernova of type I and II. While ^{53}Mn can be produced only by supernova, ^{107}Pd is mostly produced by AGB or Wolf-Rayet star, although there could be some contribution from supernova synthesis (Table 1.2).

Thermally Pulsing Asymptotic Giant Branch (TP-AGB) star

The most detailed work on nucleosynthesis of short-lived nuclides to explain their presence in the early solar system has been done on thermally pulsing AGB stars (Wasserburg et al., 1994, 1995). These are 1 to 3 $M_\odot$ evolved stars that have an inert carbon and oxygen degenerate core surrounded by a helium rich and a hydrogen rich shell with an extended convective envelope (Iben and Renzini, 1983; Iben, 1985; Lattanzio, 1995). The energy source for these stars at this stage of evolution is alternating burning of helium and hydrogen in their shells, respectively. During the He burning phase, neutrons

can be released by alpha capture on ^{13}C and/or on ^{22}Ne via the reactions, $^{13}C(\alpha,n)^{16}O$ and $^{22}Ne(\alpha,n)^{25}Mg$. These neutrons interact with seed nuclei present in the shell to synthesize different nuclides via the slow neutron capture process (s- process). The main s-process component nuclei of the solar system are considered to be synthesized in this manner (Käppeler et al., 1990).

As a result of alternate burning of He and H shells, the AGB star undergoes a repeated phases of thermal pulsations. The thermal pulsations lead to dredge up of matter from He and H shell to the convective envelope because of which the newly synthesized material from the He and H shell is mixed with the convective envelope and can be ejected out of the star in the form of stellar winds. The process of dredge up and mixing is repeated for a number of times until finally the star looses most of its envelope in the form of a planetary nebula and the remnant turning into a white dwarf.

A self-consistent model for the production of short-lived nuclides, ^{41}Ca, ^{26}Al, ^{60}Fe and ^{107}Pd has been worked out in detail by Wasserburg et al. (1994, 1995) to explain the measured abundance of these nuclides in early solar system phases. A 3 $M_\odot$ AGB star appears to be a good candidate to account for the meteorite observations. ^{41}Ca will be synthesized by neutron capture on ^{40}Ca by the $^{40}Ca(n,\gamma)^{41}Ca$ reaction along with ^{107}Pd and ^{60}Fe in the He shell during He burning, whereas, ^{26}Al is synthesized during H burning by the reaction, $^{25}Mg(p,\gamma)^{26}Al$. While the possibility of stellar wind from an AGB star initiating the collapse of the proto-solar cloud has been proposed (Cameron, 1993), the probability of association of a TP-AGB star and the proto-solar cloud if not impossible, appears to be rather small based on observational data for the current epoch (Kastner and Myers., 1994).

Wolf-Rayet star

The possible contribution of short-lived nuclides by Wolf-Rayet star to the solar nebula has been considered by Dearborn and Blake (1985, 1988). Wolf-Rayet stars are massive (ZAMS $\geq$ 40 $M_\odot$) stars that suffer very high mass loss rate of 10^{-6} - 10^{-4} $M_\odot$/yr followed by loss of its envelope. These stars go through core H burning followed subsequently by core He burning (Maeder, 1983). The burnt out regions of H, followed by He are exposed and ejected successively in WN and WC phases, respectively. The nuclei ejected in WN phase have been subjected to H burning via CNO, Na-Ne and Mg-Al cycles, and are thus rich in nitrogen, whereas, WC phase contain products of triple alpha (He burning) reaction. The broad emission spectral lines of nitrogen and of carbon and oxygen with corresponding widths of about 1000-2000 km/s, respectively, characterize the WN and WC phases.

Calculations were carried out for Wolf-Rayet stars of masses 50, 100, 150 $M_\odot$ (Dearborn and Blake, 1988). ^{26}Al is synthesized in these stars during core H burning and ^{41}Ca along with ^{107}Pd are synthesized by neutron-capture reactions during He burning.

Supernova

The possible contribution of the short-lived nuclide, ^{26}Al by supernova has been estimated by Truran and Cameron (1978), Arnett and Wefel (1978), Woosley and Weaver (1980). A detail calculation on the evolution of stars of different masses (11-30 $M_\odot$) and associated nucleosynthesis has been carried out recently by Woosley and Weaver (1995). Besides the production of short-lived nuclides, supernova explosion has also been proposed as a triggering mechanism for the gravitational collapse of the proto-solar molecular cloud (Cameron and Truran, 1977). Such an explosion is a common phenomenon in many star forming regions, particularly, in OB associations. Over a

time scale of few million years, massive star evolves and finally ejects most of its mass in a supernova explosion of type-II. The shock wave associated with the ejecta from these explosions can trigger star formation in surrounding dense molecular cloud. Thus, the production of short-lived nuclides as well as gravitational collapse of the proto-solar cloud could be a coupled phenomenon, with a supernova as the source.

During their evolution, massive stars (ZAMS $\geq$ 8 M$_\odot$) undergo a series of successive thermonuclear core burning of the fuel generated at the previous stage of its evolution. This leads to the formation of an iron core in the end. As further burning is endothermic, and photodisintegration and energy loss via neutrino emission dominates at this stage (core temperature 5×10^9 ^{o}K), the core collapses. This triggers explosion inside the star as a result of 'core-bounce' mechanism. Before this explosion, the core is surrounded by a series of shells of different thermonuclear debris. At the time of explosion, the outward moving shock wave can heat up these shells to higher temperatures because of which the thermonuclear burning will take place in the different shell at an enhanced rate for a small period, the so-called 'explosive' nucleosynthesis. Finally, the outward moving shock ejects stellar matter into the interstellar medium at very high velocities. The ejecta will contain freshly synthesized material from hydrostatic thermonuclear and explosive nucleosynthesis. ^{26}Al is produced during explosive neon, carbon and hydrogen burning by the ^{25}Mg(p,γ)^{26}Al reaction, whereas, ^{41}Ca is produced during oxygen and silicon burning.

1.4.2 Cosmogenic origin

Production of nuclides in the early solar system by energetic particles from an active early Sun was first suggested by Fowler et al. (1962). Following the discoveries of anomalies in stable isotopes and those related to short-lived nuclides in meteoritic phases, similar proposals have been revived to explain the isotopic anomalies. Cosmogenic production

of nuclides can take place in the gas or in the dust phase in the nebula or in the proto-solar cloud due to interactions of energetic particles ($>$ few MeV/n). The two different astrophysical settings proposed for such an irradiation are (i) Molecular cloud complex of which the proto-solar cloud was a part, and (ii) the solar nebula.

Most of the work carried out on cosmogenic production of nuclides in the proto-solar cloud was motivated by recent discovery of the cosmic-ray induced gamma-ray lines from Orion molecular cloud complex, a very active star formation region at present. Bloemen et al. (1994) observed broad γ-ray emission lines in the 3-7 MeV range using space-borne COMPTEL telescope and attributed their presence to de-excitation of $^{12}C^*$ and $^{16}O^*$ at 4.44 MeV and 6.13 MeV, respectively. They proposed that enhanced flux of energetic ($\sim$ 10 MeV/n) carbon and oxygen particles can interact with ambient hydrogen and helium of the molecular cloud to produce the excited nuclear states. The low-energy, heavy energetic particles can originate from various stellar sources, e.g., ejecta from evolved stars like Wolf-Rayet stars, supernova, and/or newly born low-mass stars going through high mass loss rate during their T Tauri phase. As dense molecular clouds are active star forming regions, one would expect low-energy, heavy ion cosmic rays from all these stellar sources. Clayton (1994) extended these arguments to explain the production of short-lived nuclides that were found to be present in the early solar system by assuming the proto-solar cloud to be a part of such a cloud complex. In a qualitative manner, he could explain the cosmogenic production of ^{26}Al in such a setting to explain the meteorite observations.

A detailed analysis of cosmogenic production of short-lived nuclides, ^{26}Al, ^{41}Ca and ^{53}Mn in a molecular cloud complex was carried out by Ramaty et al. (1996). In their model, low-energy, heavy ion cosmic rays (20-25 MeV/n) from various stellar sources can explain the origin of γ-rays observed in Orion molecular cloud complex and are capable of producing light isotopes of Li, Be, and B as well as the radionuclides, ^{26}Al, ^{41}Ca and

^{53}Mn. However, it was found that production of ^{26}Al to match the meteoritic observation leads to overproduction of ^{6}Li, ^{9}Be, ^{41}Ca and ^{53}Mn.

The "local" irradiation models proposed to explain isotopic anomalies in meteorite phases invoke an active early Sun going through T Tauri phase. During this pre-main sequence phase, the Sun like stars undergo high mass loss rates of about 10^{-7} $M_\odot$/yr and are also associated with enhanced emission of energetic particles as can be inferred from the observed enhanced emission of X-ray and ultraviolet radiation (≥ 10 eV) from T Tauri stars (Walter and Barry, 1991; Feigelson et al., 1991).

Some of the early attempts to explain the observed excess of ^{22}Ne and ^{16}O in various meteorite phases invoked proton irradiation from an active early Sun (Herzog, 1972; Audoze et al., 1976). A time averaged proton flux of more than 10^4-10^6 times the contemporary flux was found to be necessary to produce the observed excesses. In subsequent models (Heymann and Dziczkaniec, 1976; Heymann et al., 1978; Clayton et al., 1977; Lee, 1978; Kaiser and Wasserburg, 1983; Shu et al., 1996) for cosmogenic origin of ^{26}Al, solar energetic particle irradiation of both nebular gas and dust was discussed. Most of these models require very specific energetic particle spectra to generate the observed ^{26}Al excess in meteoritic phases. Wasserburg and Arnould (1987) discussed production of both ^{26}Al and ^{53}Mn, whereas, Clayton and Jin (1995) considered ^{26}Al and ^{41}Ca production due to interaction of energetic particle from Sun as well as anomalous cosmic rays. Clayton and Jin (1995) and Shu et al. (1996) also tried to couple the cosmogenic production of radionuclides with various nebular processes leading to the formation of the CAIs and chondrules.

As a part of my thesis work, I have carried out a detailed calculation of production of ^{26}Al, ^{41}Ca, ^{36}Cl and ^{53}Mn in CAI precursor solids of chondritic (CI) composition by energetic particle from an active early Sun. The results of these calculations discussed in chapter 5 show that co-production of all the nuclides and particularly ^{26}Al and ^{41}Ca,

18

to match the meteorite observations is not possible.

1.5 ^{26}Al as a Heat Source of Planetesimals in the Early Solar System

The parent bodies of meteorites of different types have experienced varying degrees of physical and chemical processing following their formation. These are summarized in Table 1.3. Evidence for such processing comes from chemical and petrographic studies of meteorites belonging to different types. For example, there is abundant petrographic evidence for large scale aqueous alteration in the parent bodies of primitive carbonaceous chondrites very early in their evolutionary history (Zolensky and McSween, 1988). The parent bodies of the ordinary and enstatite chondrites have suffered varying degrees of thermal metamorphism (McSween et al., 1988), whereas, those of the achondrites, stony iron and iron meteorites have undergone extensive differentiation following complete or partial melting (Hewins and Newsom, 1988). The thermal metamorphism in chondritic parent bodies suggests temperatures of 400-950°C, whereas, melting of the parent bodies of differentiated meteorites requires temperature more than 1000°C. The formation of meteorite parent bodies of a few tens to a few hundred kilometers in size, and their subsequent thermal processing took place very early in the history of the solar system, perhaps within the first few tens of million years. This inference is based on the formation ages of Ca-Al-rich refractory inclusions (CAIs) in primitive carbonaceous chondrites, some of the earliest solar system solids, and of thermally metamorphosed chondrites and differentiated meteorites (Chen and Wasserburg, 1981; Manhès et al., 1987; Göpel et al., 1989; Göpel et al., 1991; Tera et al., 1989; Lugmair and Galer, 1992). Based on the studies of extinct nuclide (^{60}Fe, ^{53}Mn) records in two differentiated meteorites, Juvinas and Chevorny Kut, Lugmair et al. (1995) have recently suggested that this time interval could be less than 6 Ma.

19

Several mechanisms have been proposed for heat generation in meteorite parent bodies that could have induced thermal processing during their early evolutionary history (Wood and Pellas, 1991). The most important among these are: (i) Energy produced due to decay of short-lived nuclides initially present in meteorite parent bodies (Urey, 1955). (ii) Electromagnetic induction heating of meteorite parent bodies by strong proto-solar winds (Sonett and Colburn, 1968; Sonett, 1969).

Table 1.3 Secondary alterations in meteorite parent bodies

Aqueous Alteration ($< 100^oC$)	Thermal metamorphism ($400 - 950^oC$)	Igneous Activity ($> 1000^oC$)
Petrographic Type		
1 —- 2 —- 3-	-3 — 4 — 5 — 6	
CI[†] CM ——-	Ordinary chondrites	Achondrites, Iron
— [CO[‡], CV]	Enstatite chondrites	and stony-iron meteorites
Carbonaceous chondrites		

[†] Carbonaceous chondrite belonging to Ivuna type
[‡] Carbonaceous chondrite belonging to Ornans type

Strong solar winds with associated enhanced magnetic fields from the pre-main sequence Sun going through the T Tauri phase can induce high electric currents in meteorite parent bodies. Because of this induction, the temperature inside the body will increase due to Joule heating. This model is discussed in detail by Herbert (1989) and Herbert et al. (1991) who suggested that heat generated by this mechanism is sufficient to explain thermal processing of meteorite parent bodies. However, this model assumes certain input parameters associated with the nature of T Tauri stars that are difficult to substantiate. Further, the question of whether Sun had gone through a highly active T Tauri stage is also not fully resolved, although there is some meteoritic evidence that suggests an active early phase of Sun (Caffee et al., 1991).

Urey (1955) proposed that radioactive nuclide, particularly the short-lived nuclide

^{26}Al ($\tau \sim 1$ Ma), could be an effective heat source of meteorite parent bodies. The choice of any particular short-lived nuclide as a plausible heat source for meteorite parent bodies is based on the requirement that the mean-life of the radionuclide should be comparable to the heat conduction time scale, which is of the order of 10^6 - 10^8 years for chondritic bodies of sizes 10 - 100 km (Scott et al., 1989). Thus the presence of short-lived nuclide like ^{26}Al in meteorite parent bodies in sufficient amount can lead to generation and accumulation of heat within the body that can result in thermal processing. The other constraint, as already noted is the time scale available for heating of meteorite parent bodies which is of the order of few tens of a million years. The prime candidates that appear to satisfy these constraints are ^{26}Al ($\tau \sim 1$ Ma) and ^{60}Fe ($\tau \sim 2.2$ Ma).

The case for ^{26}Al as a potential heat source for meteorite parent bodies has been strengthened by the observation of ^{26}Mg excess in CAIs that provide strong evidence for the presence of ^{26}Al in the early solar system (Lee et al., 1976; Wasserburg, 1985). Studies of CAIs suggest a nearly uniform initial ^{26}Al/^{27}Al value of 5×10^{-5} at the time of CAIs formation (MacPherson et al., 1995). If the meteorite parent bodies also evolved with a similar initial ^{26}Al/^{27}Al, it could have caused widespread incipient melting of these bodies. However, CAIs are primarily found in carbonaceous chondrites where it constitutes < 5 % by volume of bulk meteorite. Thus to ascertain the role of ^{26}Al as a heat source, one must find evidence for its one time presence in non-refractory phases, specifically, phases that are definite product of large scale melting or thermal metamorphism.

Several attempts have been made to establish the one time presence of ^{26}Al in non-refractory phases by looking for ^{26}Mg excess in phases that have gone through igneous or thermal metamorphic processes (Schramm et al., 1970; Hutcheon and Hutchison, 1989; Bernius et al., 1991; Kennedy et al., 1992; Zinner and Göpel, 1992; Hutcheon et al., 1994; Hutcheon and Jones, 1995; Sahijpal et al., 1994, 1995; Russell et al., 1996). The analyzed

phases include achondrites, igneous clasts found in undifferentiated meteorites, feldspar from various chondrites and igneous inclusions found in iron meteorites. In addition, Al-rich phases in meteoritic chondrules have also been analyzed to look for the presence of ^{26}Al at the time of chondrule formation that took place after the CAIs, but prior to the formation of meteorite parent bodies (Grossman et al., 1988). No definite hint for the presence of ^{26}Al was found in these studies except in three cases. These include: (1) an igneous clast from the unequilibrated chondrite, Semarkona with an initial ^{26}Al/^{27}Al of $(7.7 \pm 2.1) \times 10^{-6}$ (Hutcheon and Hutchison, 1989), (2) feldspar grains from the H4 chondrite, Ste. Marguerite meteorite with an initial ^{26}Al/^{27}Al of $(2.0 \pm 0.6) \times 10^{-7}$ (Zinner and Göpel, 1992), and (3) the recent observation in Al-rich chondrules from unequilibrated ordinary chondrites, Inman and Chainpur with initial ^{26}Al/^{27}Al values of $(9.4 \pm 6.3) \times 10^{-6}$ and $(7.9 \pm 2.7) \times 10^{-6}$, respectively (Russell et al., 1996). While the initial ^{26}Al/^{27}Al, inferred in the first case is sufficient to cause incipient melting in chondritic parent bodies, the initial ^{26}Al abundance in Ste. Marguerite feldspar grains suggests possibility of thermal metamorphism. The lower value of ^{26}Al/^{27}Al in the case of two chondrules from Inman and Chainpur compared to CAIs could be interpreted as due to a time lag between the formation of CAIs and chondrules, and suggests that these values could be the upper limit of initial ^{26}Al/^{27}Al in meteorite parent bodies.

The role of the short-lived nuclide, ^{60}Fe as a plausible heat source was suggested recently by Shukolyukov and Lugmair (1993a, b). They found ^{60}Ni excess in the differentiated meteorites, Juvinas and Chevony Kut, which could be attributed to *in situ* decay of ^{60}Fe in these meteorites. These meteorites are definite product of large scale melting and recrystallization in their parent bodies. Based on the observed differences in the ^{60}Ni excess in these two meteorites, which these authors attributed to a time difference, an initial ^{60}Fe/^{56}Fe value of 1.6×10^{-6} was inferred at the time of CAI formation. This amount of ^{60}Fe is sufficient to induce melting in meteorite parent bodies having ~ 25 weight percentage of iron, typical of H-chondrite. However, recent studies of ^{53}Mn (τ

~ 5.3 Ma) decay records in these meteorites by the same group (Lugmair et al., 1995) showed that formation time of both these meteorites is nearly the same, and led to a downward revision of initial $^{60}Fe/^{56}Fe$ at the time of CAI formation to $\sim 1.6 \times 10^{-8}$. This value is too low and rules out ^{60}Fe as a plausible heat source of meteorite parent bodies.

1.6   The Aim of the Present Study

In the present work, I have analyzed records of the two short-lived nuclides, ^{41}Ca and ^{26}Al, in refractory phases of CAIs from three primitive carbonaceous chondrites, Allende, Efremovka and Murchison, and ^{26}Al in igneous, non-refractory phases from several chondritic meteorites with the following specific aims:

1) To obtain conclusive evidence for the presence of ^{41}Ca in the early solar system.

2) To infer the most plausible source(s) of short-lived nuclides in the solar system from a combined study of ^{41}Ca and ^{26}Al in individual refractory phases of CAIs.

3) To look for evidence of ^{26}Al as a potential heat source for thermal processing of meteorite parent bodies.

The first aspect of the study is an extension of earlier work carried by Srinivasan (1994). The combined study of ^{41}Ca and ^{26}Al was carried out to look for possible correlated presence/absence of these two short-lived nuclides in refractory phases of various meteorites and has been attempted for the first time. Such correlation, if present will allow us to narrow down the plausible source(s) of these radionuclides present in the early solar system. Analytical calculations of productions of these and other short-lived nuclides by energetic particles from an active early Sun in a nebular environment were also done to compliment the experimental data. The search for ^{26}Al in several specially

selected igneous, non-refractory phases from unequilibrated and unusual chondrites was carried out to obtain evidence to support the case of ^{26}Al as a plausible heat source for meteorite parent bodies. Analytical calculations to infer the initial abundance of ^{26}Al necessary to induce thermal metamorphism/melting of meteorite parent bodies have also been performed to supplement the experimental work.

All the isotopic studies of selected meteoritic phases were carried out using an ion microprobe. In Chapter 2, the details of the experimental procedures are described. A brief description of the samples analyzed in this work is given in Chapter 3. The results obtained from the present study are given in Chapter 4. In Chapter 5, I discuss the results of K-Ca and Mg-Al isotopic data in refractory phases of CAIs and the constraints that can be put on the plausible source(s) of the short-lived nuclides present in the early solar system based on the data obtained from experimental and analytical approaches. In Chapter 6, I discuss the implication of Mg-Al isotopic data in non-refractory phases in context of thermal processing of meteorite parent bodies along with the results of analytical calculations. A summary of the present work along with possible future work in these areas is presented in Chapter 7.

Chapter 2

Experimental Techniques

2.1 Introduction

Our understanding of the various processes related to the temporal evolution of the Earth, Moon and other planetary bodies has been greatly enhanced by studies of chemical and isotopic compositions of representative samples from these objects. Various types of mass spectrometers, e.g., gas source mass spectrometers, thermal ionization mass spectrometer, secondary ion mass spectrometers, etc., have proved to be an essential tool in determining isotopic composition of terrestrial, lunar and meteorite samples and also of planetary atmospheres. The secondary ion mass spectrometer (SIMS), that can be used to obtain elemental and isotopic composition of solid samples, has been extensively used during the last couple of decades in the field of geochemistry (Shimizu et al., 1978; Shimizu and Hart, 1982a). A major advantage offered by SIMS compared to thermal ionization mass spectrometer (TIMS) is its high spatial resolution that allows *in situ* measurements of extremely small (ten to hundred microns) terrestrial and meteoritic samples. Eventhough these advantages are at the cost of a lower precision compared to TIMS, the high mass resolution secondary ion mass spectrometer has proved to be an extremely useful and the only tool at present to carry out detail *in situ* studies of

isotopic compositions in individual refractory phases of Ca-Al-rich inclusions (CAI). In the present work, which is primarily concerned with isotopic studies of K-Ca and Mg-Al systematics in refractory phases of CAIs, and Mg-Al systematics in specially selected igneous, non-refractory phases of chondritic meteorites, I have exclusively used a Cameca ims-4f secondary ion mass spectrometer (ion microprobe) for isotopic measurements. In this chapter, a brief description of this ion microprobe is presented along with the analytical techniques used in the measurements of K, Ca, Mg and Al isotopic compositions in the meteoritic phases.

2.2 Secondary Ion Mass Spectrometer (SIMS)

Matter is ejected from a solid surface via the process of sputtering when it is bombarded by energetic ions. The ejected matter consists of atomic and molecular species present in both neutral and ionic state. The ionized particles can be analyzed for their isotopic or elemental composition to get information about the composition of the solid surface. In SIMS, we make use of this principle to determine elemental and isotopic composition of solid sample. An energetic primary ion beam is used to sputter the sample surface. The ions generated from the sputtering process, termed as secondary ions, are accelerated and energy analyzed prior to passing through an electromagnet for mass (m/q) analysis. The transmitted ions of a given m/q are collected using an electron multiplier or Faraday cup to measure their intensities. In addition to its function as a mass spectrometer, the Cameca ims-4f also has imaging capability that makes it a very versatile tool. A brief description of the basic working of the Cameca ims-4f ion microprobe is presented below.

2.2.1 Primary ion column

In the sputtering process, secondary ion intensities of different species liberated from a solid sample depend upon the nature of the primary ion used for sputtering and the chemical composition of the target material. Negative primary ion (e.g., O^-) gives better secondary ion yield for electropositive elements like Mg, Al, K, Ca, Ti, Cr, etc., while the use of positive primary ion beam (e.g., Cs^+) leads to better secondary ion yield of electronegative elements like H, C, O, halogens, etc. One can also use other primary ion species like Ar, Ga, etc. depending upon the specific nature of the study. In the Cameca's ims-4f, primary ion beam from gaseous species (O, Ar, etc.) are produced by a cold cathode duoplasmatron, whereas, Cs^+ beam is produced by a specially designed microbeam source that works on the principle of thermal ionization.

Oxygen gas is introduced into the cold cathode duoplasmatron where oxygen plasma is generated by an arc discharge between the cathode and the anode kept at a potential difference of several hundred volts. An intermediate electrode and a magnetic field generated by a coil surrounding the intermediate electrode confines the plasma to a very narrow region near the anode hole. The O^- and O_2^+ charges inside the plasma are stratified with O_2^+ ions at the center of the arc and O^- ions at its periphery. The ions can be extracted from the anode hole by the relative displacement of the arc and the anode hole. This movement is brought about by mechanically moving the intermediate electrode and cathode with respect to anode. As the ions of required species diffuse out of anode hole, they are accelerated by a potential difference of up to 17.5 kV between the duoplasmatron, which is floated at high potential, and a grounded extraction electrode.

The cesium microbeam source used in the Cameca ims-4f works on the principle that vapours of Cs are ionized as they come in contact with hot tungsten metal. This results from the transfer of electron from neutral adsorbed Cs atom to conduction band of

27
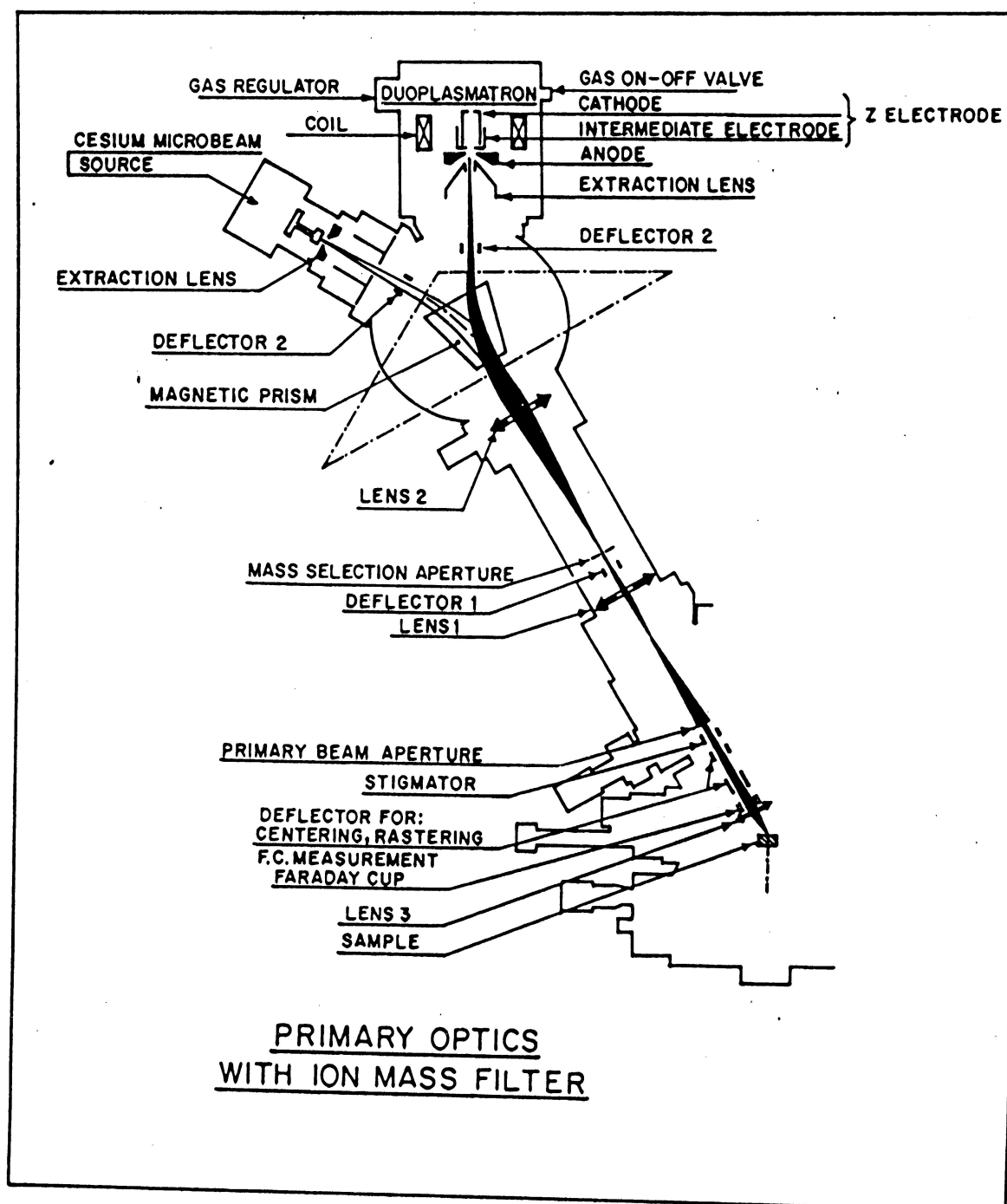
Figure 2.1: Primary column ion optics of the Cameca ion microprobe ims-4f.

tungsten at a temperature of 1100°C. Cs vapours are generated from a cesium chromate (Cs_2CrO_4) pellet kept in a reservoir at a temperature of 400°C and are passed through a hot porous tungsten metal where ionization takes place. The ions emerging out of the porous tungsten are accelerated to 10 kV by the potential gradient between the microbeam source and the extraction electrode.

Depending upon the nature of secondary ions to be analyzed, one of the three primary ion beams: O^-, O_2^+ or Cs^+, is selected and passed through a primary beam mass filter. Primary beam mass filter consists of a magnet that deflects the beam coming either from the duoplasmatron or the Cs microbeam source to the primary column. Singly or doubly charged impurity ions of hydrides and oxides associated with leak in the oxygen supply pipe or duoplasmatron surface contamination can be removed and pure $^{16}O^-$, or $^{16}O_2^+$ primary beams can be obtained with the help of the primary beam mass filter. The selected ion beam passes through a set of three electrostatic einzel lenses and deflectors in the primary column prior to bombarding the sample surface (Fig. 2.1). The intensity of the beam is controlled by the lens L1 and the primary beam aperture. Lens L2 along with the primary beam mass filter is used to maximize the beam current. The third lens L3 focusses the primary beam on the sample surface. The diameter of the focussed beam spot could be as small as few microns for primary beam current of $\leq$ 1 nanoampere. Astigmatism in the primary beam caused by off centering of primary beam from the principal optical axis of various apertures and lenses, can be removed by a pair of stigmators. The primary beam current is monitored by a Faraday cup. Stable primary currents of the order of tens of picoampere to as high as few hundred nanoampere can be obtained. The isotopic analyses performed in this work were carried out with primary current in the nanoampere range.

2.2.2   Production of secondary ions

The collisions of energetic primary beam ions with a solid surface lead to transfer of energy and momentum to the lattice atoms. As a result, the lattice bonds are broken and these atoms are set free from their lattice sites. The liberated atoms in turn undergo collisions with their neighboring atoms and continuation of this process leads to collision cascade. The net result of this collision cascade is ejection of surface atoms that have received sufficient momentum to overcome the surface barrier. The ejected particles mostly contain neutral atoms and molecular species (e.g., oxides, hydrides, dimers, etc.), with a small fraction in ionized form. Intensities of both the neutral and ionic species represent the elemental and isotopic abundances of the sample surface.

The secondary ion yield, which is the number of secondary ions emitted of a particular species per primary ion incident on the sample, depends principally upon the chemical composition of the sample (matrix effect) and the nature of the primary beam. The energy and angle of incidence of the primary beam are also important parameters. Although, the role of various parameters that determine the secondary ion yield has been studied extensively (see e.g., Benninghoven et al., 1987), it is difficult to quantify these results in absolute term as the exact processes leading to the secondary ion emission are not yet properly understood. Several models have been proposed to explain the production of secondary ions. Among these, the local thermodynamic equilibrium model proposed by Andersen and Hinthorne (1972) has been successful to some extent in quantifying the observed sputtered yields. According to this model, a plasma layer exists at the surface of sample during ion bombardment in which sputtered atoms, ions, molecules and electrons are in local thermodynamical equilibrium. Concentration of various charge species is then estimated on the basis of Saha-Eggert equation.

2.2.3 Secondary ion optics and mass spectrometer

The secondary ions generated by sputtering of a solid surface can have a wide angular as well as a large energy spread. For the typical primary beam energy used in SIMS, the energy spread of sputtered ions is $\sim$ 150 eV, whereas, angular dispersion could even be close to 2π radians. The role of secondary ion transfer optics is to produce a real, magnified and low-aberration image of the bombarded sample surface which is then transported through a double focussing mass spectrometer for energy and mass filtering. The final image produced by the mass spectrometer has only mass-dispersive property with no energy dispersion.

The real, magnified secondary ion image in the Cameca ims-4f mass spectrometer is produced by the combination of an immersion lens system and a set of three transfer einzel lenses (Fig. 2.2). One of these transfer lenses is energized at a time. The immersion lens part consists of an accelerating gap (field gradient) and an einzel lens. The sample is kept at a potential difference of 4.5 kV with respect to the grounded extraction plate. Secondary ions are accelerated in this potential gradient and emerge out from the extraction plate hole. In Fig. 2.3, trajectories of secondary ions with initial velocity perpendicular to the surface, and ions having the same energy 'E' and angle of emission 'α', are shown. After acceleration in the field gradient, ions appear to come from the virtual image A-B-C. A virtual cross over of this image is produced at C_o, where ions having same energy and initial emission angle are represented by a single point. The virtual image and virtual cross over produced by extraction electrode and sample acts as object for the immersion lens and the transfer lens. A real magnified image of sample surface and its cross over are produced in the planes of field aperture and the contrast aperture, respectively. The transfer lenses allow changes in magnification of both the surface image and its cross over, which determines the size of the image field being analyzed.
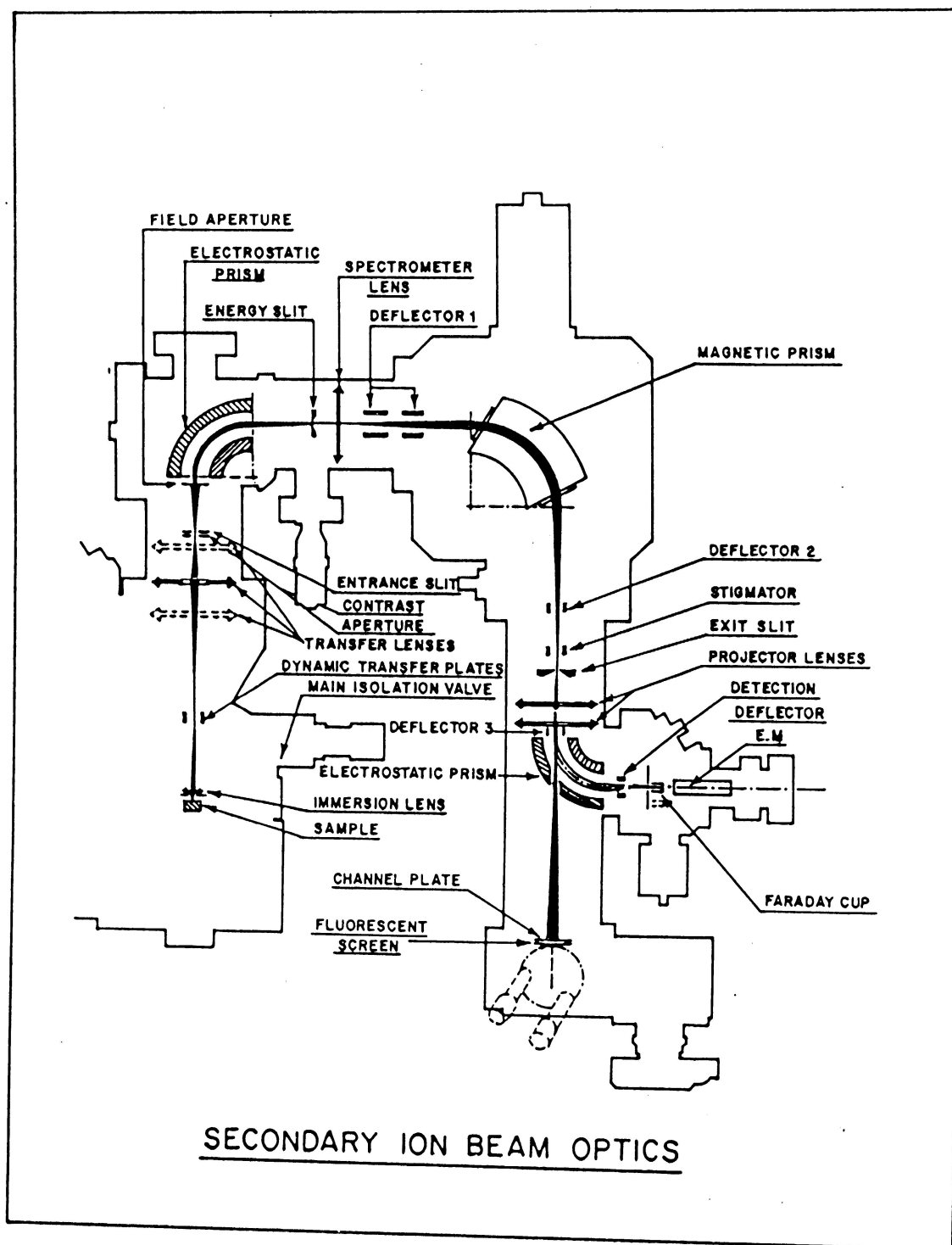
Figure 2.2: Secondary column ion optics of the Cameca ion microprobe ims-4f.
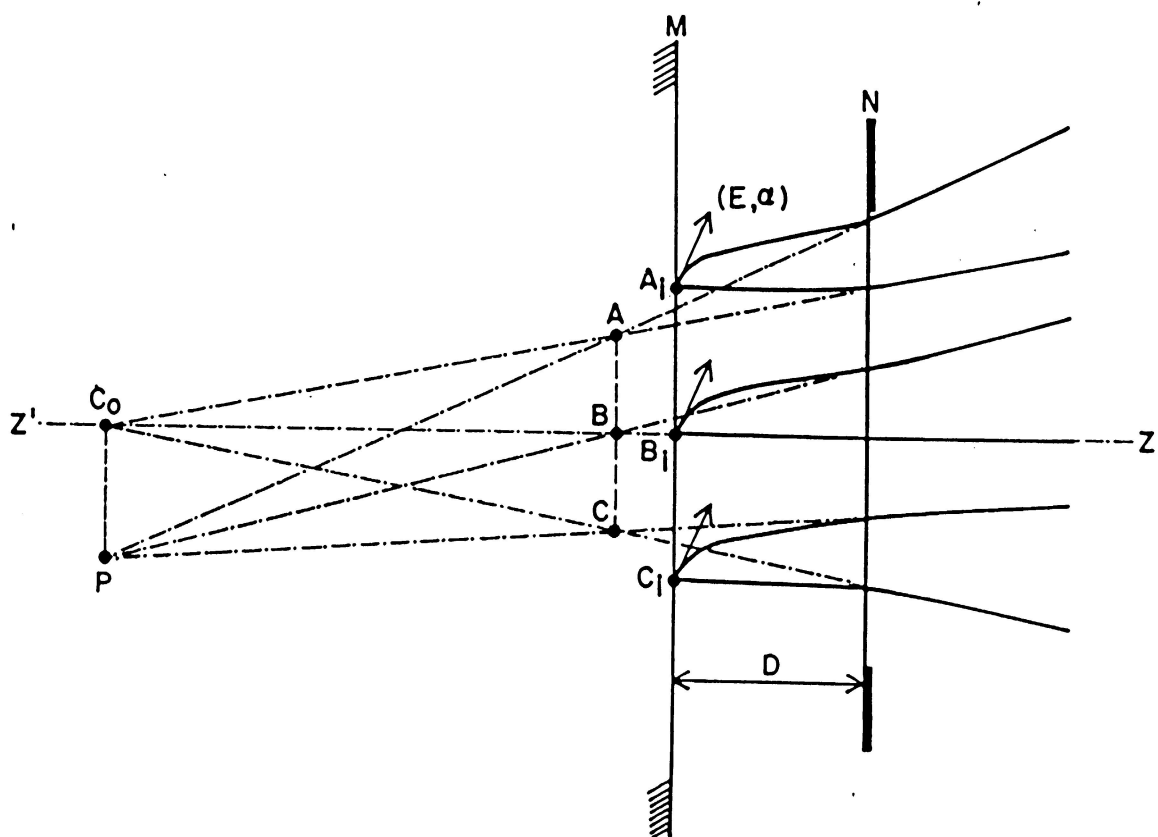
Figure 2.3: Trajectories of secondary ions emitted from sample surface.

The real magnified image of the sample and its cross over, produced at field aperture and contrast aperture, respectively, serve as object for the double focussing mass spectrometer which consists of a 90°, spherical electrostatic analyzer and a 90°, homogeneous magnetic sector. The electrostatic sector is used to reduce the momentum dispersion of the incident secondary ions having an initial energy spread of ~ 150 eV. In the electrostatic analyzer, the secondary ion beam undergoes energy dispersion, and with the help of an energy slit, a narrow energy band (usually ~ 25 eV) of this dispersed beam is selected to transmit further through the spectrometer lens into the magnetic sector. As this energy filtered beam passes through the spectrometer lens and the magnetic sector, it further undergoes an energy dispersion which is equal in magnitude and opposite in sign to that of the dispersion produced by the electrostatic analyzer. This state of achromatism is attained by tuning the spectrometer lens appropriately. Besides this energy focussing, the coupled electrostatic analyzer and magnetic sector also produce a directionally focussed sample image. This mass filtered image can be projected on channel multiplier using projector lenses. The capability of transporting image by the Cameca ims-4f ion microprobe allows the system to work as an ion microscope which facilitates mapping of lateral distribution of various elements in a sample with high spatial resolution and magnification. The final cross over of the mass filtered sample surface image is produced at the exit slit. The mass resolving power of the instrument primarily depends upon the width of the entrance and the exit slits and also on the energy band pass allowed by the energy slit.

2.2.4   Detection system

There are three modes of detecting the mass filtered secondary ions in Cameca ims-4f, ion microprobe. These are: (1) channel multiplier, (2) electron multiplier, (3) Faraday cup. The channel multiplier is coupled to a fluorescent screen and is used to visualize

the magnified mass filtered secondary ion image of the sample and its cross over. In this mode, the instrument works as an ion microscope. This mode of operation is extremely useful in tuning the instrument to high mass resolution.

In the counting mode, the secondary ions are directed toward the electron multiplier and the Faraday cup assembly with the help of an electrostatic prism. For isotopic analysis, ion counting is primarly done by using an electron multiplier. A 17 stages Cu-Be coated dynode, electron multiplier (Balzer SEV217) is used and is operated in pulse counting mode during isotopic analysis. The efficiency, dead time, and background of the counting system are checked regularly during the operation of ion microprobe. The operational efficiency of electron multiplier deteriorates with ageing of dynodes as their coating gets corroded. It is generally replaced when the efficiency goes below 70%. The 'effective' dead time of the total counting system, composed of the electron multiplier, pre-amplifier, discriminator and counting system, is generally 20 ns (nanoseconds) with a standard deviation of ~ 1 ns over a period of several weeks. It is determined from isotopic analysis of magnesium, silicon or titanium on standard samples. The background of the counting system is usually monitored on weekly basis and the static background is typically below 0.01 c/s (Fig. 2.4).

2.3   Isotopic Analysis and Mass Fractionation

The most important factor that has to be considered in isotopic studies by an ion microprobe is the interferences of various species at a given mass of interest. Such interferences can result from the presence of molecular and isobaric species in the secondary ion beam that have the same mass to charge ratio as that of the isotope of interest. The most common among the molecular interference are singly ionized hydrides, oxides, dimers etc. Doubly ionized species with (m/q) similar to the isotope of interest are also important in certain cases. Most of these interferences are resolved by high mass resolution analysis.

35

Maximum: 1 c/s
Average: 0.005 c/s
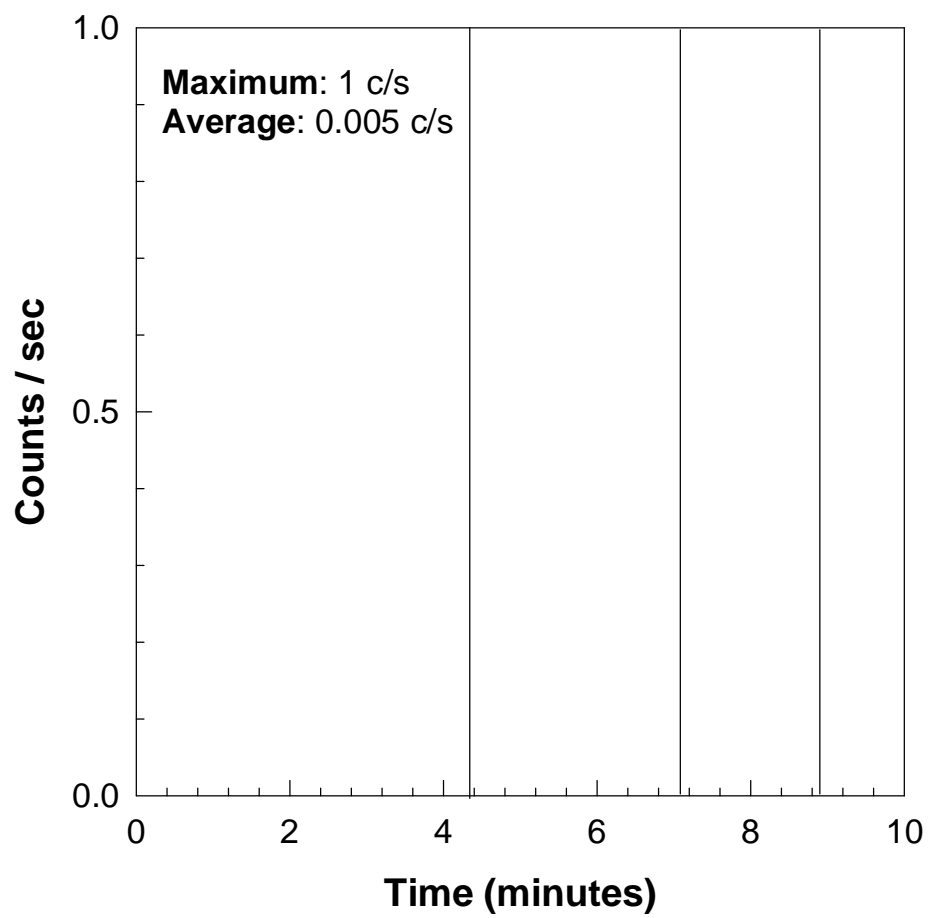
Figure 2.4: Static background of the secondary counting system at mass 40.7.

Typical mass resolution (M/ΔM; ΔM measured at 10% of the peak height) needed for resolving hydride and oxide interferences for M < 60 is $\sim$ 4,000. However, resolution of very specific isobaric interferences e.g., ^{48}Ca and ^{48}Ti needs mass resolution of $\sim$ 10,000. We have been able to achieve both high mass resolution and stability (effective ΔM/M $\leq$ 10 ppm) in our instrument in a routine manner.

The isotopic ratios measured by the ion microprobe can show departure from its true value because of isotopic mass fractionation principally taking place at the time of secondary ion emission through the sputtering process. Isotopic mass fractionation is a process in which the isotopic composition is altered in a systematic manner, whereby, there is either an enrichment of the lighter isotopes compared to heavier one or vice versa. Based on ion microprobe isotopic analyses of Li, Mg, Si, K, Ca and Zr in various minerals, Slodzian et al. (1980) observed that the lighter isotopes of all the elements are enriched relative to the heavier ones and the magnitude of the mass fractionation depends upon the difference in their masses, and also on the secondary ion energy. These observations were also supported by work carried out by Shimizu and Hart (1982b).

In general, the isotopic mass fractionation observed in a sample will be due to instrument mass fractionation as well as intrinsic mass fractionation. The later represent effect of processes that affected the samples at the time of their formation and/or subsequent evolution. The intrinsic mass fractionation effect, if present, can be determined by analyzing the sample and an analog standard under identical instrument operating condition and assinging the observed isotopic mass fractionation in the standard as due to instrument mass fractionation effect. It is always preferable to use a standard for which intrinsic mass fractionation effects have been shown to be negligible by analysis performed using thermal ionization mass spectrometry.

In the following sections, I describe the sample preparation and analytical techniques used for K-Ca and Mg-Al isotopic analysis of various meteoritic samples and

standards.

2.4 Sample Preparation and Isotopic Measurements by Ion Microprobe

Most of the samples (refractory as well as igneous inclusions) analyzed in this study were cast in standard one inch diameter epoxy mounts and polished using diamond paste and alumina powder. For analyzing individual refractory phases e.g., Murchison hibonites, the samples were mounted in small epoxy beads (≤ 2 mm) within aluminium discs and polished to expose the grain surface. We found that the later method of sample mounting greatly reduces the hydride signal because of the small amount of epoxy present in the sample-mount as compared to the standard one inch diameter epoxy mount. Reduction in hydride signal was also observed in thin section of Allende inclusion that was mounted on a glass disc. The reduction in hydride signal is extremely useful during K-Ca isotopic studies to fully resolve the ^{41}K peak from the ^{40}CaH peak. The polished sample mounts were thoroughly cleaned in an ultrasonic bath using soap solution, distilled water and ethanol in steps to remove any contamination on the sample surface during handling and polishing. The cleaned mounted samples were then coated with a 1000-1500 A thick gold film to obtain a well defined beam spot and to reduce possible sample charging effects during analysis. In the case of potassium isotopic analysis, the final cleaning prior to gold coating was done by slowly heating the mounted samples in ultrapure water (filtered through Millipore ^{TM}Milli-Q-Plus-System) for a period of one to two hours. This ensures the removal of any extraneous potassium on the sample surface that could have come during the sample preparation procedure. The samples were documented in detail using an optical and a scanning electron microscope.

2.4.1 Magnesium isotopic measurement

The measurement of magnesium isotopic composition in various meteoritic phases and terrestrial standards were carried out at a mass resolution of $\sim$4,000, adequate to resolve hydride (NaH^+, MgH^+) and other molecular ($^{48}Ca^{++}$, $^{48}Ti^{++}$) interferences at the masses of interest (Fig. 2.5). A focused $^{16}O^-$ primary ion beam of energy 17 kV was used and the beam current was typically 1-2 nanoamperes with a beam spot size of $\leq$ 10 μm on the sample surface. Lower beam currents with smaller beam spot sizes were used while analyzing very small Al-rich (Mg-poor) phases surrounded by Mg-rich phases, particularly in the case of igneous inclusions of chondritic meteorites. This was done to avoid contributions to the ion signal from the surrounding Mg-rich phases. This, however, reduces the secondary ion signals in these cases that resulted in higher statistical uncertainities (lower precision) in the measured isotopic ratios.

Isotopic analyses were carried out in peak jumping mode by cycling the magnet through the mass sequence 24(^{24}Mg), 25(^{25}Mg), 26(^{26}Mg) and 27(^{27}Al). When the Al/Mg ratio of any analyzed sample was very high and the count-rate for ^{27}Al exceeded a few times 10^5, ^{27}Al was excluded from the isotopic analysis and the $^{27}Al^+/^{24}Mg^+$ ratio was determined independently both before and after individual analysis. A typical analysis consisted of 20-25 blocks, with each block representing 5 cycles of data. The deviations in the measured magnesium isotopic ratios ($^{26}Mg/^{24}Mg$ and $^{25}Mg/^{24}Mg$) from their reference values were obtained using the relation.

$$\Delta^i Mg = \left(\frac{\left(\frac{^iMg}{^{24}Mg}\right)_{sample}}{\left(\frac{^iMg}{^{24}Mg}\right)_{ref.}} - 1 \right) \times 1000 \text{ permil}, \quad (i = 25,\ 26) \tag{2.1}$$

The reference magnesium isotopic ratios used by us are: ($^{25}Mg/^{24}Mg$) = 0.12663 and ($^{26}Mg/^{24}Mg$) = 0.13932 (Catanzaro et al., 1966). Correction for instrumental and
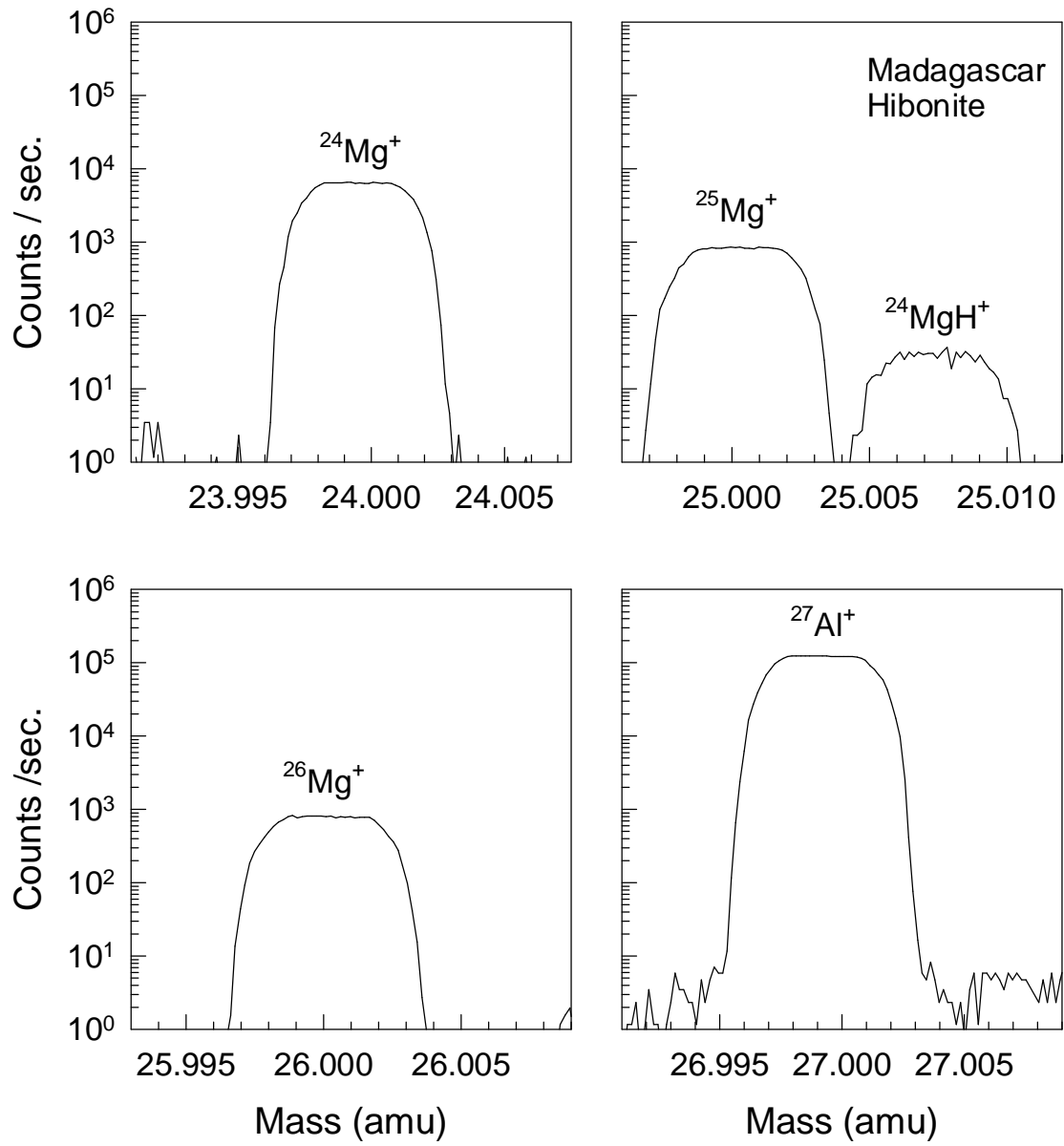
Figure 2.5: Mass spectra of Mg and Al isotopes in Madagascar Hibonite taken at a mass resolution, $M/\Delta M \sim 4{,}000$.

intrinsic (sample) isotopic mass fractionation was done using the linear mass fractionation relation, Δ^{26}Mg $= 2\ \Delta^{25}$Mg, to calculate any excess ^{26}Mg as:

$$\delta^{26}Mg = \Delta^{26}Mg - 2\Delta^{25}Mg \tag{2.2}$$

In the case of terrestrial anolog of meteorite phases, δ^{26}Mg should be zero within experimental uncertainities. We have analyzed a set of standards and showed this to be true under our instrument operating conditions (Table 2.1).

Since the secondary ion yield of a given element depends on the chemical composition of the target and its lattice structure, determination of elemental abundance ratios from the measured ion intensities require a knowledge of relative ion yields of different elements from a given matrix. This can be determined by analyzing terrestrial standards whose elemental composition is precisely known from measurements made by using other analytical technique, e.g., electron probe. We have analyzed terrestrial analog standards of the meteoritic phases investigated in this work to determine the relative ion yield factor (λ), by using the relation:

$$\lambda = \frac{\left(\frac{^{27}Al}{^{24}Mg}\right)_{e.p}}{\left(\frac{^{27}Al^+}{^{24}Mg^+}\right)_{i.p}} \tag{2.3}$$

where e.p. and i.p. stands for electron probe and ion probe data, respectively. The λ values obtained in this work are shown in Table 2.2.

Table 2.1. Magnesium isotopic analyses of terrestrial standards

Sample	Number of analyses	$^{27}Al/^{24}Mg$ $\pm 2\sigma_m$	$\delta^{26}Mg(\%)$ $\pm 2\sigma_m$
Lake County Plagioclase*	3	218.60 ± 1.10	-1.25 ± 1.85
Burma Spinel*	3	2.53 ± 0.01	0.36 ± 1.44
Madagascar Hibonite[†]	3	31.69 ± 0.11	-0.63 ± 1.20
Melilite[‡]	3	1.03 ± 0.01	1.45 ± 1.59

* National Museum of Natural History, Smithsonian Institution, Washington, D C.
[†] Curien et al. (1956)
[‡] Vernadsky Institute, Moscow

Table 2.2. Relative yield factor (λ) for Mg-Al isotopic analyses

Sample	$^{27}Al^+/^{24}Mg^+$	Yield (λ)
Lake County Plagioclase	172.09	1.27
Spinel *	1.98	1.28
New York Spinel	2.02	1.26
Burma Spinel	1.98	1.28
Madagascar Hibonite	22.64	1.40
Melilite *	0.98	1.04

* Vernadsky Institute, Moscow

2.4.2 Potassium isotopic measurements

The potassium isotopic measurements were carried out using a focused 17 kV $^{16}O^-$ primary beam with current generally of the order of 1.5 to 4 nanoamperes. The spot size was made as small as possible for the given primary current and was typically < 10 μm. Secondary ions from a restricted area of the sample surface (~ 10 μm) were accepted during isotopic analysis by limiting the size of the field aperture. This was done to avoid contributions from neighbouring phases with relatively high K content and also possible

surface contamination from outside the sputtered beam spot. The energy distribution of the secondary ions were monitored both before and after each run to ensure that there was no significant change in the energy band over which the secondary ions were accepted for mass analysis. The stability of the magnet, the effective deadtime and efficiency of the counting system were checked routinely using standard procedures (see e.g., Goswami and Srinivasan, 1994). Prior to each analysis, a preburn of the sample spot was carried out for a period of about 15-30 minutes to remove any surficial potassium and to achieve a steady Ca/K value. In the case of Murchison hibonites, magnesium analyses were usually carried out prior to potassium analyses on **the same spot** with relatively low primary current.

K-Ca isotopic studies of terrestrial and meteoritic phases with high Ca/K were carried out at a mass resolution of ~ 5000 that is sufficient to resolve the major interference of ^{40}CaH at mass ^{41}K (see Fig. 2.6). Although K has three isotopes (39, 40 and 41), it is not possible to resolve ^{40}K from ^{40}Ca when Ca is present. Thus for all practical purposes K can be considered as a two isotope system in the present case. Further, the interference of $[^{40}Ca^{42}Ca]^{++}$ cannot be resolved at this mass resolution and was determined indirectly. The magnitude of the other unresolved doubly charged interference $[^{26}Mg^{56}Fe]^{++}$ was checked by looking for $[^{25}Mg^{56}Fe]^{++}$ signal at mass 40.46 amu under our operating condition for K isotopic studies. High mass resolution spectra obtained around this mass with long integration time did not reveal any signal above our system background. This was also expected because of the very low content of Fe (FeO<1%) in all the analyzed phases, and the much lower secondary ion yield of Fe relative to Ca. Possible interference from $[^{50}Ti^{16}O_2]^{++}$, that is separated from the ^{41}K mass peak by ~ 0.0055 amu and is nearly well resolved under our operating conditions, was also checked by analyzing terrestrial perovskite and looking for $[^{46}Ti^{16}O_2]^{++}$ signal at mass 39.971 amu (separated from the ^{39}K mass peak by ~ 0.007amu) using high primary beam current and a $^{40}Ca^+$ count rate of $\sim 7 \times 10^6$ s^{-1}. No detectable signal was found

and we can rule out contribution from $[^{50}\mathrm{Ti}^{16}\mathrm{O}_2]^{++}$ to the signal at mass 41 (^{41}K) under our operating condition (typical ^{40}Ca$^+$ count rates of $< 2 \times 10^6$ c/s). Contributions from additional interferences (e.g., $[^{27}\mathrm{Al}_2{}^{28}\mathrm{Si}]^{++}$, $[^{25}\mathrm{Mg}^{16}\mathrm{O}]^+$) can be neglected as they are well resolved under our operating conditions. Finally, as the count rate at mass ^{41}K is generally a few orders of magnitude smaller than ^{40}CaH in the high Ca/K phases, we have checked for possible scattering from the hydride peak that may contribute to the ^{41}K counts during K isotopic analysis. Contribution due to scattering from the ^{40}Ca peak towards the signal at mass 41 can be ruled out under our operating condition as we could not detect any signal above our counting system background in the mass region around 40.7 amu even for ^{40}Ca count rate of $\sim 2 \times 10^7$ s^{-1}, which is almost an order of magnitude higher than the value normally encountered during K isotopic analysis. The measured ion intensity at the mass 41 peak can therefore be written as:

$$[mass(41)]^+ \;=\; \left[^{41}K\right]^+_{true} \;+\; \left[^{40}Ca^{42}Ca\right]^{++} \;+\; \left[^{40}CaH\right]^+_{tail} \;+\; dyn.bg. \qquad (2.4)$$

where dyn. bg. refers to the dynamic background of the counting system. Since it is not possible to directly measure $[^{40}\mathrm{Ca}^{42}\mathrm{Ca}]^{++}$ count rate, we correct for it following the approach of Hutcheon et al. (1984) by finding the magnitude of $[^{40}\mathrm{Ca}^{43}\mathrm{Ca}]^{++}$ signal at mass 41.5 and assuming :

$$\frac{(^{40}Ca^{43}Ca)^{++}}{^{43}Ca^+} = \frac{(^{40}Ca^{42}Ca)^{++}}{^{42}Ca^+} \qquad (2.5)$$

The $[^{40}\mathrm{Ca}^{43}\mathrm{Ca}]^{++}$ signal, which can be monitored at m/q=41.5, was found to be extremely low (<0.5c/s) in both terrestrial and meteoritic phases under our operating condition. The value of $[^{40}\mathrm{Ca}^{43}\mathrm{Ca}]^{++}/^{43}\mathrm{Ca}^+$ was therefore obtained independently in meteoritic as well as terrestrial analog phases by using high primary current and long
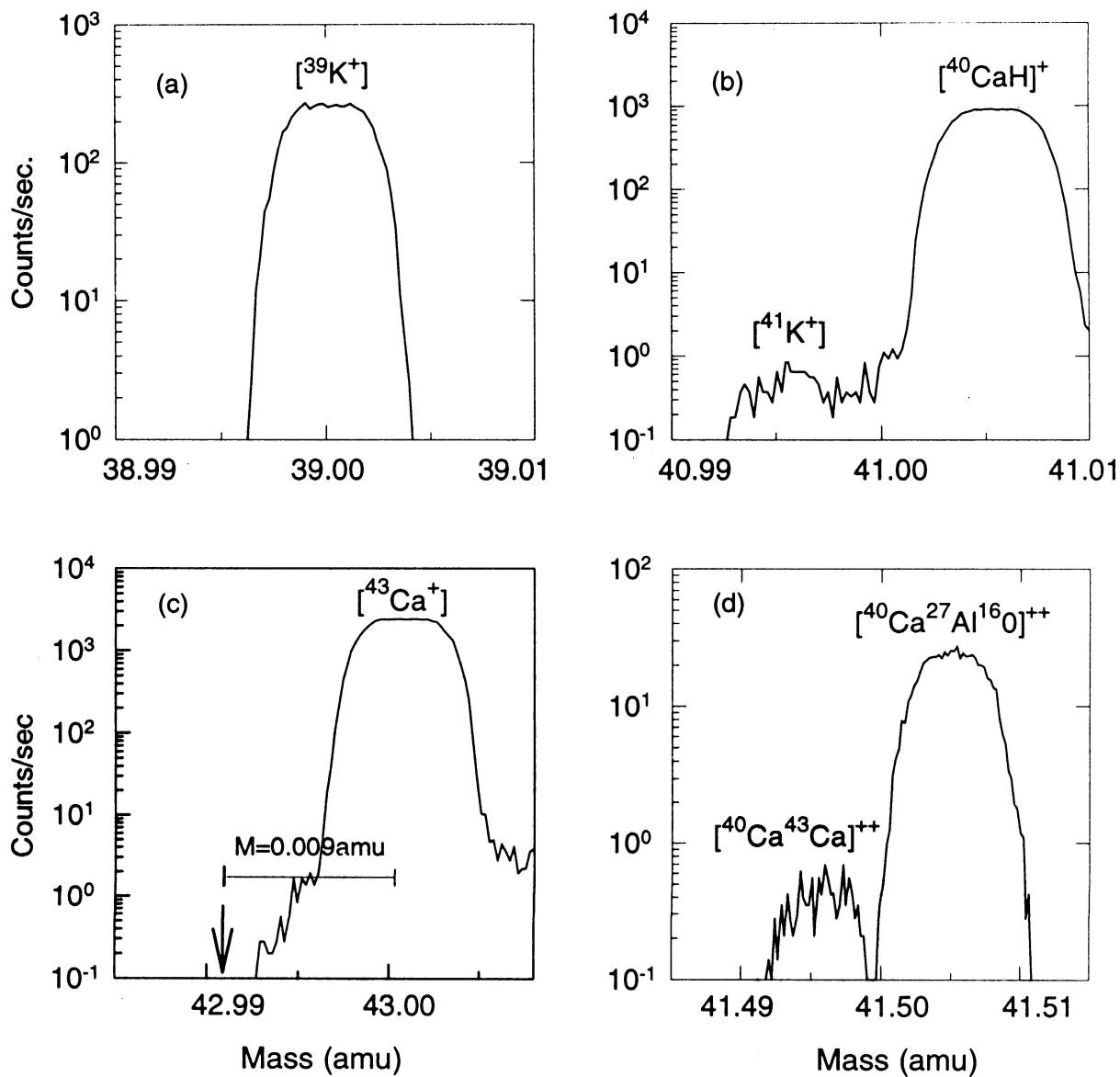
Figure 2.6: Mass spectra at masses 39(K), 41(K), 43(Ca) and 41.5 [(^{40}Ca^{43}Ca)$^{++}$] taken at a mass resolution, $M/\Delta M \sim 5,000$.

acquisition time at mass 41.5 to achieve reasonable precision. The position of the $[^{40}Ca^{43}Ca]^{++}$ peak could be easily identified in perovskite and can be accurately located in the case of other phases (melilite, fassaite and hibonite) based on the $[^{40}Ca^{27}Al^{16}O]^{++}$ peak that is separated from the $[^{40}Ca^{43}Ca]^{++}$ peak by 0.009amu (see Fig. 2.6). We have obtained the values for the $[^{40}Ca^{43}Ca]^{++}/^{43}Ca^{+}$ ratio for all the analyzed mineral phases, as one could expect a dependence of this ratio on the matrix composition (Hutcheon et al., 1984). The measured values for this ratio in terrestrial and meteoritic phases are shown in Fig. 2.7. Except for hibonite, the values for the other mineral phases are very close to each other. The results shown in Fig. 2.7 clearly demonstrate our ability to reproduce this ratio in all the analyzed mineral phases and we can use the measured values with confidence for the correction of the $[^{40}Ca^{42}Ca]^{++}$ interference.

Possible contribution to the signal at mass 41 due to scattering from the hydride peak was generally monitored by obtaining the count rate at mass $(^{43}Ca - \Delta M)$ or $(^{42}Ca - \Delta M)$ where ΔM is given by the relation:

$$\Delta M = \frac{i}{41} \cdot \left[M(^{40}CaH) - M(^{41}K) \right] \simeq 0.009amu \qquad (2.6)$$

where i = 42, 43.

The contribution due to scattering from the $^{40}CaH^{+}$ peak towards signal at mass 41 is estimated as:

$$\left[^{40}CaH \right]_{tail} (c/s) = signal\, at\, \left(^{i}Ca - \Delta M \right) (c/s) \cdot \frac{^{40}CaH^{+}}{^{i}Ca^{+}} \qquad (2.7)$$

where i = 42, 43.

In the case of Efremovka CAIs this contribution was found to be $< 5\%$ of the total signal at mass 41 except in a couple of cases. A major improvement on experimental procedure
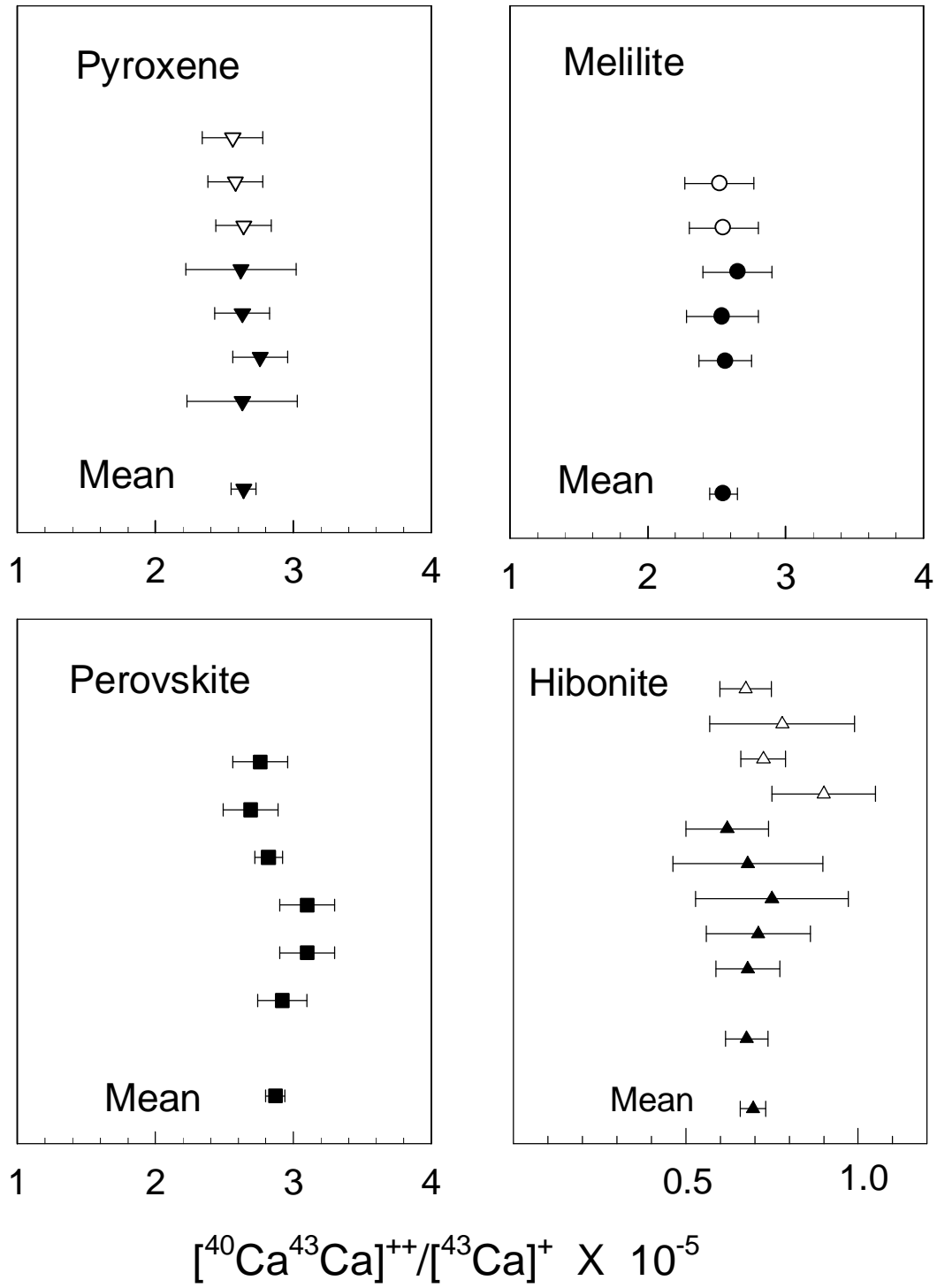
Figure 2.7: $[^{40}\text{Ca}^{43}\text{Ca}]^{++}/^{43}\text{Ca}^{+}$ ratio for different terrestrial (filled symbols) and meteoritic (open symbols) phases.

made during this study is the approach used to analyze single grains of refractory phases using the epoxy bead mounting method. With a smaller volume of epoxy in these beads compared to standard one inch diameter epoxy mounted polished section for the Efremovka CAIs, we found a very significant reduction in the hydride signal, and the $(^{40}CaH)^+$ and $(^{41}K)^+$ peaks were fully resolved (Fig. 2.8). Because of this, the contribution of the scattering from (^{40}CaH) peak to ^{41}K count rate became negligible in most of the single grain analysis. However, as a matter of precaution, the hydride tail was monitored in all the isotopic analysis. The background of the counting system was checked in both static and dynamic mode of operation. In the static mode the system background was always < 0.005 c/s. The dynamic background of the counting system was monitored by including mass 40.7 (acquisition time 30 s) during analysis of terrestrial phases. It was found to be somewhat higher than the static background and had a value of ≤ 0.01 c/s.

Potassium isotopic analysis was carried out by cycling the magnet through the masses, ^{39}K, ^{41}K, ^{40}CaH, $(^{42}Ca - \Delta M$; if necessary), ^{42}Ca, $(^{43}Ca - \Delta M)$ and ^{43}Ca in the peak-jumping mode. The peak center for ^{41}K could be ascertained accurately from the ^{40}CaH peak. The counting times at masses $39(^{39}K)$ and $41(^{41}K)$ were typically 30-45 and 60-90 seconds, respectively. The counting time at mass $(^{42}Ca - \Delta M)$ or $(^{43}Ca - \Delta M)$, used for monitoring the hydride contribution, was typically 10 s. Each analysis consisted of 10-12 blocks of 5-6 cycles each, which lasted for a duration of 90 to 120 minutes. The data reduction was done on block level basis. The value of $(^{41}K^+/^{39}K^+)_{true}$ was evaluated for each block of data in a given analysis and the resultant data set was used to get the mean value and associated uncertainties for the analysis. The $[^{40}Ca^{42}Ca]^{++}$ correction at block level was based on the independently determined value for $[^{40}Ca^{43}Ca]^{++}/^{43}Ca^+$ in meteoritic and terrestrial analog phases (Fig. 2.7) and the measured $^{42}Ca^+/^{39}K^+$ values for each block. The contribution due to scattering from the hydride peak was corrected by using the mean value of $[^{42}Ca-\Delta M]^+/^{42}Ca^+$ or $[^{43}Ca-\Delta M]^+/^{43}Ca^+$ for the

whole analysis and the $[^{40}\text{CaH}]^+/^{39}\text{K}^+$ ratio for each block.

Studies of K-Ca isotopic systematics using ion microprobe involve the determination of the relative sensitivity factor (relative ion yield) for K and Ca in suitable terrestrial analogs of the meteoritic phases. We have analyzed specially prepared samples of pyroxenes and anorthositic glass with high Ca/K ratios to obtain this value. The results obtained by us are shown in Table 2.3. The value of the relative sensitivity factor λ, defined as $[(^{39}\text{K}^+/^{40}\text{Ca}^+)/(^{39}\text{K}/^{40}\text{Ca})]$, obtained from analysis of the anorthositic glass is somewhat lower than those from pyroxenes and suggests a possible matrix-dependent effect. As most of the analyzed meteoritic phases are pyroxenes and have Ca/K values higher than the anorthositic glass, we have used the mean value of 3.2 for the sensitivity factor for obtaining Ca/K ratios. We note here that in determining the $^{39}\text{K}^+/^{40}\text{Ca}^+$ ratio for the pyroxene with extremely low K content (CAI-PX-1), we faced the problem of contribution from K external to the sample. The λ value for this sample given in Table 2.3 is based on the measured $^{39}\text{K}^+/^{40}\text{Ca}^+$ ratios close to (and including) the lowest value obtained for this pyroxene. In the absence of standard samples of perovskite, hibonite and melilite with known Ca/K ratios, we have used a λ value of 3.2 for these phases also.

Table 2.3. Relative yield factor (λ) for K-Ca isotopic analyses

Sample*	K (ppm)	Ca/K	λ**
Pyroxene 1 (Ti-Px-1)	8	2.1×10^4	3.34 ± 0.10
Pyroxene 2 (CAI-Px-1)	0.06	3.0×10^6	3.08 ± 0.20
Anorthositic Glass An-Mg-5	17	8.6×10^3	2.47 ± 0.10

*Samples prepared at Caltech (Courtesy I.D. Hutcheon).
**Relative yield factor favouring K. Errors are $2\sigma_m$.
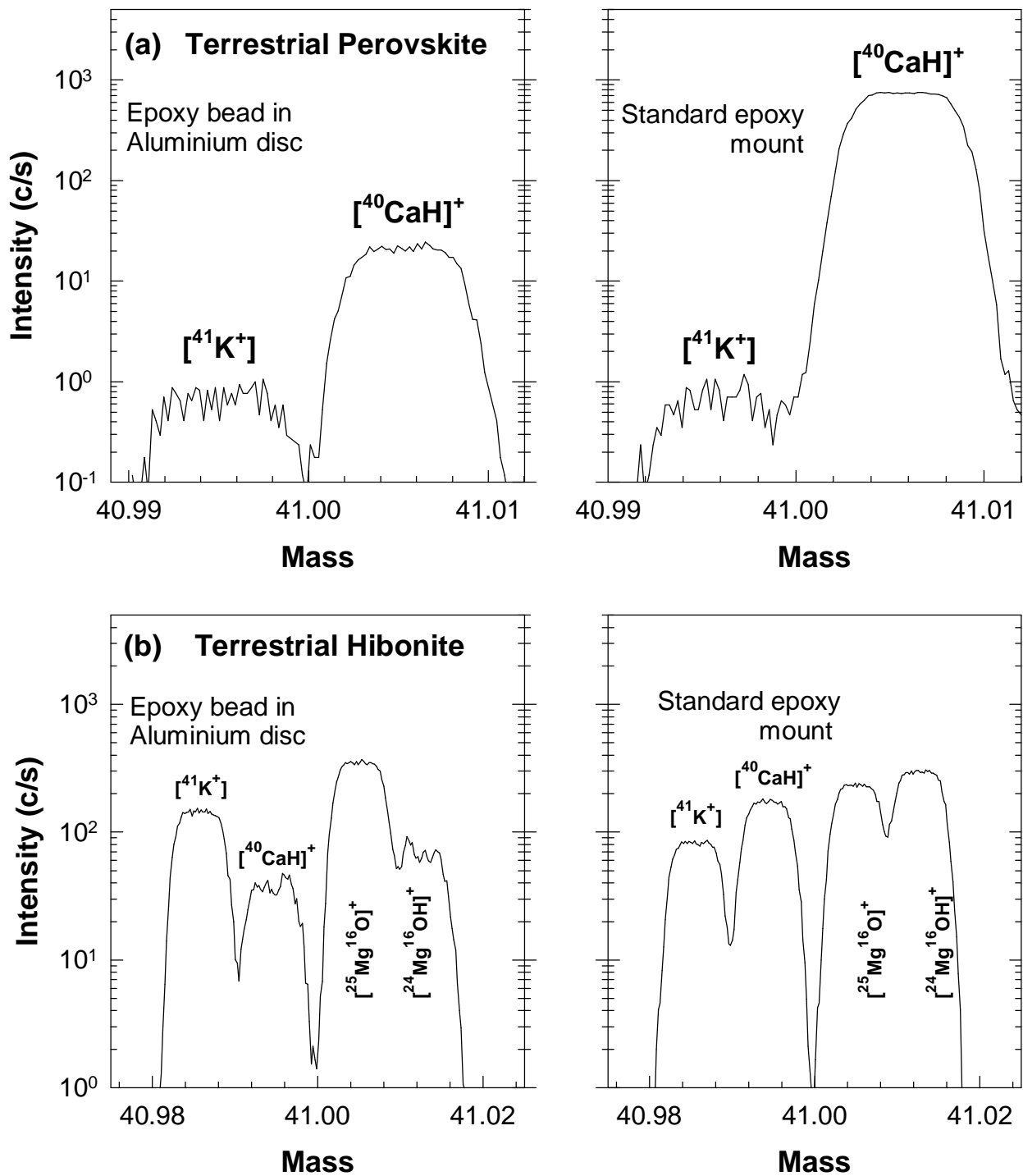
Figure 2.8: High mass resolution spectra around mass 41 taken for samples in standard one inch epoxy mounts and ~ 2 mm epoxy bead in Aluminium discs for: (a) Perovskite, (b) Hibonite. Strong suppression of the hydride signal in the epoxy bead mount is clearly evident.
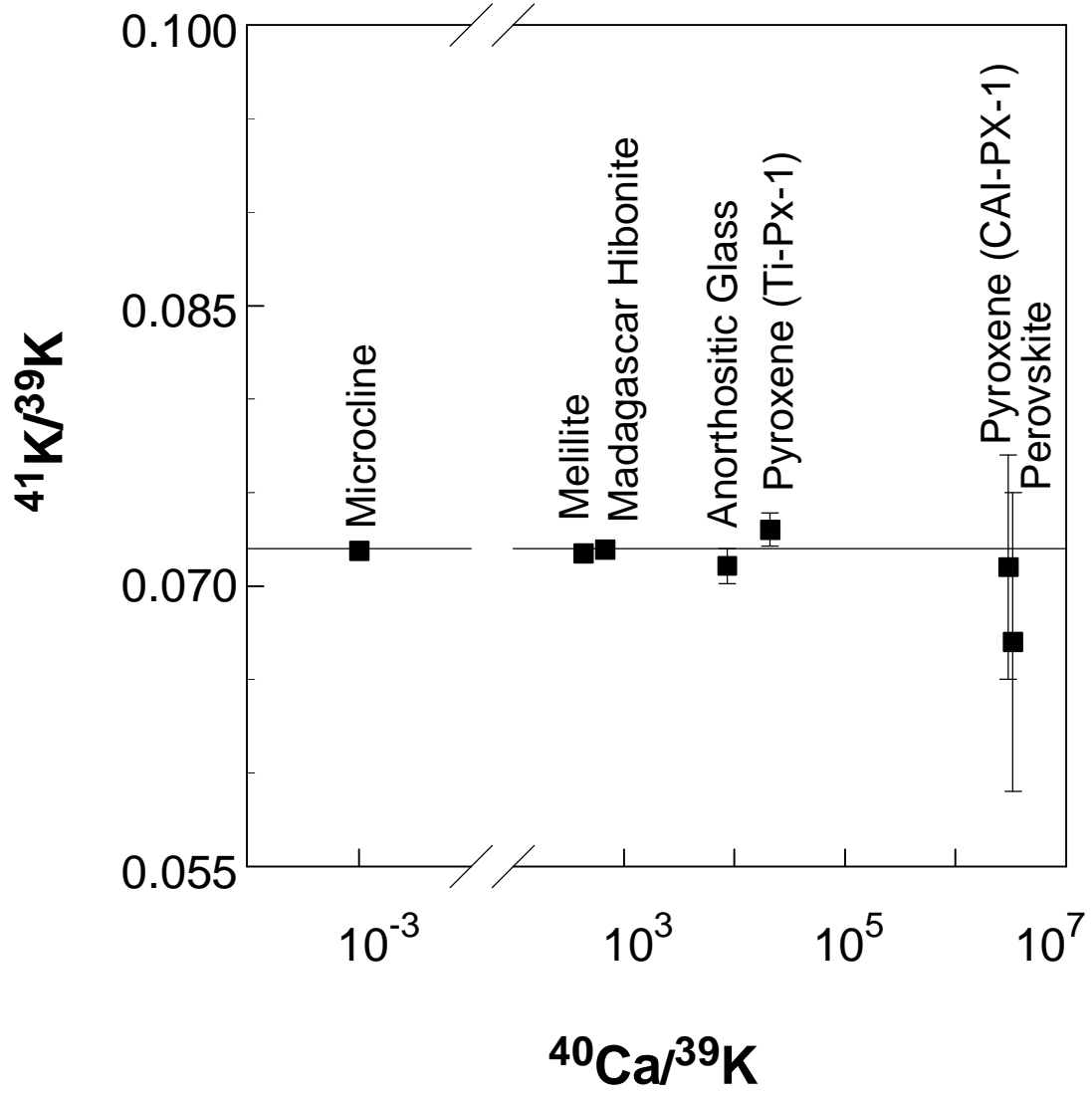
Figure 2.9: K isotopic composition of terrestrial standards with extreme variations in Ca/K ratios. The solid line denotes normal K isotopic composition (^{41}K/^{39}K = 0.072).

In order to ensure that the procedure adopted by us for K-Ca isotopic studies of meteoritic phases with high Ca/K ($>10^5$) can provide accurate $^{41}K/^{39}K$ ratios, we have analyzed a set of terrestrial minerals with Ca/K ratios varying over nine orders of magnitude. The analyzed samples include Madagascar hibonite, perovskite, melilite, microcline (USNM # 143966), and pyroxenes (Ti-Px-1 and CAI-Px-1). The results obtained from this study are shown in Table 2.4 and Fig. 2.9. As in the case of determination of the sensitivity factor, the data for the pyroxene with lowest K content is based on a couple of analyses where the inferred $^{40}Ca/^{39}K$ ratio was close to the expected value of 3×10^6. The $^{41}K/^{39}K$ values in all the cases are close to the reference value of 0.072 (Garner et al., 1975), within the limits of our experimental uncertainties. As ^{40}K is excluded from analysis routine, it is not possible to determine the fractionation corrected residual for ^{41}K (i.e., $\delta\,^{41}K$). However normal K isotopic composition was found for terrestrial minerals with Ca/K ratios ranging from 10^{-3} to $\sim 3 \times 10^6$ (Fig. 2.9), and suggests that isotopic mass fractionation in the case of potassium must be small ($\leq$ a few per mil/amu). It may be noted that instrumental mass fractionation generally favours the lighter isotopes and as such it will tend to suppress the signal at ^{41}K relative to ^{39}K. On the other hand, since the meteorite samples analyzed by us include some coarse-grained CAIs that are considered to be evaporative residues (e.g., MacPherson et al., 1988), one may expect an enrichment of the heavy isotope ^{41}K relative to ^{39}K. However, the magnitude of instrumental mass fractionation in ion microprobe is generally more than that of intrinsic mass fractionation and as the measured isotopic ratios in all the terrestrial phases are close to the reference value, we have neglected any possible effect of isotopic mass fractionation in analyzing the K isotopic data. We note here that a value of ~ 4 per mil per amu for instrumental mass fractionation has been reported recently by Humayun and Clayton (1995) who have analyzed K isotopic compositions in a variety of terrestrial and meteorite samples using an ion microprobe. The measured normal potassium isotopic composition in the terrestrial phases (Fig. 2.9) also provide credence

and validity to the approach used by us to correct the hydride, the doubly charged calcium interferences as well as the absence of other doubly charged interferences under our instrument operating conditions.

Table 2.4. Potassium isotopic analyses of terrestrial standards

Sample	Number of analyses	$^{40}Ca/^{39}K$	$^{41}K/^{39}K$ $\pm 2\sigma_m$
Microcline*	1	1.1×10^{-3}	0.0719 ± 0.0001
Melilite†	1	4.3×10^2	0.0718 ± 0.0002
Madagascar Hibonite	2	6.2×10^2	0.0718 ± 0.0004
Anorthositic Glass ** (An-Mg-5)	2	8.6×10^3	0.0716 ± 0.0009
Pyroxene 1** (Ti-Px-1)	2	1.7×10^4	0.0731 ± 0.0005
Pyroxene 2** (CAI-Px-1)	3	3.0×10^6	0.073 ± 0.008
Perovskite†	4	4.5×10^6	0.072 ± 0.006

*US National Museum Standard (USNM 143966).
**Samples prepared at Caltech (Courtesy I. D. Hutcheon).
†Sample obtained from Vernadsky Institute, Moscow.

Chapter 3

Sample Description

Refractory phases from three carbonaceous chondrites, Efremovka, Murchison and Allende were analyzed in the present work for their K-Ca and Mg-Al isotopic composition. Refractory inclusions (CAIs) in primitive meteorites, particularly those from the Allende (CV3) and Murchison (CM) chondrites have served as important probes to understand the early stages of the formation of the solar system (e.g., Grossman, 1980; MacPherson et al., 1988). The relevant information has come from detailed mineralogical, chemical and isotopic analyses of these refractory phases. The refractory phase assemblages in Murchison contain higher temperature oxide phases (e.g., hibonite, perovskite, spinel, etc., with very little silicates) compared to the Allende CAIs that are mostly devoid of hibonites and have abundant refractory silicates (e.g., fassaite, melilite, anorthite). Some of the Allende CAIs also show distinct signatures of secondary alterations, whereas, CAIs from another CV3 meteorite, Efremovka, analyzed by us appear to be more pristine than the Allende inclusions with very little evidence of secondary alteration. This is also supported by petrographic, REE and, trace element studies of Efremovka CAIs (Ulyanov et al., 1982, 1988; Ulyanov and Kolesov, 1984; Nazarov et al., 1982, 1984; Goswami et al., 1994; Sylvester et al., 1993). A brief description of the refractory samples from these three meteorites analyzed in this work is presented in this chapter. In addition, we also

describe the igneous, non-refractory phases from several chondritic meteorites that were analyzed to look for the presence of ^{26}Al at the time of formation of these phases.

3.1 Refractory phases and inclusions

3.1.1 Allende CAIs

Three CAIs, HAL, EGG3 and USNM 3529-42 from the Allende (CV3) meteorite were analyzed in the present work. A brief description of these inclusions is presented below.

HAL (Hibonite ALlende)

The hibonite inclusion HAL consists of three coarsely crystalline white large crystals of pure hibonite surrounded by a narrow black rim of devitrified glass rich in aluminum and iron (Allen et al., 1980; Table 3.1). In addition, there is a thick (~ 2 mm) sequential multilayered, fine grained outer rim consisting of both volatile (nepheline, sodalite, Ca-phosphate, grossular) as well as refractory (perovskite and hibonite) phases. Mineralogic and petrologic studies of these rims suggest that they were formed by accretion of an assemblage of grains that condensed from a cooling nebular gas. Pentlandite, nickel iron and barrel-shaped olivine crystals (minerals typical of Allende matrix) are also found in the outer layer and increase in abundance towards its exterior. The results obtained from isotopic analyses of O, Mg, Ca and Ti make HAL one of the most unusual inclusion among the category termed as FUN (Fractionation and Unknown Nuclear effects) inclusion (Lee et al., 1979, 1980; Fahey et al., 1987). It shows large Ca isotopic fractionation effects (~ 7.5 % /amu) favoring heavier isotopes with additional superposed nuclear effects. Titanium shows a small positive fractionation of ~ 4.4 % /amu with a presence of small nuclear effects in the neutron rich isotope ^{50}Ti. The oxygen isotopic

compositions of different refractory phases in the HAL inclusion suggest that this inclusion sampled an anomalous reservoir rich in ^{16}O, and has experienced fractionation as well as partial exchange of oxygen with a reservoir of normal isotopic composition (Lee et al., 1979). The magnesium isotopic composition in the rim of HAL was found to be normal, whereas, a very small excess of ^{26}Mg was found in hibonite with an initial ^{26}Al/^{27}Al $= (5.2 \pm 1.7) \times 10^{-8}$. No intrinsic mass fractionation could be measured for magnesium. Based on isotopic composition, petrology and mineral studies, it appears that HAL is a volatilization residue that back-reacted with normal solar nebular matter at low temperature. We have analyzed a fragment of HAL hibonite (Fig. 3.1) for K isotopic composition.

EGG3

EGG3 is a subspherical large (1.5 cm diameter) coarse grained inclusion, composed primarily of Ti-rich fassite, anorthite, spinel and melilite (Wark and Wasserburg, 1980; Wark and Lovering, 1980, 1982). The mineralogy is consistent with Type B1 category. The entire inclusion is extensively veined by a fine-grained alteration material. Based on textural and chemical features, there are indications that some of the melilite, specifically near the rim of the inclusions, were formed by a secondary metamorphic event rather than primary crystallization from a melt (Meeker et al., 1983). The metamorphic event might have taken place on a small planetary body as a result of which pyroxene was replaced by melilite.

Table 3.1. Composition of refractory phases
from Allende and Murchison inclusions

Inclusions:	HAL[*] Hibonite	EGG3[**] Pyroxene	BB-4[†] Hibonite	SH-7[‡] Hibonite
SiO_2	< 0.02	40.40	0.40	0.30
TiO_2	0.71	7.14	3.65	4.6-5.3
Al_2O_3	89.95	17.29	84.69	76.62
FeO	0.32	0.03	-	< 0.1
MnO	-	-	-	-
MgO	<0.01	9.40	2.88	2.2-2.5
CaO	8.71	24.84	8.26	8.58
Cr_2O_3	< 0.02	-	-	-
V_2O_3	< 0.02	0.46	-	-
Sum	99.74	99.56	99.88	92.85

[*] Allen et al. (1980)

[**] Meeker et al. (1983)

[†] Taken by averaging the 4 and 5 enteries of table-1
from MacPherson et al. (1983)

[‡] Assumed to be similar to composition of SH-4 (MacPherson et al., 1983)
for major elements. Minor element composition was taken from
Hashimoto et al. (1986)

The magnesium isotopic analysis of plagioclase and spinel in EGG3 inclusion was carried out by Armstrong et al. (1984). An initial ^{26}Al/^{27}Al value of $\sim 4.9 \times 10^{-5}$ was inferred which is typical of the least altered Type B1 CAI (MacPherson et al., 1995), and suggests that magnesium isotopic composition of EGG3 was not disturbed by the high temperature metamorphic event or during the production of low temperature secondary phases. K isotopic data obtained by Hutcheon et al. (1984) provided a hint for excess ^{41}K seen in some of the pyroxene grains of this CAI which they attributed to decay of ^{41}Ca. However, the K-isotopic signature in EGG3 appeared to be disturbed.

In the present study, pyroxene grain from a small portion of EGG3 (Fig. 3.2; Table 3.1) was analyzed for potassium isotopic composition. The samples of HAL and
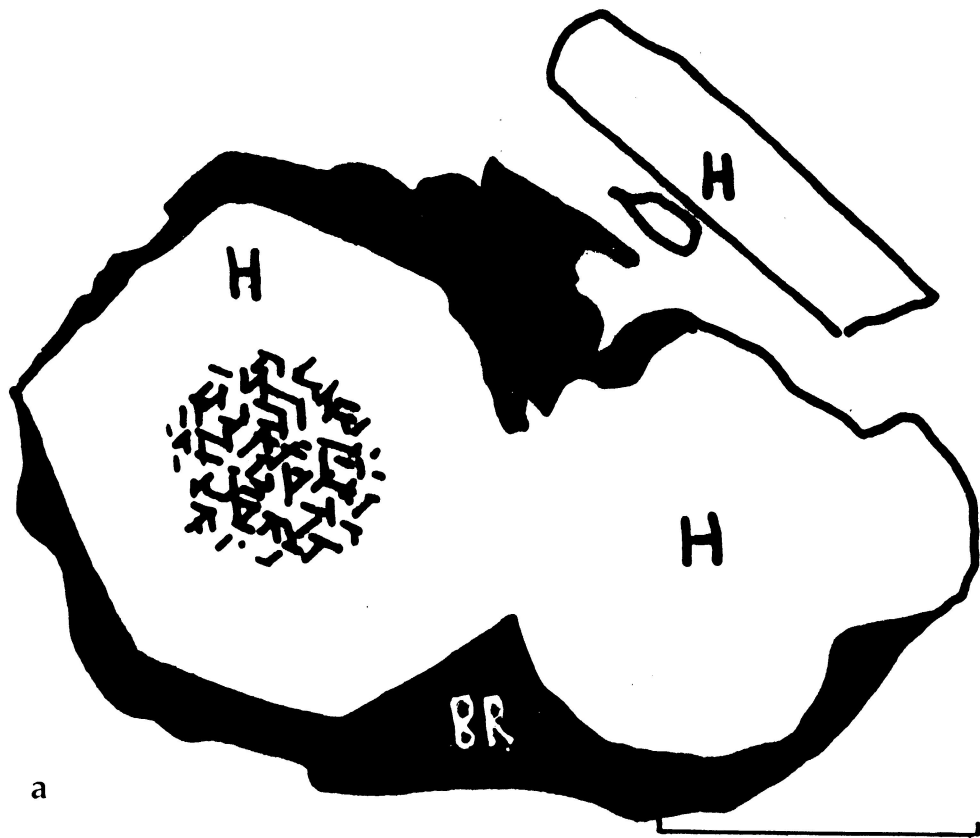
Figure 3.1: (a) The sketch of inclusion HAL in Allende (Allen et al., 1980). Hibonite crystals (H) are surrounded by a black rim (BR) and a friable, multilayered rim sequence. Scale bar is 0.5 mm. (b) Optical photomicrograph of the hibonite crystal studied in this work. The hibonite crystal is ~ 800 μm across.

EGG3 were obtained from Caltech. (courtesy, G. J. Wasserburg and I. D. Hutcheon).

USNM 3529-42

USNM 3529-42 is a unique spinel and hibonite-rich, melilite-bearing Allende inclusion having two diverse lithologies, one spinel-rich (SR) and the other spinel-poor (SP) (MacPherson et al., 1986). Most of the inclusion (SR) is a dense intergrowth of spinel, hibonite and melilite with minor metal beads, fassaite and secondary anorthite that embays and apparently replaces melilite. Secondary phases such as grossular, nepheline and sodalite are virtually absent. The texture of this lithology suggests crystallization from a melt. The melilite-rich region (SP lithology) is attached to one side of SR and resembles normal Allende fluffy Type A (FTA) inclusions. It shows no evidence of having been molten. As both the lithologies are petrologically dissimilar and show no petrographic gradations near the interface, the inclusion might have resulted from a collision between SR and a FTA (SP). However the same initial magnesium isotopic composition in both the lithologies suggests that either there was a complete magnesium isotopic exchange between the two lithologies or both objects coincidently had the same initial magnesium isotopic composition. In the present work, we have carried out magnesium and potassium isotopic analyses of hibonites from two hibonite-rich regions of 3529-42 section #2 (Fig. 3.3; Table 3.2). This sample was obtained from Smithsonian Institute (courtesy, G. J. MacPherson). We have measured both Mg and K isotopic compositions in hibonites from this inclusion.

3.1.2   Murchison (CM) Hibonites

One of the main aim of the present work was to look for correlated presence/absence of the two short-lived nuclides, ^{41}Ca and ^{26}Al in early solar system phases. Such a study can be best done by analyzing refractory phases with high Al/Mg (≥ 10) and Ca/K
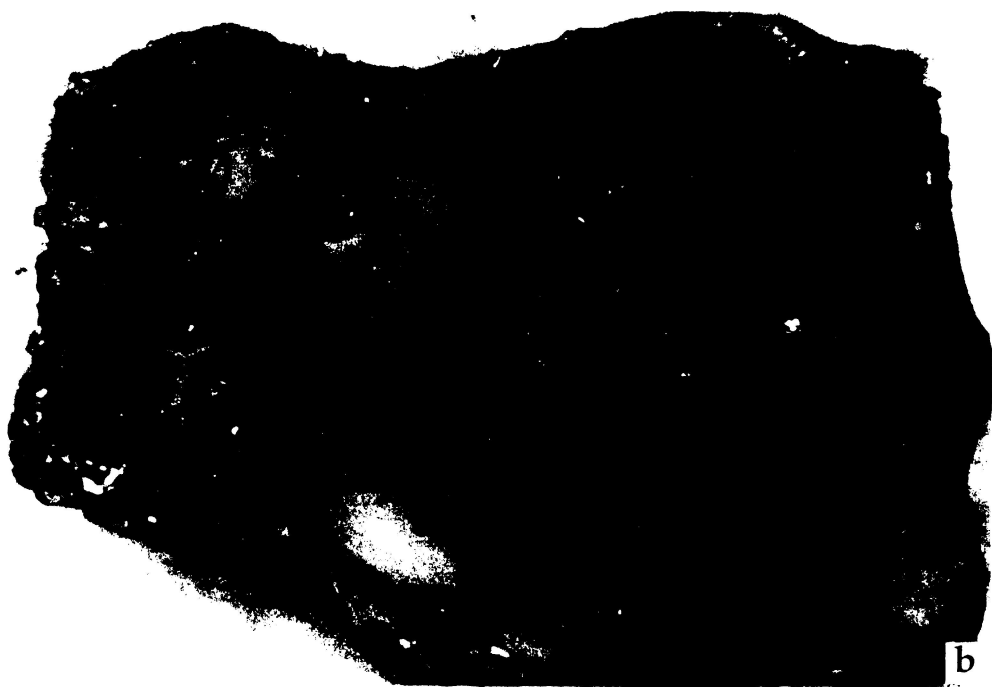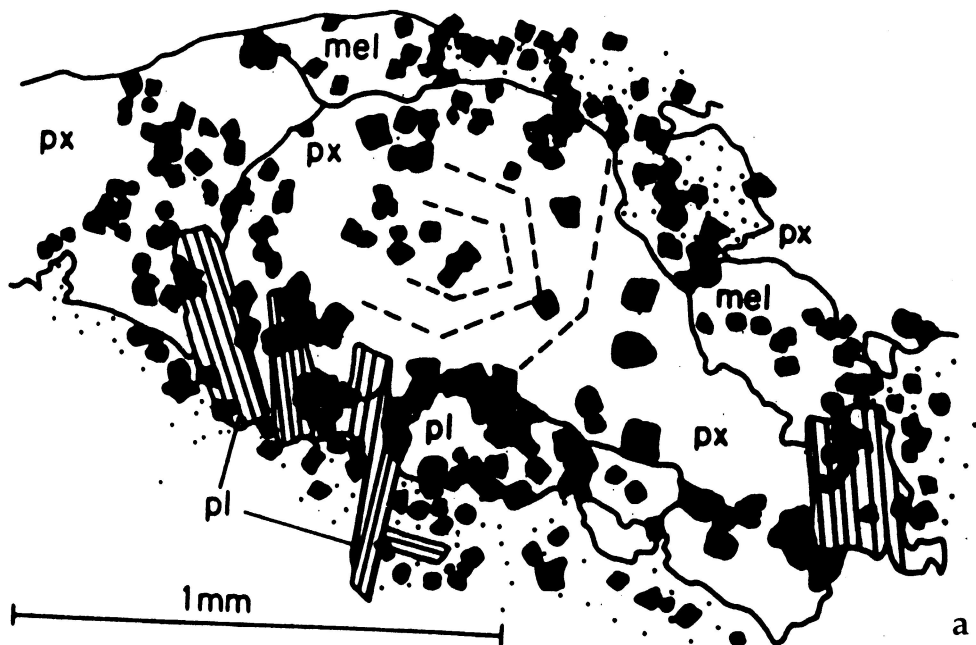
Figure 3.2: (a) Subophitic pyroxene (px) with concentric crystals (dashed lines) and plagioclase (pl) enclose spinel (black) in inclusion EGG3 of Allende meteorite. Stippled areas are alteration. (b) Optical photomicrograph of pyroxene analyzed for K isotopic composition.
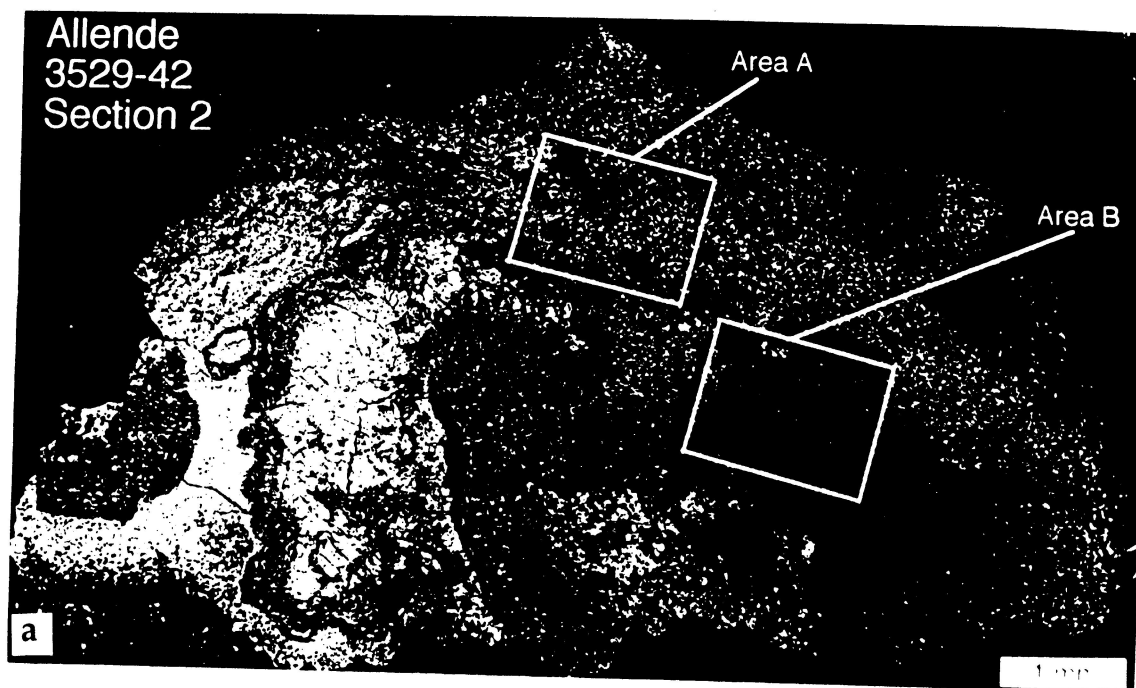
Figure 3.3: (a) Backscattered electron photomicrograph of Allende CAI, USNM 3529-42 (#2). Hibonites from two marked areas, namely, A and B were analyzed for K and Mg isotopic composition. (b) Backscattered electron photomicrograph of hibonite laths in 3529-42 analyzed by ion microprobe. Scale bar is 40 μm.

($\geq 3 \times 10^5$) ratio, so that both Mg-Al and K-Ca isotopic measurements can be done on the same phase. The refractory phase that best suits this requirement is hibonite. In addition to the hibonites from Allende meteorite, we have studied several hibonites from the Murchison (CM) chondrite. Four blue spherules containing spinel and hibonite, and four platelet type irregular thin chips of hibonites were selected for potassium and magnesium isotopic analyses. These hibonites were hand-picked at the Enrico Fermi Institute, Chicago (courtesy, A. M. Davis) from HF/HCl insoluble residue of a large piece of Murchison meteorite that was processed for the separation of interstellar dust (Amari et al., 1994). Most of these objects are 50 - 100 μm in size. The spheroidal shapes of the blue spherules suggest that they could have solidified from melt droplets (MacPherson et al., 1983). The origin of the platelet type hibonite is not exactly understood. It is not clear whether the hibonites occur as isolated grains or were part of some refractory inclusions that got disaggregated during accretion of the Murchison parent body or during separation procedure.

Table 3.2. Major element composition of Murchison and Allende hibonites*

Phases	SH-7	CH-B2	CH-B5	CH-B7	CH-A4	CH-A3	CH-A5	USNM 3529-42
TiO_2	5.4	5.6	4.9	5.5	5.0	5.9	5.3	6.4
Al_2O_3	83.0	83.7	84.6	82.5	84.6	78.7	85.5	78.3
MgO	2.6	1.8	1.6	1.8	1.6	6.6	0.1	9.5-3.6
CaO	9.3	9.2	9.4	9.8	8.9	8.2	9.4	8.6
SUM	100	100	100	100	100	100	100	100

* Hibonite composition for various inclusions were evaluated on the basis of SEM-EDX data. The composition of SH-7 was taken as standard

In addition to these spinel-hibonite spherules and platelet type hibonites, two well documented inclusions, a blue object, BB-4 and a hibonite-rich inclusion SH-7 from Murchison meteorite were also analyzed. BB-4 is a spheroidal object ($\sim$ 100 μm

diameter) composed of intergrown spinel and hibonite. The magnesium isotopic data obtained by Hutcheon et al. (1980) suggest an initial $^{26}Al/^{27}Al \sim 5 \times 10^{-5}$ at the time of formation of this inclusion.

SH-7 is a 2 mm diameter, hibonite rich inclusion that was found on a broken surface of the Murchison meteorite. The analyzed inclusion consists almost entirely of hibonite which poikilitically encloses 1-8 μm euhedral perovskite crystals and sparse 5-10 μm melilite grains (Hashimoto et al., 1986). Spinel is absent in this inclusion. No secondary alteration phases were found in the inclusion. The minor and trace element contents of the inclusion are within the range of composition of hibonites found in other spinel-hibonite inclusions (MacPherson et al., 1983). Magnesium isotopic composition showed absence of ^{26}Al at its formation time. An initial $^{26}Al/$ ^{27}Al of $< 3.6 \times 10^{-6}$ was estimated in hibonite. The oxygen isotopic composition of SH-7 deviates from the normal trend seen in most of the refractory phases from other CAIs. The samples of BB-4 and SH-7 were provided by L. Grossman and A. M. Davis of Enrico Fermi Institute, Chicago.

Representative photomicrographs of hibonites and hibonite bearing inclusions from Murchison meteorite analyzed in this study are shown in Fig. 3.4. Representative chemical compositions of hibonites from Murchison and Allende meteorites are presented in Table 3.1 and Table 3.2.

3.1.3 Efremovka CAIs

Three coarse grained CAIs, E40, E44, E65, and a large multizoned hibonite-rich inclusion (E50) from Efremovka were analyzed to look for excess ^{41}K in them. E40, E44 and E65 are Type B1 inclusions with pyroxene-rich cores and melilite-rich mantles. The petrographic details and mineral chemistry of these inclusions are reported by Ulyanov
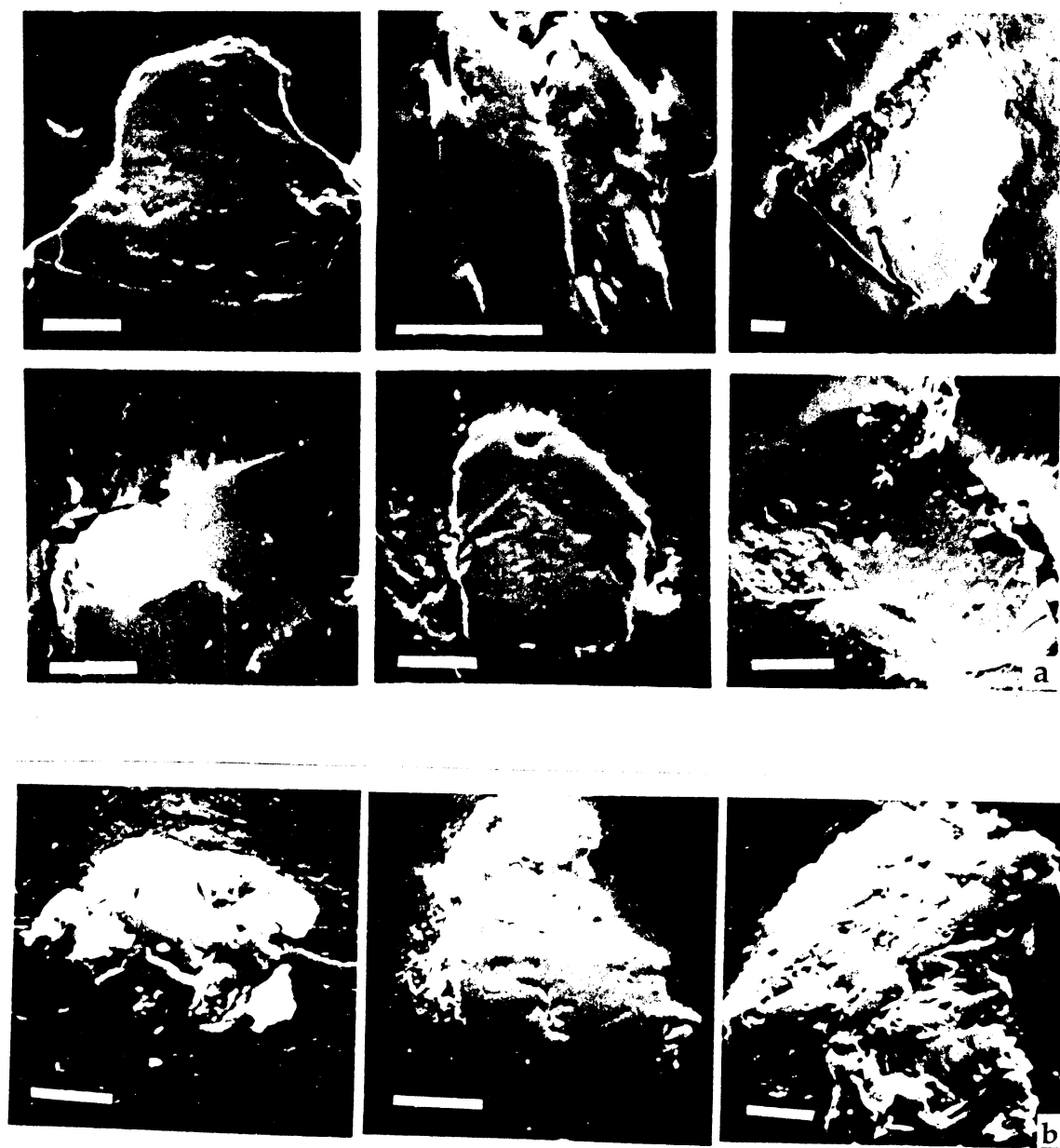
Figure 3.4: Backscattered electron photomicrograph of epoxy mounted hibonites (fig. a) and spinel-hibonite inclusions (fig. b) from Murchison meteorite. Scale bar is 40 μm.

et al. (1982, 1988); Nazarov et al. (1982, 1984) and summarized by Goswami et al. (1994) (Table 3.3). Secondary alteration products are nearly absent in these inclusions. All the inclusions have a 20 to 30 μm thick multilayered rim with a layer sequence of (as one moves outward from the inclusion) spinel ($\pm$ perovskite), melilite, and an outer layer of pyroxene that is zoned from Ti-Al-rich fassaite to aluminous diopside. Hibonite is also present in some of the spinel-melilite layer of E40 rim. The spinel grains in the interior of E40 are relatively large (up to about 100 μm in the core). The spinel grains are in general isometric crystals that are poikilitically enclosed by pyroxenes and melilite. Metal grains and anorthite are generally present in the core region although some times they are also present in the mantle. The abundance of Fe-Ni metal decreases from E65 to E40 to E44. The pyroxenes in these inclusions show variations in their TiO$_2$ content from 2.5 % in E65 to 14.5 % in E40. The pyroxenes are zoned; the smaller ones show simple zoning (Ti-rich core and Ti-poor rim) and the larger ones show complex zoning. The compositional data and stoichiometric considerations suggest that a good fraction of Ti in these inclusions is present in the trivalent state. Melilite in all the inclusions show compositional zoning with the core being rich in akermanite content (55-70 mole %) while it decreases in the near rim region (10-30 mole %). All the three inclusions have well-behaved Mg-Al isochrons with initial ^{26}Al/^{27}Al close to the canonical value of 5×10^{-5} (Goswami et al., 1994). Petrographic, chemical and isotopic data for these Efremovka CAIs suggest them to be more prisitine than the Allende CAIs.

E50 is a large ($\sim$ 1 cm) multizoned hibonite-rich inclusion containing a melilite-pervoskite zone, a melilite-spinel zone, a melilite-spinel perovskite zone and the hibonite rich zone. Small ($\leq$10 μm) perovskite grains are extremely abundant in the melilite-perovskite zone. The spinel grains are small and are poikilitically enclosed by melilite. In the hibonite-rich zone, the hibonite has a lath like structure, and the spinel grains present in this zone are interwoven with melilite. Representative photomicrographs of Efremovka CAIs are shown in Fig. 3.5 and 3.6. We have analyzed pyroxene grains of

E40, E44, E65 for K isotopic composition and hibonites in E50 for both Mg and K isotopic compositions.

<div align="center">

**Table 3.3. Composition of refractory phases
in Efremovka CAIs[*]**

Phase:	Pyroxene[**]			Mel	Pev	Hib
CAI:	E40	E44	E65		E50	
SiO$_2$	42.23	44.68	45.39	25.17	0.68	-
TiO$_2$	6.51	4.00	2.54	0.00	56.76	7.25
Al$_2$O$_3$	16.32	13.67	16.67	31.74	1.09	79.81
FeO	0.05	-	0.54	0.22	0.04	-
MnO	-	0.03	0.02	-	0.11	-
MgO	9.87	12.50	11.43	2.65	0.05	4.73
CaO	25.47	24.99	25.78	39.94	41.09	7.92
Na$_2$O	-	0.08	0.06	0.19	0.15	0.23
K$_2$O[+]	0-0.01	0-0.06	0-0.04	0-0.13	0.03-0.10	0-0.16
Cr$_2$O$_3$	0.10	0.03	0.05	-	-	-
V$_2$O$_3$	0.07	0.02	-	-	-	-
SUM	100.6	100.1	102.5	100	100.1	100.1

</div>

[*]Mel: Melilite; Pev: Perovskite; Hib: Hibonite
[**]The pyroxenes show simple to complex zoning in titanium composition;
data are representative of low-Ti zones.
[+]The spread refers to measured range in different grains
Note: "-" Indicates no measurement.

3.2 Igneous Objects from Chondrites

We have analyzed Mg-Al isotopic systematics in plagioclase phases of igneous, non-refractory objects from two unequilibrated chondrites, Dengli and Severnyi Kolchim, both belonging to the H3 group, and from the Tsarev meteorite belonging to L5 group of chondrites. In addition, Al-rich phases in chromite chondrules and inclusion from
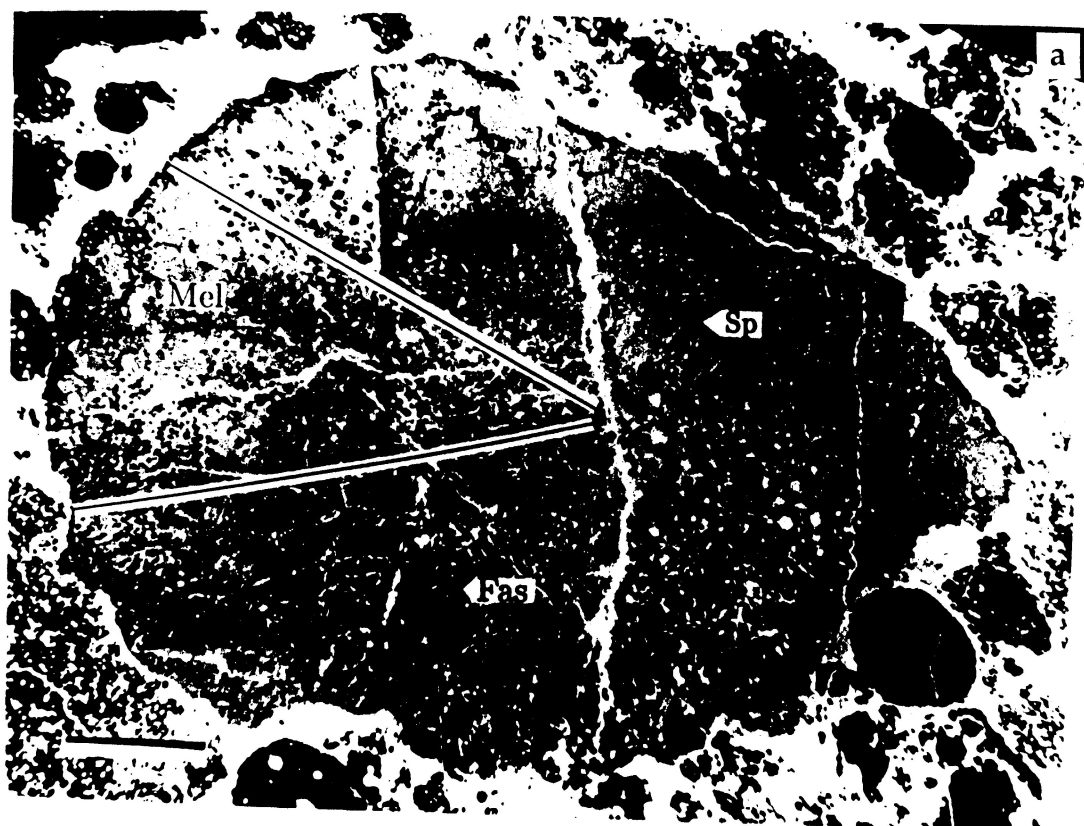
Figure 3.5: Backscattered electron photomicrographs of polished sections of the Efremovka CAIs, E40 (fig. a) and E44 (fig. b). The dominant mineral species (melilite: Mel; spinel: Sp; pyroxene: Fas and anorthite: An) are marked on the photomicrographs. Scale bar is 1 mm in each case.
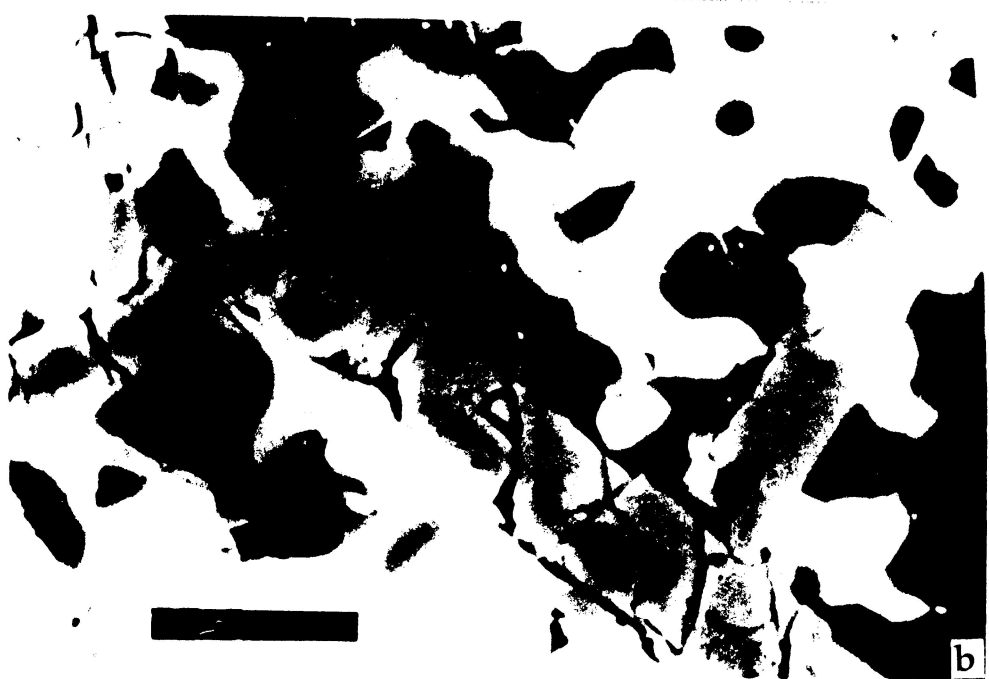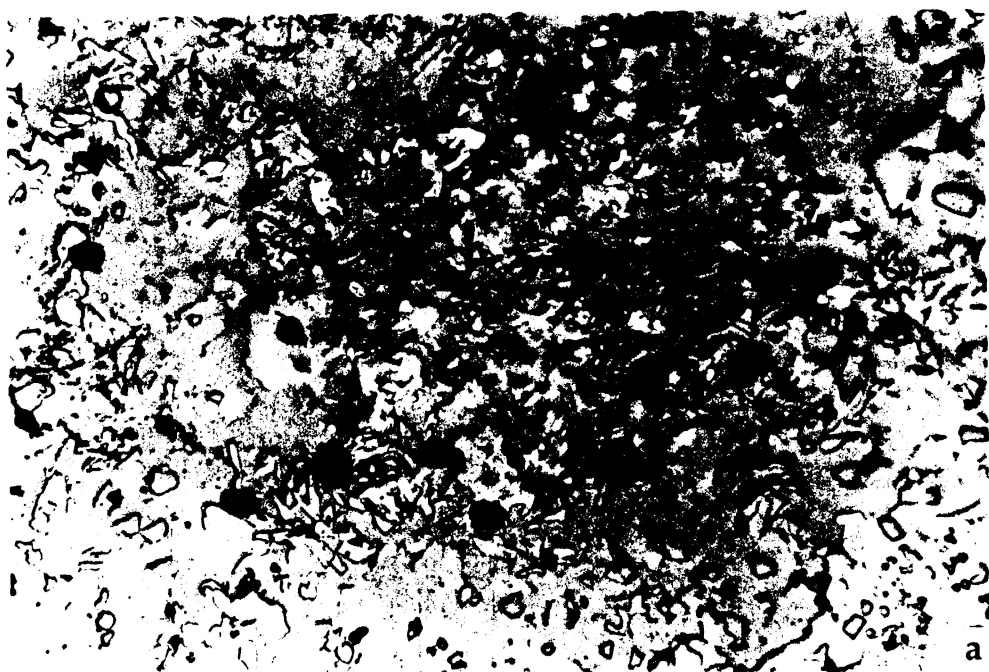
Figure 3.6: Optical photomicrograph of a polished hibonite-rich section of the Efre-movka CAI E50 (fig. a). The hibonite has a lath like structure, the spinel grains present in this zone are interwoven with melilite. The backscattered electron image (fig. b) shows lath like hibonite crystals. Scale bar is 20 μm.

the unequilibrated H-chondrite, Raguli and anorthite grains separated from the multi-component meteorite breccia Kaidun were also chosen for analyses.

The basaltic inclusion in the **Tsarev** (L5) chondrite consists of Ca-rich pyroxene and minor orthopyroxene grains embedded in a glassy plagioclase matrix and is characterized by a fine grained magmatic texture (Migdisova et al., 1992; 1994). The chemical composition of Ca-rich pyroxene and plagioclase in the inclusion is similar to that of the host chondrite. However, the phase proportion in the former is similar to that of eutectic (basaltic) mixture. The similarity in the chemical compositions suggests that the basaltic inclusion and the host chondrite are genetically related. Partial melting of host chondritic material by which plagioclase-pyroxene fraction was melted and separated from residual olivine and orthopyroxene has been proposed as the mode of formation of this inclusion. The basaltic inclusion was most probably formed by rapid solidification of melt without equilibration with residual solid.

The **Dengli** (H3) unequilibrated chondrite is a complex chondritic breccia containing several angular clasts and inclusions (Ivanova et al., 1992; Ivanova et al., 1993). The plagioclase phases from a silica-bearing inclusion, an angular clast (clast number 2 of Ivanova et al., 1992) and a chondrule were analyzed by us. The silica-bearing inclusion has a round shape and consists of orthopyroxene, clinopyroxene, feldspar and silica (probably crystobalite). The angular clast is composed of olivine, Al-rich clinopyroxene and feldspar. The presence of clinopyroxene and Ca-rich feldspar indicates its similarity with achondrites, and suggests an igneous origin for this silica bearing inclusion.

Table 3.4. Composition of plagioclase phases from
igneous objects in chondrites

| | Tsarev[*] | Severnyi[†] Kolchim | Dengli[‡] | |
			Silica-bearing	Igneous clast
SiO_2	54.70	45.60	49.50	54.50
Al_2O_3	21.59	35.30	33.50	27.30
FeO	0.18	0.82	0.30	1.00
MgO	0.10	0.09	-	0.42
CaO	2.04	16.60	15.40	9.10
TiO_2	0.09	0.01	0.10	0.13
MnO	0.03	0.04	0.35	< 0.05
Na_2O	8.33	1.51	2.60	6.10
K_2O	1.49	0.04	<0.05	0.10
Cr_2O_3	0.03	0.85	-	0.01

[*] Migdisova el al. (1992)
[†] Nazarov et al. (1993)
[‡] Ivanova et al. (1992)

The igneous object in the unequilibrated chondrite **Severnyi Kolchim** (H3) consists of olivine grains surrounded by Ca-rich pyroxene and Ca-rich feldspar (Nazarov et al., 1993). The presence of Ca-rich feldspar and pyroxene with the absence of metal grains suggest that the clast was formed by igneous process on a differentiated parent body. However, the mineral chemistry, particularly the higher Fe/Mg ratio in olivine grains relative to that of the late crystallizing phases is difficult to explain in this scenario.

Presence of chromite chondrules and inclusions in the **Raguli** (H3) meteorite has been reported by Krot and Ivanova (1992) and Krot et al. (1992). These objects consist of chromite and plagioclase phases with minerals like ilmenite, pyroxene and phosphate as accessory phases. Several models have been proposed to explain the origin of chromite chondrules and inclusions (Ivanova and Krot, 1994). These include melting and recrystallization of pre-solar aggregates to form chondrules and inclusions, and secondary alteration of nebular condensate in meteorite parent body or in an oxidizing
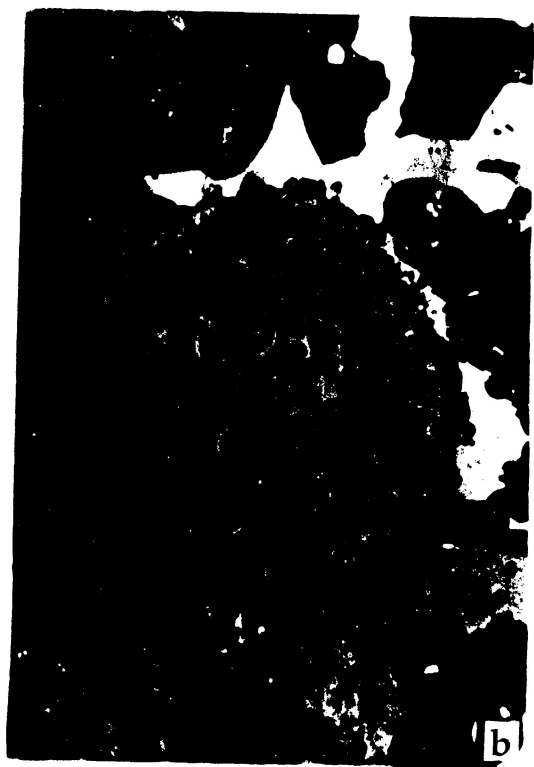
Figure 3.7: (a) Optical photomicrograph of a section of Severnyi Kolchim (H3) meteorite. Inset shows an igneous inclusion ($\sim 800~\mu$m) analyzed for Mg-Al isotopic systematics. (b), (c) Optical photomicrograph of a chromite chondrule and an inclusion ($\sim 200~\mu$m across), respectively, from Raguli (H3) meteorite. The light portions in the chondrule and inclusion are chromite, whereas, dark portions represent plagioclase.

environment. Although, these phases are not product of thermal processing in meteorite parent bodies, they can provide additional clues about distribution of ^{26}Al during different epochs in the early solar system. In the present study, plagioclase phases from two chromite chondrules and one inclusion were analyzed.

Kaidun meteorite is a heterogeneous multi-component meteorite breccia comprising of carbonaceous and enstatite chondrites (Ivanov, 1989). The major constituents of this meteorite have a composition close to type CM chondrite. Xenoliths with composition resembling type CI and two distinct types of enstatite chondrites (EL3 and EH5) are also found within the dominant CM type. This multi-component meteorite breccia perhaps was formed in a series of events causing compaction of these four types of meteorites. The origin of the anorthite grains separated from the carbonaceous matrix by crushing and hand picking are not exactly known, but has been included in the present study because of the unique nature of the Kaidun meteorite.

Representative photomicrographs of the igneous objects analyzed in this work are shown in Fig. 3.7. Chemical composition of a selected plagioclase phases is shown in Table 3.4.

Chapter 4

Results

In this chapter we present the results obtained from the K-Ca and Mg-Al isotopic analyses of the refractory phases and inclusions from the Efremovka, Allende and Murchison meteorites. In addition, Mg-Al isotopic systematics for the igneous, non-refractory objects form various chondrites analyzed in this study are also presented.

4.1   Potassium Isotopic Composition

4.1.1   Refractory phases in Efremovka (CV3) meteorite

The results obtained in the present study of K isotopic composition in refractory phases of Efremovka CAIs are given in Table 4.1. The $^{40}Ca/^{39}K$ values were computed from the measured $(^{42}Ca^+/^{39}K^+)$ ratio, using a relative sensitivity factor of 3.2 favouring K for all the analyzed phases and a normal $^{40}Ca/^{42}Ca$ ratio of 151.02. The hibonite grains in E50 are small and it is difficult to carry out high precision isotopic analysis without possible interference from surrounding relatively K-rich (Ca/K $\sim 10^4$) phases (presumably altered products present in melilite). Nonetheless we have been able to analyze a few hibonite grains where contributions towards K signal from the neighbouring phases are expected

to be small. This could be inferred from the measured intensities of the Mg^+, Al^+, Ca^+ and Ti^+ ions from the analyzed spot before and after each analysis. Although melilite has typically a low Ca/K ratio (a few times 10^4) we could locate several spots in E50 where this value exceeds 10^5 and are suitable for K-isotopic studies. The results obtained, however, suggest possible disturbance in K isotope systematics in melilite from E50 and we have included data for only a few analyses in Table 4.1 to illustrate both the presence as well as absence of ^{41}K excess in melilite with high Ca/K ratios. All the ^{41}K/^{39}K values given in Table 4.1 have been corrected for contributions to the signal at mass 41 from the unresolvable $[^{40}Ca^{42}Ca]^{++}$ interference and from the tail of the ^{40}CaH peak following the procedures described in chapter 2. The typical signal at mass ^{41}K ranges from 0.5 to 0.8c/s when the Ca/K ratio exceeds 5×10^5. The measured count rate at mass 41 (averaged over individual analysis) and its decomposition to various components are shown in Fig. 4.1 for the analyzed pyroxenes with Ca/K $\geq 10^6$ as well as for terrestrial perovskite and pyroxene with high Ca/K ratio. The ^{39}K count rate for the pyroxene with the highest Ca/K ratio (E44; pyroxene 2) decreased by a factor of two after the first three blocks of analysis and remained relatively stable for the remainder seven blocks of analysis. The data for this pyroxene presented in Table 4.1 and Fig. 4.1 refer to the result obtained from the last seven data blocks.

The contribution to the signal at mass 41 due to scattering from the hydride peak, estimated from the count rate at the mass (^{42}Ca-Δ M) or (^{43}Ca-Δ M), was generally less than 5% of the signal at ^{41}K except in a couple of cases that probably reflect less than optimal instrument tuning (peak shape) and operating conditions. We have not made explicit correction for the background of the counting system as the indirect correction for $[^{40}Ca^{42}Ca]^{++}$ interference at mass 41 already takes this into account. Note that the magnitude of this correction is based on independent analysis with long acquisition time (60-90s per cycle) at mass 41.5. The magnitude of the $[^{40}Ca^{42}Ca]^{++}$ contribution to the signal at mass 41 is proportional to the count rate at mass 42 (^{42}Ca) and the
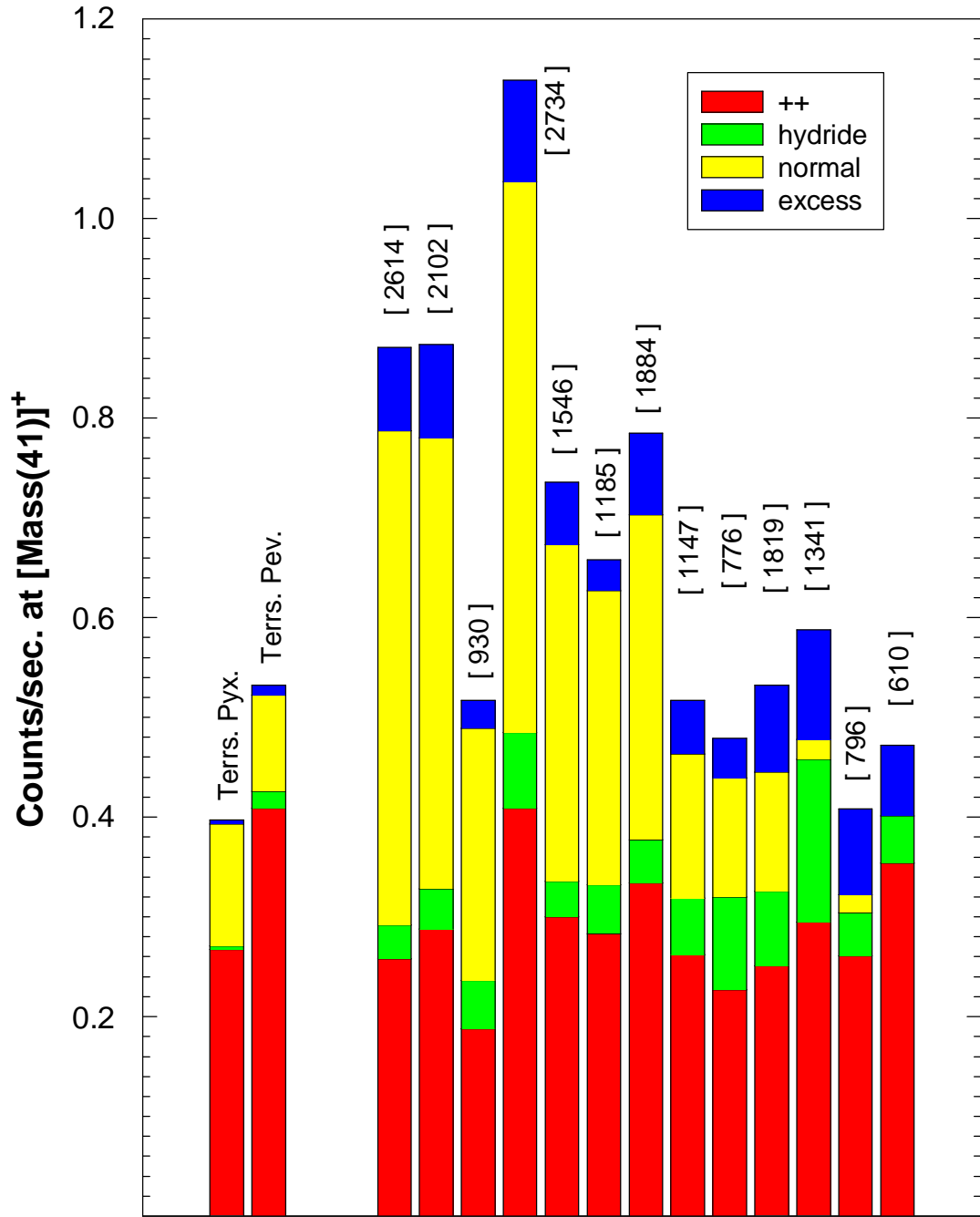
Figure 4.1: Decomposition to various components (Double plus, hydride, normal and excess) of count rates at mass 41 for various pyroxenes from Efremovka CAIs with $Ca/K > 10^6$. The total counts at mass 41 in each case is also shown. Data for terrestrial pyroxene and perovskite are also shown.

variations in this signal seen in Fig. 4.1 reflect variations in the measured $^{42}Ca^+$ count rates primarily due to the differences in the primary beam current used during individual analysis. The data shown in Fig. 4.1 clearly suggest the presence of an excess signal at mass 41(^{41}K) varying from 0.04 to 0.12c/s. The excess count rates are much above our system background ($\leq$0.01c/s) and account for $\sim$ 8 to 20% of the measured count rates at this mass except for a couple of cases.

The $^{41}K/^{39}K$ ratios for the analyzed phases from the Efremovka CAIs, evaluated following the procedures described in chapter 2, along with the data for terrestrial pyroxene and perovskite are plotted as a function of their $^{40}Ca/^{39}K$ ratios in Fig. 4.2. Data points with Ca/K > 3 $\times$ 10^5 show clear evidence of excess ^{41}K with measured $^{41}K/^{39}K$ values higher than the reference value of 0.072. The error bars in the measured $^{41}K/^{39}K$ ratios are mainly governed by counting statistics at mass 41 and 39 (typically of the order of $\leq$ 3% at 1σ level), and the error associated with the doubly-charged calcium interference. In some analyses the error bars are rather large due to the spread in the measured $^{42}Ca/^{39}K$ ratio. Note that the uncertainty in the mean value for this ratio affects the error estimation for ($^{41}K/^{39}K$) while making corrections for the doubly charged calcium interference and also the error on the estimated value of $^{40}Ca/^{39}K$. A correlation of the excess ^{41}K with the measured $^{40}Ca/^{39}K$ ratio of the analyzed phases is clearly evident in the data shown in Fig. 4.2.

It is therefore reasonable to assume that the excess in ^{41}K is due to *in situ* decay of the short-lived nuclide, ^{41}Ca that was incorporated 'live' into the CAIs at the time of their formation, and, we can write:
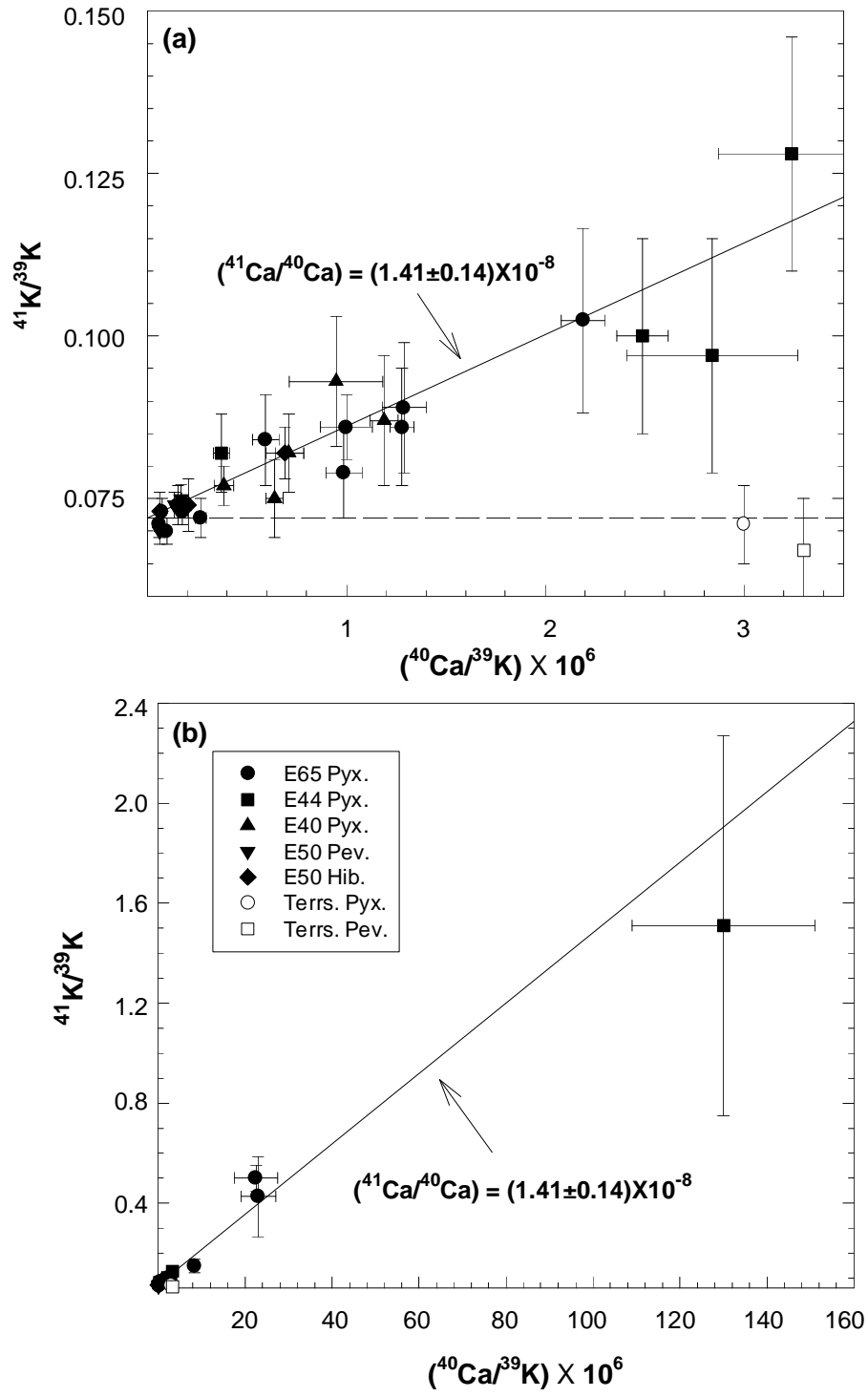
Figure 4.2: K isotopic composition of different phases from Efremovka CAIs plotted as a function of their Ca/K ratios. The error bars are $2\sigma_m$. The dashed line represents normal terrestrial standard value for $^{41}K/^{39}K = 0.072$.

$$\left(\frac{^{41}K}{^{39}K}\right)_{m(true)} = \left(\frac{^{41}K}{^{39}K}\right)_{i} + \left(\frac{^{41}K^{*}}{^{39}K}\right)$$

$$= \left(\frac{^{41}K}{^{39}K}\right)_{i} + \left(\frac{^{41}Ca}{^{40}Ca}\right)_{i} \left(\frac{^{40}Ca}{^{39}K}\right)_{m} \tag{4.1}$$

where i represents the initial ratio, m(true) refers to the measured(true) ratio and '*' represents the radiogenic component. This relation represents the evolution of the K-Ca isotopic system in the Efremovka CAIs (assuming a closed system), and the intercept and slope of the best-fit line represented by this relation give the initial ^{41}K/^{39}K and ^{41}Ca/^{40}Ca values at the time of closure of the K-Ca isotope system in the CAIs. The data shown in Fig. 4.2 yield a value of $(1.41 \pm 0.14) \times 10^{-8}$ for the initial ^{41}Ca/^{40}Ca at the time of formation of Efremovka CAIs (error quoted here and in the remainder of the thesis are $2\sigma_m$). They also suggest a value of (0.0706 ± 0.0007) for the initial ^{41}K/^{39}K which is close to the reference value of 0.072. Both these initials are very close to the earlier result reported by Srinivasan et al. (1994) based on a sub-set of the total data presented here. Even though the Ca/K values for most of the data points lie between $(0.3 - 3) \times 10^{6}$, the correlation holds true even for phases with very high Ca/K ratios of $\sim 2 \times 10^{7}$ and $\sim 10^{8}$ (Fig. 4.2b). Decomposition of the signal at mass 41 for the analysis that yielded the highest Ca/K ratio and where the contribution from natural ^{41}K is below our detection limit (^{39}K$^{+}\sim 0.01$c/s), yields an initial ^{41}Ca/^{40}Ca of $(1.10 \pm 0.56) \times 10^{-8}$. The value of the slope of the correlation line obtained by us is higher than the value of $(8 \pm 3) \times 10^{-9}$ reported by Hutcheon et al. (1984). However, a majority of the data points (4 out of 6) with high ^{40}Ca/^{39}K ($> 5 \times 10^{5}$) reported by Hutcheon et al. (1984) fall closer to the correlation line obtained by us. We have already noted that we suspect movement of K in E50 melilites and they are not included in Fig. 4.2 and also while obtaining the initial Ca and K isotopic ratios. The low Ca/K values for melilite in other Efremovka CAIs, unfortunately, do not allow us to make an in-depth study of this problem.

Table 4.1 Efremovka K-Ca isotopic data

Sample	$^{40}\text{Ca}/^{39}\text{K}$ $\pm 2\sigma_m$	$^{41}\text{K}/^{39}\text{K}^{\dagger}$ $\pm 2\sigma_m$
Efremovka CAIs		
E40 (type B1)		
Pyroxene 1	$(6.39 \pm 0.44) \times 10^5$	0.075 ± 0.006
Pyroxene 2	$(7.11 \pm 0.70) \times 10^5$	0.082 ± 0.006
Pyroxene 3	$(1.19 \pm 0.07) \times 10^6$	0.087 ± 0.010
Pyroxene 4	$(9.48 \pm 2.34) \times 10^5$	0.093 ± 0.010
Pyroxene 5	$(3.83 \pm 0.49) \times 10^5$	0.077 ± 0.003
E44 (type B1)		
Pyroxene 1	$(2.84 \pm 0.43) \times 10^6$	0.097 ± 0.018
Pyroxene 2	$(1.30 \pm 0.21) \times 10^8$	1.510 ± 0.760
Pyroxene 3	$(2.49 \pm 0.13) \times 10^6$	0.100 ± 0.015
Pyroxene 4	$(3.24 \pm 0.37) \times 10^6$	0.128 ± 0.018
Pyroxene 5	$(3.71 \pm 0.41) \times 10^5$	0.082 ± 0.006
E50 (Hibonite-Rich)		
Perovskite 1	$(1.69 \pm 0.01) \times 10^5$	0.075 ± 0.002
Perovskite 2	$(5.95 \pm 0.01) \times 10^4$	0.070 ± 0.002
Perovskite 3	$(1.36 \pm 0.01) \times 10^5$	0.074 ± 0.002
Melilite 1*	$(1.17 \pm 0.10) \times 10^6$	0.096 ± 0.012
Melilite 2*	$(1.71 \pm 0.25) \times 10^6$	0.108 ± 0.028
Melilite 3*	$(7.37 \pm 0.47) \times 10^5$	0.065 ± 0.005
Hibonite 1	$(6.11 \pm 1.15) \times 10^4$	0.073 ± 0.003
Hibonite 2	$(2.04 \pm 0.17) \times 10^5$	0.074 ± 0.004
Hibonite 3	$(6.91 \pm 0.96) \times 10^5$	0.082 ± 0.004

Efremovka (Continued)

Sample	$^{40}\text{Ca}/^{39}\text{K}$ $\pm 2\sigma_m$	$^{41}\text{K}/^{39}\text{K}^{\dagger}$ $\pm 2\sigma_m$
E65 (type B1)		
Pyroxene 1	$(7.30 \pm 0.81) \times 10^4$	0.073 ± 0.002
Pyroxene 2	$(2.67 \pm 0.29) \times 10^5$	0.072 ± 0.003
Pyroxene 3	$(5.86 \pm 0.85) \times 10^4$	0.071 ± 0.002
Pyroxene 4	$(9.73 \pm 1.33) \times 10^4$	0.070 ± 0.002
Pyroxene 5	$(1.75 \pm 0.28) \times 10^5$	0.073 ± 0.002
Pyroxene 6	$(1.52 \pm 0.04) \times 10^5$	0.074 ± 0.003
Pyroxene 7	$(9.87 \pm 0.95) \times 10^5$	0.079 ± 0.007
Pyroxene 8	$(5.94 \pm 0.67) \times 10^5$	0.084 ± 0.007
Pyroxene 9	$(1.28 \pm 0.06) \times 10^6$	0.086 ± 0.009
Pyroxene 10	$(2.19 \pm 0.11) \times 10^6$	0.102 ± 0.014
Pyroxene 11	$(1.29 \pm 0.11) \times 10^6$	0.089 ± 0.010
Pyroxene 12	$(1.00 \pm 0.13) \times 10^6$	0.086 ± 0.005
Pyroxene 13	$(8.30 \pm 0.76) \times 10^6$	0.149 ± 0.026
Pyroxene 14	$(2.30 \pm 0.40) \times 10^7$	0.427 ± 0.160
Pyroxene 15	$(2.25 \pm 0.50) \times 10^7$	0.501 ± 0.051

†Values are corrected for $(^{40}\text{Ca}^{42}\text{Ca})^{++}$ interference. The values for $[^{40}\text{Ca}^{43}\text{Ca}]^{++}/^{43}\text{Ca}^+$ ratio in pyroxene, melilite, perovskite and hibonite are $(2.64 \pm 0.09) \times 10^{-5}$, $(2.55 \pm 0.10) \times 10^{-5}$, $(2.87 \pm 0.07) \times 10^{-5}$ and $(6.95 \pm 0.61) \times 10^{-6}$ respectively. The magnitude of $(^{40}Ca^{42}Ca)^{++}$ correction is given by:

$$[^{40}\text{Ca}^{43}\text{Ca}]^{++}/^{43}\text{Ca}^+ \times (^{42}\text{Ca}^+/^{40}\text{Ca}^+) \times (^{40}\text{Ca}^+/^{39}\text{K}^+), \text{ where, } (^{40}\text{Ca}^+/^{42}\text{Ca}^+) = 151.02$$

*Data not included to calculate the slope and intercept of the evolution diagram.

In addition to the conventional isochron plot of $^{41}\text{K}/^{39}\text{K}$ vs. $^{40}\text{Ca}/^{39}\text{K}$, we have also plotted $^{41}\text{K}/^{40}\text{Ca}$ as a function of $^{39}\text{K}/^{40}\text{Ca}$ (Fig. 4.3), which avoid plotting ratios of two quantities with large uncertainities (e.g., $^{41}\text{K}/^{39}\text{K}$) on individual axis. The slope of the best-fit line in this representation give the initial $^{41}\text{K}/^{39}\text{K}$, while the intercept, the initial $^{41}\text{Ca}/^{40}\text{Ca}$. The values obtained are (0.0712 ± 0.0012) and $(1.29 \pm 0.29) \times 10^{-8}$, respectively, consistent with the values noted earlier.
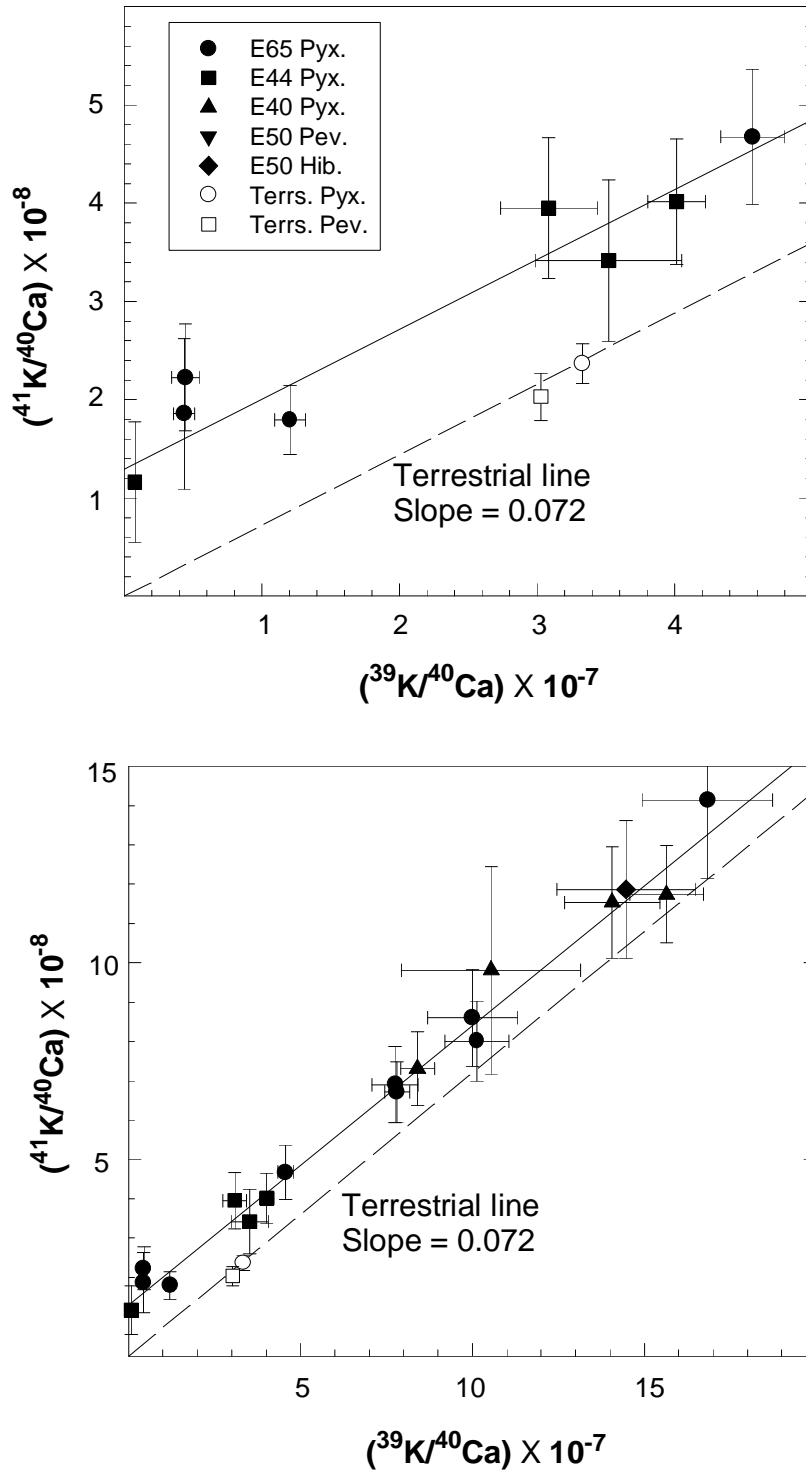
Figure 4.3: $^{41}K/^{40}Ca$ vs $^{39}K/^{40}Ca$ plot for Efremovka CAIs. The data yield an initial $^{41}K/^{39}K$ value of 0.0712 ± 0.0012 and $^{41}Ca/^{40}Ca$ of $(1.29 \pm 0.20) \times 10^{-8}$. The error bars are $2\sigma_m$.

4.1.2 CAIs from the Allende (CV3) meteorite

HAL

The results obtained from potassium isotopic analyses of HAL hibonite are presented in Table 4.2. We found spatial inhomogeneity in K concentration within the HAL hibonite. In the first two analyses, the ^{39}K count rate was resonably high, and the measured ^{41}K/^{39}K ratio after appropriate corrections for $[^{40}$Ca^{42}Ca$]^{++}$ interference, reveal no excess in ^{41}K/^{39}K ratio over the normal value of 0.072. In the third analysis, the ^{39}K count rate was below our detection background. After correcting the measured ^{41}K/^{42}Ca ratio for this analysis for double-plus calcium interference, the residual excess in ^{41}K provides an upper limit for initial ^{41}Ca/^{40}Ca of 3×10^{-9}. The first three results are plotted in Fig. 4.4 along with the results obtained from potassium isotopic analyses of USNM 3529-42 hibonites. The first two data points plot on the normal ^{41}K/^{39}K values along with the terrestrial samples. As the abundance of ^{39}K in case of third analysis is below our detection limit, a lower limit value for ^{40}Ca/^{39}K of 2.6×10^7 was selected to represent the data. The arrow represents the expected evolution of a closed K-Ca isotopic system for an initial ^{41}Ca/^{40}Ca value of 3×10^{-9}. The results from two additional analyses given in Table 4.2 do not show any excess in ^{41}K/^{39}K ratio over its normal value within our experimental uncertainties. Because of their low precesion, these data points are not represented in Fig. 4.4. Based on the data, we infer a value of 3×10^{-9} as an upper limit for the initial ^{41}Ca/^{40}Ca at the time of formation or final closure of K-Ca isotopic systematics in HAL hibonite.
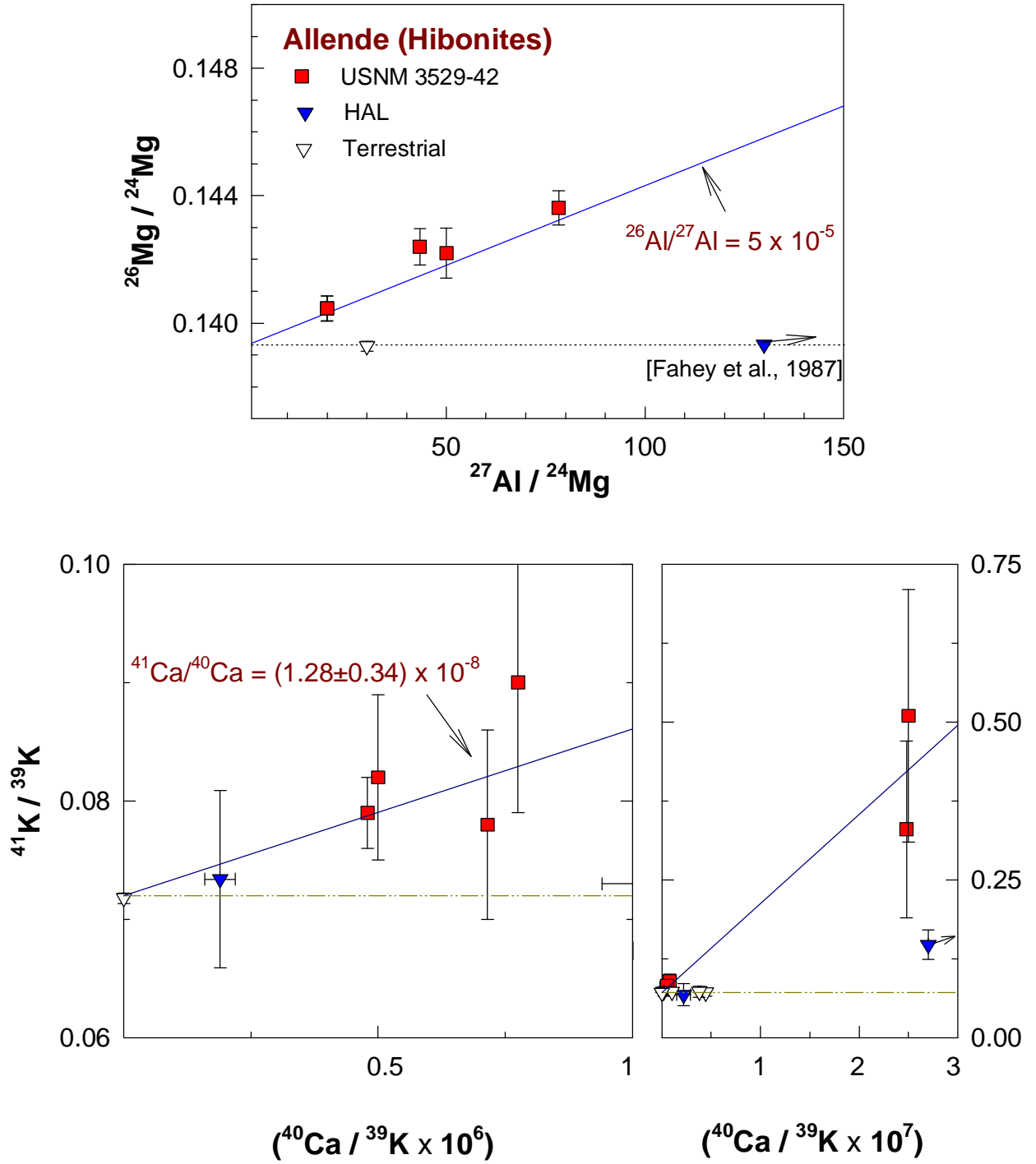
Figure 4.4: Mg and K isotopic composition of hibonites from the Allende inclusions; USNM 3529-42 and HAL, plotted as a function of their Al/Mg and Ca/K ratios, respectively. The error bars are $2\sigma_m$.

Table 4.2 K-Ca isotopic data of Allende CAI HAL

Analysis Number	Mass 41 c/s	$(^{41}\text{K}/^{39}\text{K})_m$[†] $\pm 2\sigma_m$	$^{40}\text{Ca}/^{39}\text{K}$ ($\times 10^5$) $\pm 2\sigma_m$	$(^{41}\text{K}/^{39}\text{K})_c$[‡] $\pm 2\sigma_m$
1	0.643	0.102 ± 0.030	(22.0 ± 7.0)	0.068 ± 0.017
2	1.155	0.076 ± 0.008	(1.9 ± 0.3)	0.073 ± 0.0075
3	0.077	-	-	-
4	0.090	-	-	-
5	0.049	-	-	-

(continue)

Analysis Number	$(^{41}\text{K}/^{42}\text{Ca})_m$ $\pm 2\sigma_m$	$[^{40}Ca^{42}\text{Ca}]/^{42}\text{Ca}$ $\pm 2\sigma_m$	$(^{41}\text{K}/^{42}\text{Ca})_{expected.}$[*] $\pm 2\sigma_m$	$(^{41}\text{K}/^{42}\text{Ca})_{excess.}$[**] $\pm 2\sigma_m$
		($\times 10^{-6}$)		
1	(22.4 ± 2.7)	(7.0 ± 0.6)	(16.4 ± 4.7)	No excess
2	(199.0 ± 28.0)	(7.0 ± 0.6)	(189.0 ± 28.0)	(2.7 ± 0.4)
3	(8.8 ± 1.70)	(7.0 ± 0.6)	Nil	(1.5 ± 1.8)
4	(11.4 ± 5.8)	(7.0 ± 0.6)	(4.2 ± 6.6)	No excess
5	(5.7 ± 1.8)	(7.0 ± 0.6)	(0.5 ± 1.0)	-ive

[†] Experimentally measured value of $^{41}\text{K}/^{39}\text{K}$

[‡] Corrected value of $^{41}\text{K}/^{39}\text{K}$ for $[^{40}\text{Ca}^{42}\text{Ca}]^{++}/[^{42}\text{Ca}]^+$ and hydride

[*] Expected value based on the measured $^{39}\text{K}/^{42}\text{Ca}$ ratio

[**] Excess is obtained by subtracting $(^{41}\text{K}/^{42}\text{Ca})_{expected}$ from the corrected value of $(^{41}\text{K}/^{42}\text{Ca})$ for double plus and hydride

'-' $^{41}\text{K}/^{42}\text{Ca}$ and $^{39}\text{K}/^{42}\text{Ca}$ were measured instead of $^{41}\text{K}/^{39}\text{K}$ in these analyses because of low count rates at masses 39 and 41

EGG3

The potassium concentration in the pyroxene grain from EGG3 analyzed in this work was also found to be spatially inhomogeneous. We could analyze eight spots that have reasonably high ^{39}K count rates. All these analyses show excess in $^{41}\text{K}/^{39}\text{K}$ ratio. The results are shown in Table 4.3 and plotted in Fig. 4.5. An initial $^{41}\text{Ca}/^{40}\text{Ca}$ value of $(1.17 \pm 0.22) \times 10^{-8}$ can be inferred on the basis of this excess. Our data, therefore, confirm the hint for an excess in ^{41}K in this sample reported earlier by Hutcheon et al. (1984). If we include the data obtained by Hutcheon et al. (1984) in estimating the

initial $^{41}\text{Ca}/^{40}\text{Ca}$, a value of $(8.5 \pm 1.5) \times 10^{-9}$ is obtained. In one of the analysis (# 9 of Table 4.3), the ^{39}K count rate went below our background level after the third block of analysis. The measured $^{41}\text{K}/^{42}\text{Ca}$ ratio in this case when corrected for $[^{40}\text{Ca}^{42}\text{Ca}]^{++}$ contribution, yield an initial $^{41}\text{Ca}/^{40}\text{Ca}$ value of $(1.32 \pm 0.35) \times 10^{-8}$. We assign a lower limit value of 6.5×10^8 for $^{40}\text{Ca}/^{39}\text{K}$ for this analysis based on the ^{40}Ca count rate and assuming ^{39}K to be present at background level (i.e., ~ 0.01 c/s).

Table 4.3 K-Ca isotopic data of Allende inclusion EGG3

Sample	$^{40}\text{Ca}/^{39}\text{K}$ $\pm 2\sigma_m$	$^{41}\text{K}/^{39}\text{K}$ $\pm 2\sigma_m$
Pyroxene 1	$(2.67 \pm 0.20) \times 10^5$	0.079 ± 0.005
Pyroxene 2	$(5.20 \pm 1.31) \times 10^5$	0.086 ± 0.008
Pyroxene 3	$(1.42 \pm 0.26) \times 10^6$	0.088 ± 0.013
Pyroxene 4	$(2.09 \pm 0.34) \times 10^6$	0.102 ± 0.009
Pyroxene 5	$(3.34 \pm 0.23) \times 10^6$	0.086 ± 0.019
Pyroxene 6	$(7.49 \pm 4.19) \times 10^6$	0.19 ± 0.03
Pyroxene 7	$(7.75 \pm 2.54) \times 10^7$	0.55 ± 0.40
Pyroxene 8	$(7.13 \pm 3.06) \times 10^7$	0.84 ± 0.22
Pyroxene 9	6.50×10^8	7.9 ± 3.3

4.2 Potassium and Magnesium Isotopic Composition in Hibonites

4.2.1 Efremovka hibonites (E50)

Both potassium and magnesium isotopic compositions were measured in hibonites from the Efremovka CAI E50. Excess ^{26}Mg was found in all analyses. This can be noted in Fig. 4.6 where the new data are plotted along with earlier data reported by Goswami and Srinivasan (1994) that suggested a well behaved Mg-Al isotope systematics for E50 with initial $^{26}\text{Al}/^{27}\text{Al}$ of $(4.87 \pm 0.87) \times 10^{-5}$. The Mg isotopic data obtained in this
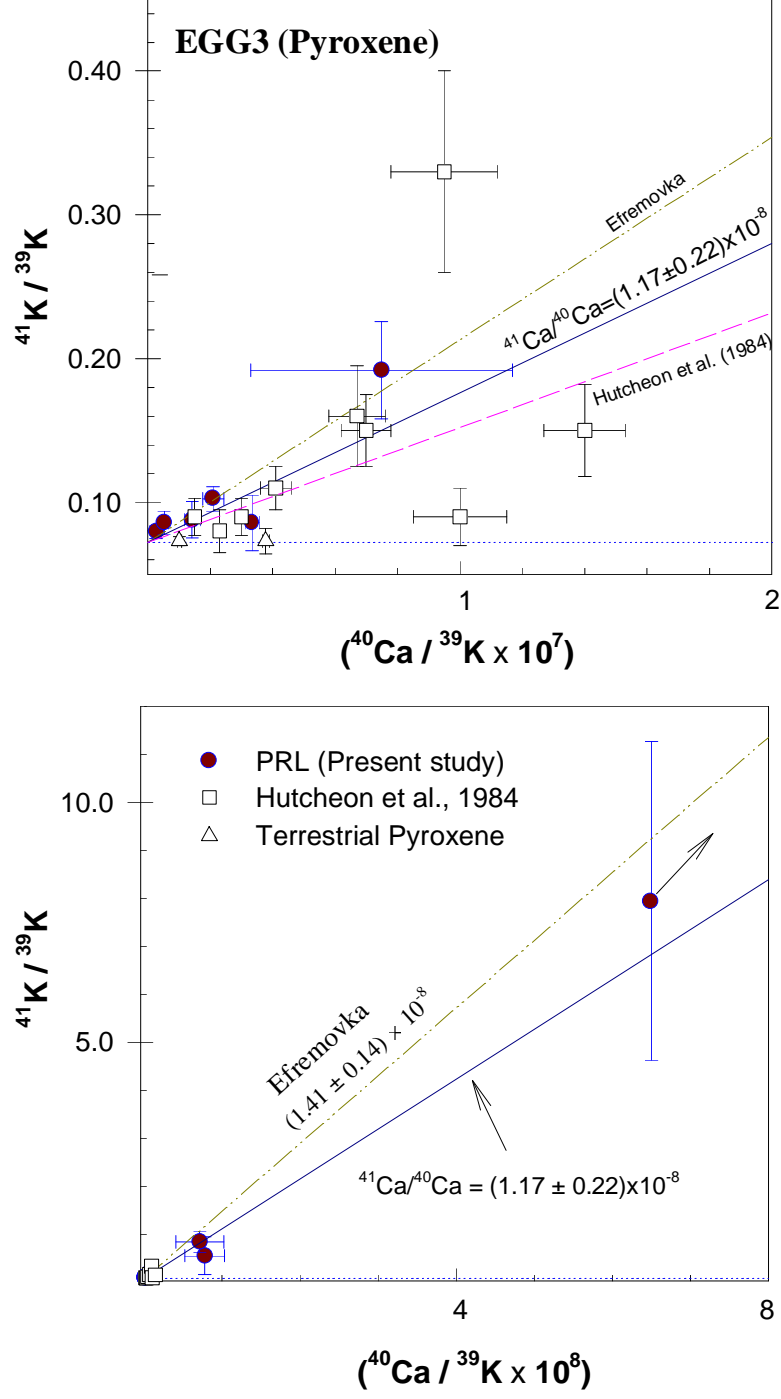
Figure 4.5: K isotopic composition of pyroxene from EGG3 inclusion plotted as a function of their Ca/K ratio. The error bars are $2\sigma_m$.

work are consistent with the earlier data and the initial ^{26}Al/^{27}Al value obtained from the combined data set is indistinguishable from the earlier result. We also note here that the Efremovka CAIs E40 and E65 also have well behaved Mg-Al isotope systematics with initial ^{26}Al/^{27}Al values of $(3.4 \pm 1.0) \times 10^{-5}$ and $(3.99 \pm 0.27) \times 10^{-5}$, respectively, while the CAI E44 shows evidence for Mg-isotopic exchange between anorthite and melilite while the pyroxenes appear to be unaffected (Goswami et al., 1994).

4.2.2   Murchison (CM) Hibonites

The results obtained from the K-Ca and Mg-Al isotopic analyses of individual hibonite grains as well as hibonite-bearing inclusions from the Murchison meteorite are presented in Table 4.4. The initial ^{41}Ca/^{40}Ca inferred from the individual analysis is also presented in the table. The data reduction in the case of Murchison hibonites were carried out in a manner similar to that of Efremovka, except that the epoxy bead mounting method has reduced the contribution from the tail of ^{40}CaH peak to ^{41}K peak to negligible level (< 1 %) of the signal at mass ^{41}K. The salient features of the results obtained from the Murchison hibonites are:

(1) Excess in ^{41}K that can be attributed to the *in situ* decay of ^{41}Ca was found to be present in some of the hibonites.

(2) The K-Ca and Mg-Al isotopic systematics for individual hibonite grains as well as hibonite-bearing inclusions indicate correlated presence/absence of the two short-lived nuclides, ^{41}Ca and ^{26}Al, at the time of formation of these phases.

An initial ^{41}Ca/^{40}Ca ratio of $(1.07 \pm 0.40) \times 10^{-8}$ was inferred from K isotopic analysis of hibonite CH-B6 that also show an initial ^{26}Al/^{27}Al ratio of $\sim 5 \times 10^{-5}$. Hibonites from blue spherules CH-A2, -A3 and -A5 indicate presence of excess ^{41}K. An initial value for ^{41}Ca/^{40}Ca of $(1.10 \pm 0.34) \times 10^{-8}$ was inferred from the combined data
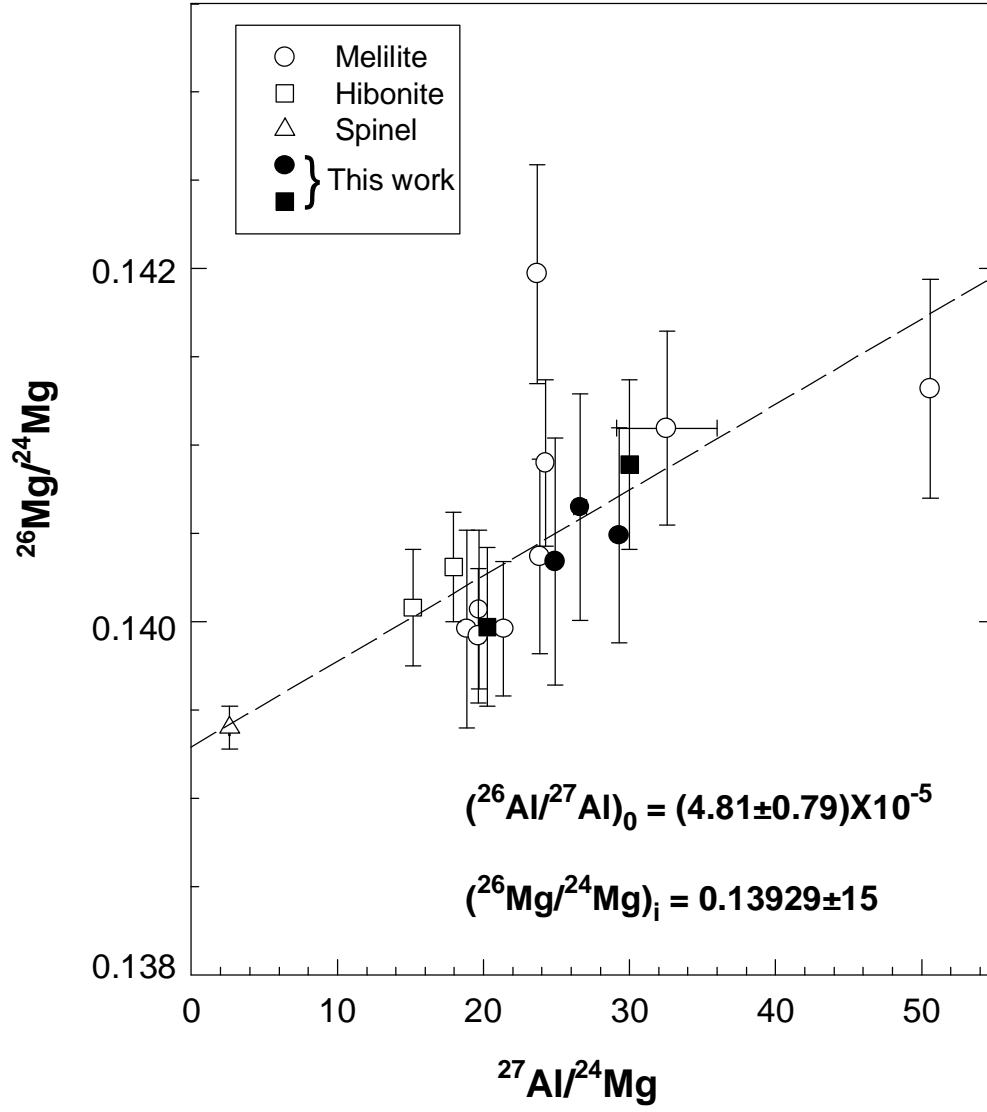
Figure 4.6: Mg isotopic composition of refractory phases from Efremovka E50 inclusion plotted as a function of their Al/Mg ratio. The error bars are $2\sigma_m$.

Table 4.4 Murchison Hibonites: K-Ca and Mg-Al isotopic Data

Sample	$^{40}Ca/^{39}K$ $\pm 2\sigma_m$	$^{41}K/^{39}K$ $\pm 2\sigma_m$	$(^{41}Ca/^{40}Ca)_{ini.}$[†] $\pm 2\sigma_m$	$^{27}Al/^{24}Mg$ $\pm 2\sigma_m$	$\delta^{26}Mg$ (‰) $\pm 2\sigma_m$	$(^{26}Al/^{27}Al)_{ini.}$[‡] $\pm 2\sigma_m$
CH-A2	$(3.21 \pm 0.29) \times 10^5$	0.075 ± 0.004	9.4×10^{-9}	18	4.61 ± 1.59	3.6×10^{-5}
CH-A3	$(7.25 \pm 4.00) \times 10^4$	0.076 ± 0.003	5.5×10^{-8}	29	16.19 ± 3.18	7.7×10^{-5}
CH-A4	$(1.32 \pm 0.41) \times 10^6$	0.070 ± 0.010	$<6 \times 10^{-9}$	130	-2.82 ± 4.11	$<1 \times 10^{-6}$
CH-A5	$(5.24 \pm 0.54) \times 10^5$	0.081 ± 0.010	1.7×10^{-8}	1782	174.7 ± 12.23	1.4×10^{-5}
CH-B2	$(8.75 \pm 3.66) \times 10^6$	0.075 ± 0.025	$<3 \times 10^{-9}$	108	2.43 ± 3.14	$<7 \times 10^{-6}$
CH-B5	$(2.96 \pm 0.86) \times 10^6$	0.072 ± 0.007	$<2 \times 10^{-9}$	130	-2.90 ± 3.60	$<8 \times 10^{-7}$
CH-B6	$(6.78 \pm 0.78) \times 10^5$	0.082 ± 0.010	–	–	–	–
	$(1.04 \pm 0.13) \times 10^6$	0.090 ± 0.014	Isochron	–	–	Isochron
	$(2.41 \pm 0.10) \times 10^6$	0.094 ± 0.012	$(1.07 \pm 0.40) \times 10^{-8}$	121	–	$(5.1 \pm 0.4) \times 10^{-5}$
	$(2.13 \pm 0.27) \times 10^6$	0.096 ± 0.020	–	–	–	–
CH-B7	$(2.42 \pm 0.26) \times 10^6$	0.070 ± 0.012	$<4 \times 10^{-9}$	110	-0.08 ± 5.66	$<7 \times 10^{-6}$
BB-4	$(4.91 \pm 0.28) \times 10^5$	0.077 ± 0.004	1.02×10^{-8}	12	3.40 ± 2.56	4.2×10^{-5}
	$(3.28 \pm 0.38) \times 10^5$	0.078 ± 0.009	1.8×10^{-8}			
SH-7	$(4.24 \pm 2.08) \times 10^6$	0.073 ± 0.013	$<3 \times 10^{-9}$	77	1.32 ± 3.49	$<8 \times 10^{-6}$

Initial $^{41}Ca/^{40}Ca$[†] and $^{26}Al/^{27}Al$[‡] estimated at the time of formation of hibonites

for these hibonites. We note here that the low precesion of this data set makes it difficult to obtain initial ^{41}Ca/^{40}Ca ratios in each individual case. The low precesion in the data was due to the low count rates of ^{41}K in the analyzed phases resulting from the use of low primary beam current in order to avoid contributions of K from neighbouring phases. Hibonites from the inclusion BB-4, however, show well resolved excess in ^{41}K above its normal value of 0.072. Excess in ^{26}Mg over its normal value of 0.13932 was also found to be present in all these hibonites. Attributing this excess to *in situ* decay of ^{26}Al in these hibonites, we obtain an initial value for ^{26}Al/^{27}Al of $(5.02 \pm 0.44) \times 10^{-5}$.

Isotopic analysis of hibonite from the blue spherules, CH-A4, and hibonite fragments, CH-B2, -B5, -B7, as well as SH-7 do not show any excess in ^{41}K. An upper limit of 6×10^{-9} for initial ^{41}Ca/^{40}Ca can be inferred from the measured ^{41}K/^{39}K ratios in these samples. All these hibonites also show absence (or near absence) of ^{26}Mg excess with an upper limit of 7×10^{-6} for initial ^{26}Al/^{27}Al. The results obtained from K and Mg isotopic analyses of the Murchison hibonites are presented in Fig. 4.7 and Fig. 4.8, respectively.

4.2.3   Allende (CV3) hibonite (USNM 3529-42)

Isotopic analyses of K and Mg in hibonites from USNM 3529-42 inclusion confirmed the presence of ^{41}Ca and ^{26}Al at the time of formation this CAI. An initial ^{41}Ca/^{40}Ca ratio of $(1.28 \pm 0.34) \times 10^{-8}$ and an initial ^{26}Al/^{27}Al ratio of $(5.7 \pm 1.0) \times 10^{-5}$ were inferred from the data, presented in Table 4.5 and plotted in Fig. 4.4. Except in one case, there is an excess in ^{41}K/^{39}K ratio over its normal value of 0.072 for all the analyzed grains. Eventhough the hibonite grains in this inclusion are relatively bigger than those in Efremovka CAI E50, the movement of potassium into some of these grains from neighbouring phases made it difficult to locate spots with high ^{40}Ca/^{39}K signal; we could find only two grains that have ^{40}Ca/^{39}K $> 10^7$. The magnesium isotopic data
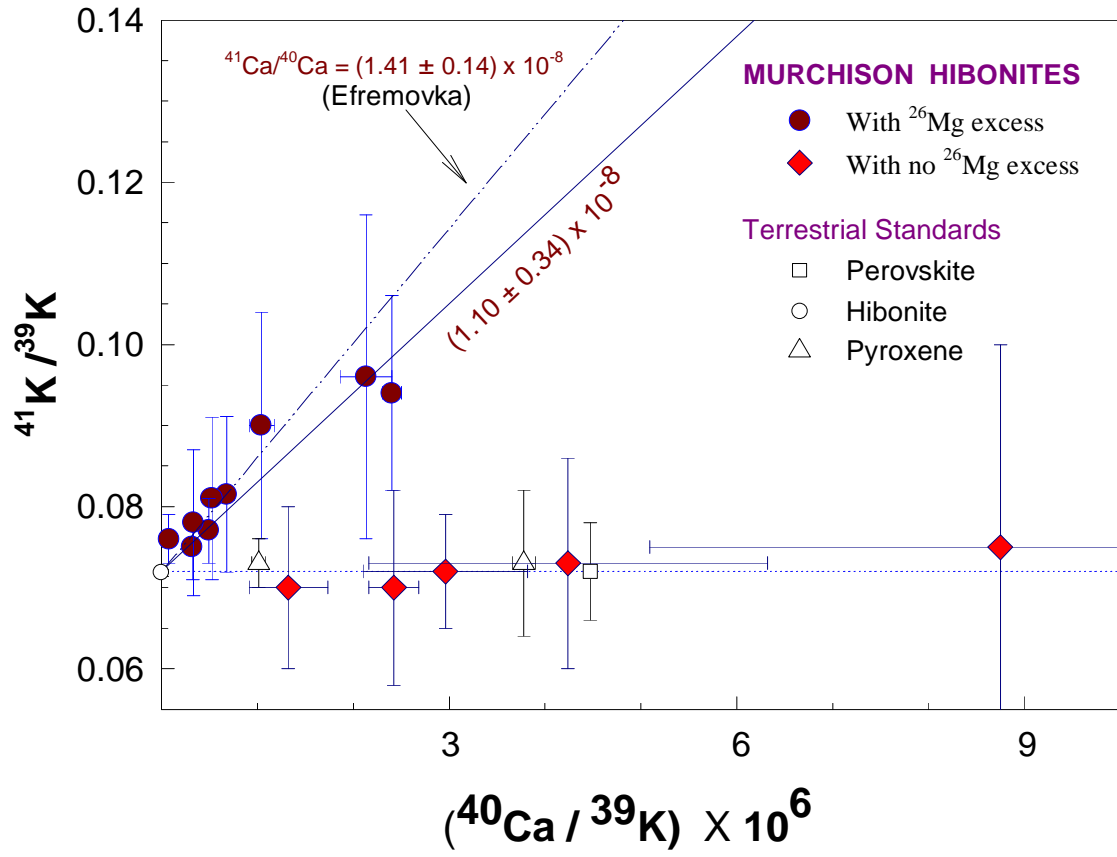
Figure 4.7: K isotopic composition in Murchison hibonites plotted as a function of their Ca/K ratio. The error bars are $2\sigma_m$.
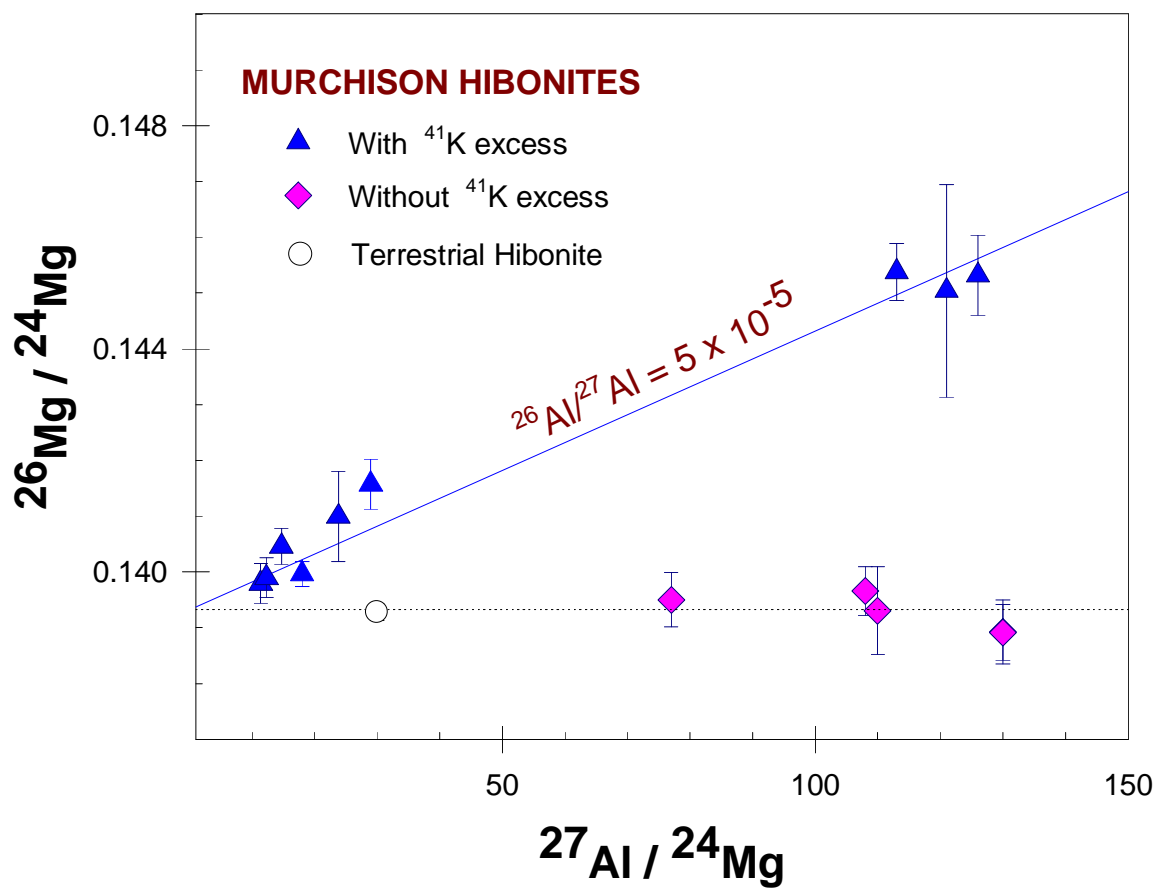
Figure 4.8: Mg isotopic composition in Murchison hibonites plotted as a function of their Al/Mg ratio. The error bars are $2\sigma_m$.

obtained on the same grains following potassium isotopic analysis also show a clear excess in ^{26}Mg.

Table 4.5 K-Ca and Mg-Al isotopic data of
Allende inclusion USNM 3529-42

Sample	^{40}Ca/^{39}K $\pm\, 2\sigma_m$	^{41}K/^{39}K $\pm\, 2\sigma_m$	^{27}Al/^{24}Mg $\pm\, 2\sigma_m$	δ^{26}Mg(‰) $\pm\, 2\sigma_m$
Hibonite #1	2.48×10^7	0.33 ± 0.14	43.3	21.96 ± 4.12
Hibonite #2	2.50×10^7	0.51 ± 0.20	50.0	20.87 ± 5.63
Hibonite #3	$(7.15 \pm 1.07) \times 10^5$	0.078 ± 0.008	20.7	7.23 ± 2.64
Hibonite #4	$(4.79 \pm 0.78) \times 10^5$	0.079 ± 0.003	78.3	30.9 ± 3.80
Hibonite #5	$(7.75 \pm 0.12) \times 10^5$	0.090 ± 0.011	-	-
Hibonite #6	$(5.00 \pm 0.78) \times 10^5$	0.082 ± 0.007	19.9	8.22 ± 2.82

4.3 Magnesium Isotopic data for Igneous Objects from Chondrites

The results obtained from the measurement of Mg isotopic composition in plagioclase phases found in igneous objects from all the chondritic meteorites selected for this study are given in Table 4.6. In Fig. 4.9, we have plotted the measured values of ^{26}Mg/^{24}Mg for the meteorite samples as a function of their ^{27}Al/^{24}Mg ratio along with the data for terrestrial plagioclase used as a standard. If radiogenic excess in ^{26}Mg is present in any of the analyzed phases, the measured ^{26}Mg/^{24}Mg ratio should be higher than 0.13932, the reference value. The magnesium isotopic composition in most of the analyzed phases are normal within our experimental uncertainties. The low ^{27}Al/^{24}Mg for two out of three analyses of Raguli plagioclase suggest contribution to Mg signal from surrounding chromite.

Two of the Kaidun anorthite grains show definite excess of ^{26}Mg with δ^{26}Mg = 4.2 $\pm$ 1.6 ‰ and 4.0 $\pm$ 2.4 ‰ and suggest an initial ^{26}Al/^{27}Al $\sim$ 1.6 $\times$ 10^{-6} at the time of their formation. However, the other anorthite grains analyzed from the same
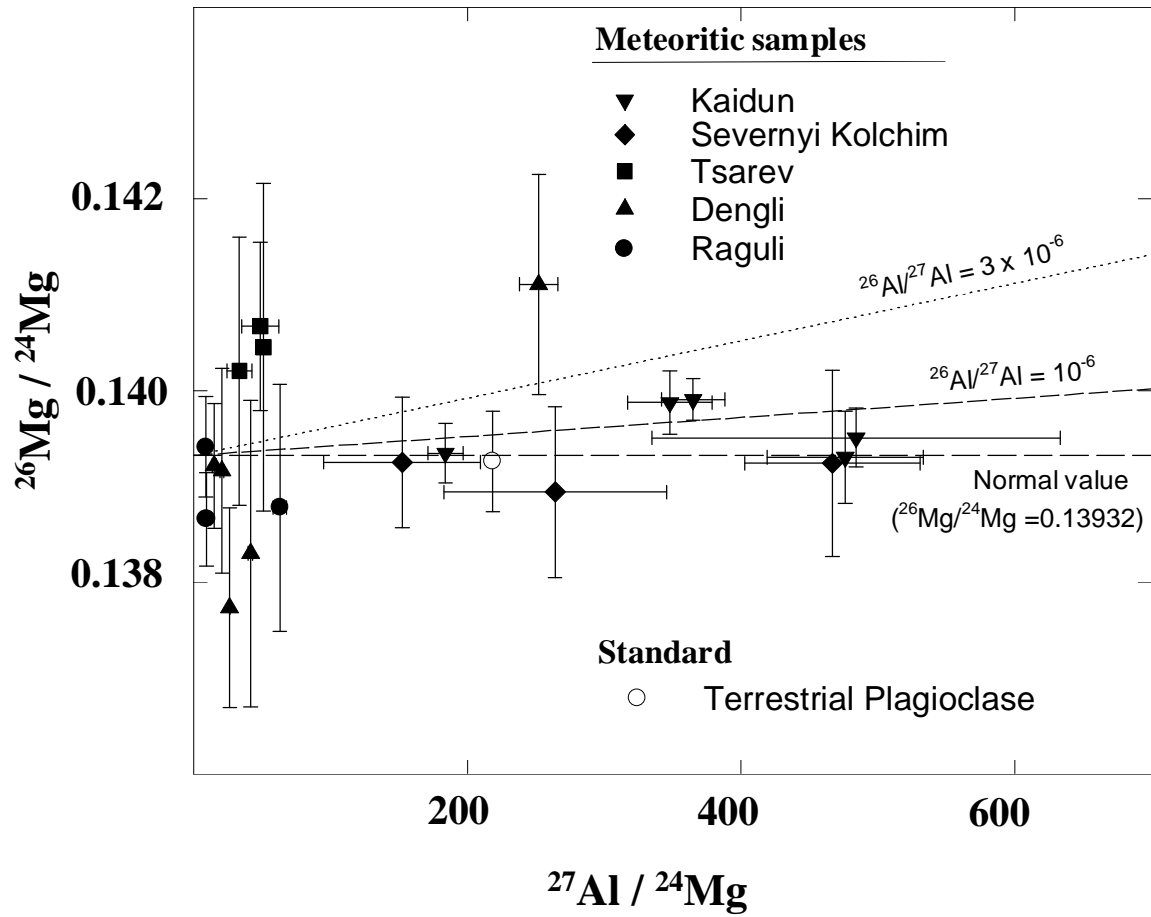
Figure 4.9: Mg isotopic composition of plagioclase phases from igneous inclusions in different chondritic meteorite, plotted as a function of their Al/Mg ratios.

meteorite have normal magnesium isotopic composition with an upper limit of 10^{-6} for initial ^{26}Al/^{27}Al.

The results obtained from analyses of igneous inclusion from the Severnyi Kolchim (H3) meteorite suggest absence of ^{26}Mg excess within our experimental uncertainities. An upper limit of 2×10^{-6} for initial ^{26}Al/^{27}Al can be inferred from the data.

The experimental uncertainities in case of data from the basaltic inclusion from Tsarev (L5) and igneous clasts from Dengli (H3) are rather large. This resulted from the use of low primary beam current (beam diameter ≤ 10 μm) for these analyses. This was necessary to avoid contribution from surrounding Mg-rich phases while analyzing the small plagioclase laths ($\sim$ 10 - 20 μm in width). All the analyses from these two meteorites indicate absence of ^{26}Mg excess except for one data-point for a silica bearing inclusion in Dengli. An initial value of $(7.0 \pm 4.6) \times 10^{-6}$ for ^{26}Al/^{27}Al can be inferred based on this data point.

Table 4.6 Mg-Al data for plagioclase phases
in chondritic meteorites

Sample details	$^{27}Al/^{24}Mg$ $\pm 2\sigma_m$	$\delta^{26}Mg(\%)$ $\pm 2\sigma_m$
Kaidun (Multi-breccia)		
Anorthite # 1	365±23	4.22±1.57
Anorthite # 2	184±13	0.19±2.22
Anorthite # 3	476±57	-0.13±3.47
Anorthite # 4	484±149	1.35±2.21
Anorthite # 5	348±31	3.99±2.39
Severnyi Kolchim (H3)		
(Igneous object)		
Analysis # 1	152.3±57.3	-0.48±4.85
Analysis # 2	264.2±81.5	-2.74±6.40
Analysis # 3	466.7±64.1	-0.59±7.00
Tsarev (L5)		
(Basaltic inclusion)		
Analysis # 1	33.4±8.9	6.34±10.05
Analysis # 2	48.7±13.5	9.70±6.28
Analysis # 3	50.9±5.3	8.14±12.26
Dengli (H3)		
Clast # 2; 1	26.3±0.2	-11.39±7.46
Clast # 2; 2	20.7±1.3	-1.17±7.68
Clast # 2; 3	41.6±1.6	-7.35±11.53
Silica bearing inclusion	252.2±14.1	12.64±8.28
Chondrule	15.1±1.4	-0.76±4.71
Raguli (H3)		
Chromite chondrule # 1	62.96±5.00	-3.90±9.26
Chromite chondrule # 2	8.83±0.29*	0.65±3.78
Chromite-Plagioclase inclusion	9.31±0.06*	-4.77±3.48

Chapter 5

Source(s) of Short-lived Nuclides in the Early Solar System and Time Scales

The implications of the results obtained from the K-Ca and Mg-Al isotopic analyses of individual refractory phases and CAIs from the primitive meteorites, Murchison, Efremovka and Allende are discussed in the present chapter. The two most important results obtained in this study are:

(1) Excess ^{41}K was found in all the CAIs from the Efremovka meteorite analyzed in this work and also in several samples from Allende and Murchison meteorites. The observed excess in ^{41}K also correlates with the measured ^{40}Ca/^{39}K ratio in the analyzed phases and clearly demonstrates the one time presence of ^{41}Ca in the analyzed phases. The initial value for ^{41}Ca/^{40}Ca at the time of their formation was estimated to be $(1.38 \pm 0.13) \times 10^{-8}$ (Fig. 5.1).

(2) Observation of correlated presence/absence of the two short-lived nuclides, ^{26}Al and ^{41}Ca, in CAIs as well as individual refractory phase (hibonite) from Efremovka, Allende and Murchison meteorites. They are either present with their
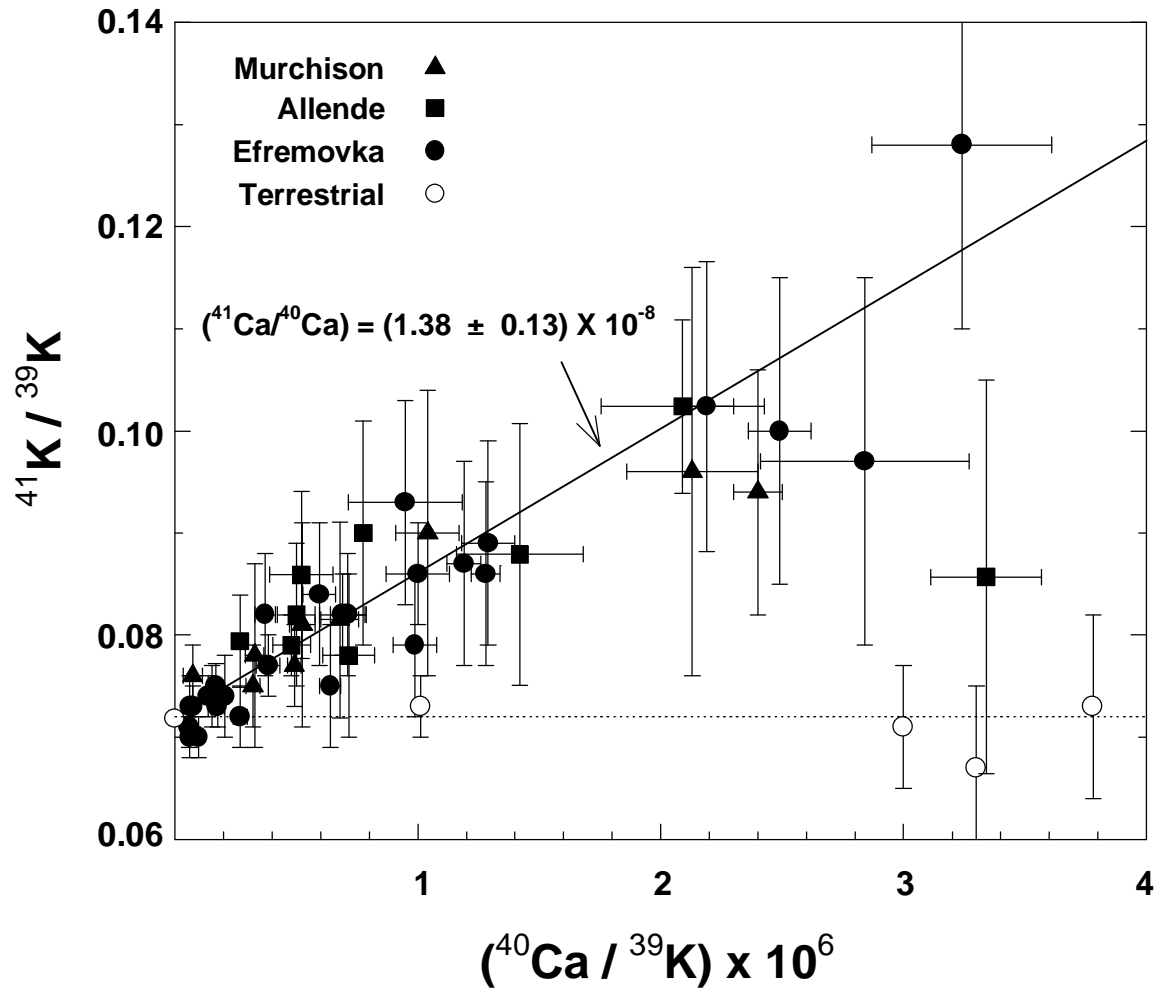
Figure 5.1: K-Ca isotopic systematics in refractory phases from the meteorites, Efremovka, Allende and Murchison.

characteristic initial values of $\sim 1.4 \times 10^{-8}$ for ^{41}Ca/^{40}Ca, and $\sim 5 \times 10^{-5}$ for ^{26}Al/^{27}Al or are absent/occur in very low abundances (Fig. 5.2). This result, obtained for the first time in this study, suggests that ^{41}Ca and ^{26}Al are coupled either in their original production site(s) or were thoroughly mixed in some parcels of proto-solar cloud before they were incorporated into the refractory phases.

In the following, we will discuss these observations to infer the most plausible source(s) of these two short-lived nuclides present in the early solar system from among the various sources proposed so far and discussed briefly in chapter 1. We show that the correlated presence/absence of the two short-lived nuclides in individual refractory phases helps us to better constrain the source(s) of the short-lived nuclides. Before discussing this aspect, we briefly consider the implications of the absence of signatures of these radionuclides in certain refractory phases analyzed in this work.

5.1 Distribution of ^{41}Ca and ^{26}Al in the Early Solar System

While the presence of excess ^{41}K and ^{26}Mg in refractory phases is attributed to the presence of the radionuclides, ^{41}Ca and ^{26}Al, respectively, at the time of formation of these phases, the absence of such an excess in some of the refractory phases analyzed in this work can be due to several causes. These include: (i) a heterogeneity of these radionuclides in the solar nebula (due to variable mixing of the source material with the nebular material), (ii) late formation of these phases, and (iii) reprocessing of material and/or redistribution of Mg and K isotopes as a result of multiple secondary events affecting the refractory phases in the early solar system.

Based on detailed petrographic and magnesium isotopic studies of refractory inclusions from Allende (Podosek et al., 1991), Vigarano (MacPherson and Davis, 1993)
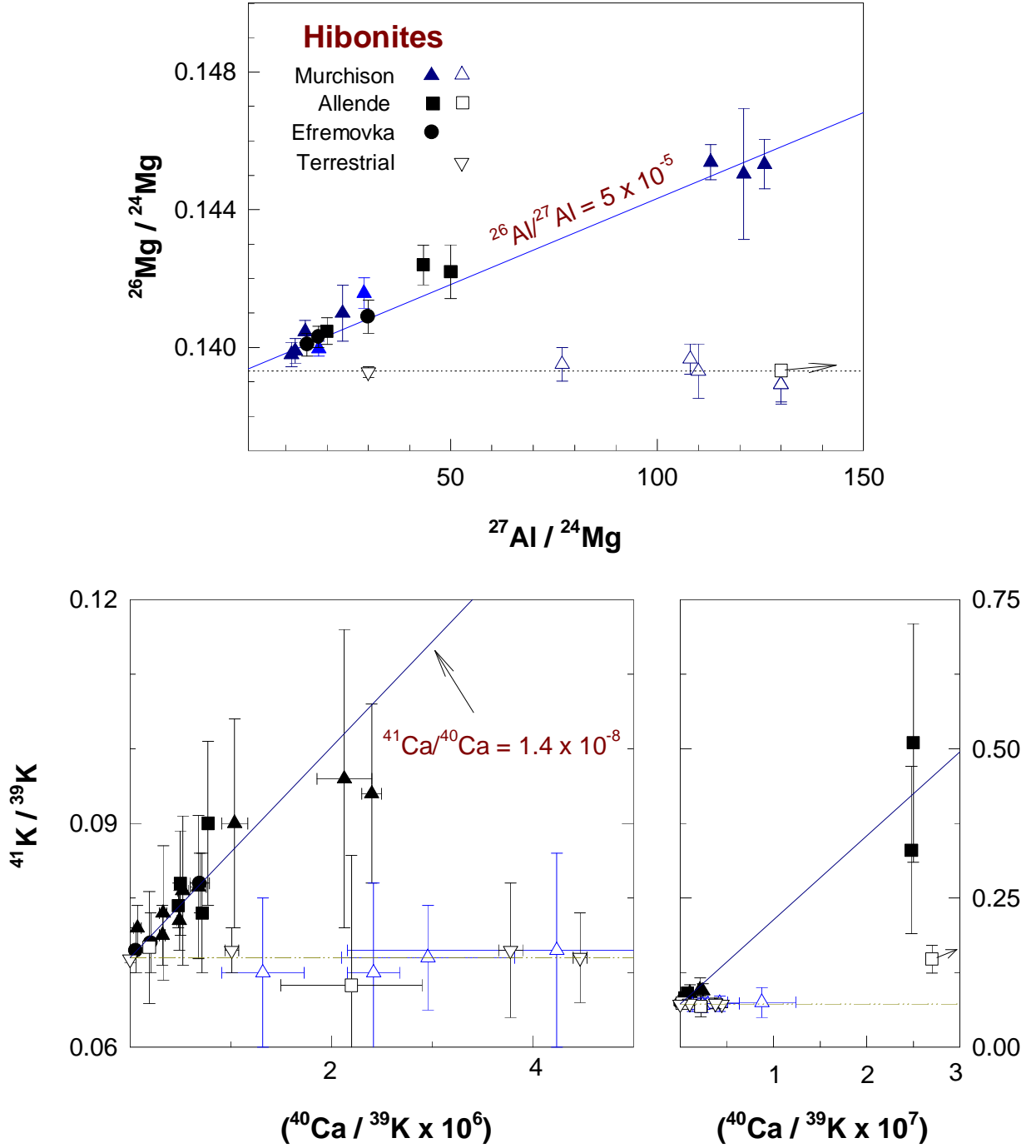
Figure 5.2: K-Ca and Mg-Al isotopic systematics in hibonites from the meteorites, Efremovka, Allende and Murchison. Hibonites devoid of ^{26}Mg excess (open symbols; top panel) also do not have ^{41}K excess (lower panel).

and Leoville (Caillet et al., 1993) meteorites, a correlation was observed between the presence of disturbed Mg-Al isotopic systematics and secondary alteration effects. The observed secondary alterations must have taken place within the first few million years after the formation of CAIs, that resulted in Mg-isotopic redistribution between the adjoining mineral phases leading to either complete erasure of the signatures of ^{26}Mg excess or reducing the initial ^{26}Al/^{27}Al value to less than the canonical value of 5×10^{-5}. The relatively low value of $(8.5 \pm 1.6) \times 10^{-9}$ for ^{41}Ca/^{40}Ca in the case of Allende EGG3 inclusion (based on combined data obtained by us and Hutcheon et al., 1984), as compared to the value of $\sim 1.4 \times 10^{-8}$ seen in Efremovka CAIs may be attributed to possible disturbances in K-Ca isotopic systematics in this CAI. This is consistent with the petrographic studies of EGG3 inclusion which also suggest presence of secondary alteration effect in this CAI (Meeker et al., 1983). The Mg-Al isotopic systematics of the inclusion was however not affected significantly as indicated by the inferred initial value of 5×10^{-5} for ^{26}Al/^{27}Al (Armstrong et al., 1984).

In the case of HAL hibonite, eventhough, its petrographic studies reveal secondary alteration presumably taking place in a nebular environment (Allen et al., 1980), the absence of ^{41}Ca and low abundance of $(5.4 \pm 1.3) \times 10^{-8}$ for ^{26}Al/^{27}Al (Fahey et al., 1987) would be difficult to explain on its basis as it would require a rather large time interval of ~ 7 Ma for the closure of the Mg-Al isotopic system. The preservation of nuclear isotopic anomalies in calcium and titanium found in this CAI (Lee et al., 1979, 1980) over such a time scale seems to be very difficult. Thus, heterogeneous distribution of ^{26}Al and ^{41}Ca in the solar nebula appears to be a more plausible reason for the absence of these radionuclides in HAL hibonite as well as some of the Murchison hibonites analyzed in this work. Isotopic heterogeneity in the solar nebula has also been proposed earlier to explain the absence of ^{26}Mg excess in FUN inclusions and in CM hibonites (MacPherson et al., 1995). The magnesium and oxygen isotopic analyses of corundum grains from Murchison meteorite by Virag et al. (1991) also suggest the presence of more

than one ^{26}Al component in the solar nebula. Although the absence of ^{26}Al and ^{41}Ca in some of the analyzed phases in the present study could represent an inhomogeneity in the distribution of these two nuclides in the solar nebula, the fact remains that they are both present in their canonical abundances in all the petrographically unaltered Efremovka and Allende CAIs. Further, as the petrographic context of the Murchison hibonites are unknown, we shall assume that the initial ^{26}Al/^{27}Al and ^{41}Ca/^{40}Ca were uniform in the solar nebula, atleast in the region of CAI formation, with an initial value of 5×10^{-5} and 1.4×10^{-8}, respectively, in the remainder of our discussion.

5.2   Source(s) of the Short-lived Nuclides, ^{26}Al and ^{41}Ca in the Early Solar System

The two proposals made to explain the presence of the short-lived nuclides, ^{41}Ca and ^{26}Al in the early solar system phases are:

(i) presence (or production) of these short-lived nuclides in the early solar system that were incorporated 'live' into the CAIs during their formation, followed by *in situ* decay within these objects,

(ii) contribution from variable amounts of "fossil" ^{41}K and ^{26}Mg of radiogenic origin locked in refractory stardust that are part of the initial components of the solar nebula from which the CAIs were formed.

Apart from these, an alternate mechanism for producing ^{41}Ca could be cosmogenic production by secondary neutrons during recent cosmic ray exposure of the meteorites [via (n,γ) reaction with ^{40}Ca present in the CAIs or refractory phases] and its subsequent decay. In order to explain the presence of ^{41}Ca with the observed initial ^{41}Ca/^{40}Ca ratio of $\sim 1.4 \times 10^{-8}$ in the various analyzed refractory phases, a neutron

fluence of $\sim 3 \times 10^{16}$ cm^{-2} is necessary. The expected secondary neutron fluence in a meteorite depends mainly on three parameters: the cosmic ray exposure duration, the preatmospheric size and the chemical composition of the meteorite. The preatmospheric size is an important parameter as the production of secondary neutrons within a meteorite increases with shielding depth and reaches a maximum at a shielding depth of $\sim$ 100-150 gm cm^{-2}. The Efremovka meteorite has a cosmic ray exposure age of ~ 11Ma (Murty et al., 1995, 1996; Mazor et al., 1970), whereas, Allende and Murchison meteorites have relatively low cosmic ray exposure ages of ~ 5.2 Ma and ~ 2 Ma, respectively (Fireman and Göbel, 1970; Hohenberg et al., 1990). As the estimated neutron fluence in Allende is rather low, $< 10^{15}$cm^{-2} (Göbel et al., 1982), the presence of ^{41}Ca in the Allende refractory phases due to production by secondary neutrons during cosmic ray exposure of the meteorite is not possible. In the case of Efremovka, its preatmospheric size is expected to be much smaller than Allende for which the recovered mass exceed 2 tons compared to 21 kg for Efremovka. Thus, the neutron fluence experienced by Efremovka is not expected to be much higher than that of Allende. In fact, recent noble gas data for Kr and Xe and for cosmogenic ^{36}Cl in bulk samples of Efremovka (Murty et al., 1995, 1996) suggest that the neutron fluence experienced by Efremovka is almost a factor of ten lower than the value for Allende. A large preatmospheric size for the Efremovka meteorite is also ruled out by preliminary data for cosmic ray produced nuclear tracks in Efremovka as well as the measured activities of ^{36}Cl, ^{26}Al and ^{10}Be in this meteorite and the cosmogenic ^{22}Ne/^{21}Ne ratio of 1.11 obtained from noble gas data (Murty et al., 1996). Thus, the possibility of cosmogenic production of ^{41}Ca in Efremovka can be ruled out.

An additional argument against the cosmogenic production of ^{41}Ca by secondary neutrons is the absence of ^{41}K excess in HAL hibonite from Allende meteorite and some individual hibonite grains from Murchison meteorite. It would be difficult to explain the presence as well as absence of ^{41}K excess in different phases of the same meteorite if

the production took place during the recent cosmic ray exposures of these meteorites in interplanetary space. Therefore, the possibility that the observed ^{41}K excess in refractory phases and CAIs of these meteorites is due to production by secondary neutrons during their cosmic ray exposures in the interplanetary space can be ruled out.

5.2.1 "Fossil" origin of the short-lived nuclides in the early solar system

The possibility that the short-lived nuclides found in early solar system solids (CAIs) could be of "fossil" origin was proposed by Clayton (1977, 1982, 1986). In this model the decay of the short-lived nuclides took place within interstellar grains that had preferentially incorporated such nuclides in their stellar formation sites. The case for the possible presence of excess ^{41}K of "fossil" origin in refractory inclusions of primitive meteorites, which would enhance the ^{41}K/^{39}K ratio in these objects above the normal solar system value, was specifically noted by Clayton (1977). The proposed scenario involves the formation of refractory condensates (stardust) in stellar environment (e.g., supernova envelope) that are enriched in their refractory element concentrations (e.g., Ca) compared to the volatile (e.g., K) and as such they will have high Ca/K ratio and also excess ^{41}K from ^{41}Ca decay. Since these stellar condensates are expected to be an important component of the solar nebula they will find their way into the CAIs that can inherit excess ^{41}K from the stellar condensates. While this scenario has its own appeal and excess ^{41}K has been detected in interstellar dust (Amari et al., 1995), it does not readily explain the observed correlation between excess ^{41}K and ^{40}Ca/^{39}K in the refractory phases unless one makes the *ad hoc* assumption of mixing between components of arbitrary compositions. However, petrographic studies of the analyzed Efremovka CAIs clearly show that they were formed via crystallization of refractory melts and one would expect complete K isotopic equilibration during their formation which rules out preservation of signals resulting from varying degrees of mixing of distinct components

within individual CAIs. Thus, although the presence of a very small amount of "fossil" ^{41}K and ^{26}Mg in the CAIs cannot be ruled out unequivocally, we do not consider this to be the primary source for the observed excess of ^{41}K and ^{26}Mg in the analyzed CAIs and refractory phases.

The ^{41}K excess in the analyzed refractory phases and CAIs, and its correlation with ^{40}Ca/^{39}K can therefore be best explained by considering the presence of live ^{41}Ca in the early solar system at the time of CAI formation. The presence of live ^{41}Ca and ^{26}Al in the early solar system may be due to any one or more of the following processes:

(i) introduction of freshly synthesized ^{41}Ca and ^{26}Al from specific stellar site(s) to the solar nebula,

(ii) production of ^{41}Ca and ^{26}Al in early solar system matter by nuclear reactions initiated by energetic particles from an active (T Tauri) early Sun,

(iii) irradiation of the proto-solar cloud by energetic particles within a molecular cloud complex.

If the first alternative is true then the presence of the short-lived nuclides, ^{41}Ca and ^{26}Al in CAIs puts an extremely stringent constraint on the value of Δ, the time interval between the last nucleosynthetic input to the solar nebula and the formation of some of the first solar system solids (CAIs). We shall first discuss the other two possibilities before discussing this aspect in detail.

5.2.2 Production of ^{41}Ca and ^{26}Al by energetic particle irradiation

Irradiation by an active early Sun

As discussed in the introductory chapter, the possibility of production of nuclides (radiogenic as well as non-radiogenic) due to energetic particles irradiation in the solar nebula has been suggested by several groups. In this scenario, the short-lived nuclides are produced due to interaction of energetic particles from an active early Sun with solar system matter. One can consider *in situ* production of nuclides in CAIs as well as their production in nebular gas and dust prior to the formation of the CAIs. Several proposals were made to explain the enhanced abundances of both radiogenic and non-radiogenic nuclides in meteoritic matter by considering an enhanced flux of energetic particles from the early Sun (Heymann and Dziczkaniec, 1976; Heymann et al., 1978; Clayton et al., 1977; Lee, 1978; Kaiser and Wasserburg, 1983; Clayton and Jin, 1995; Shu et al., 1996). Evidence for an active early Sun, with a time averaged proton flux of $\sim$ 100 to 1000 times more than the contemporary average (based on lunar sample data), has been obtained recently from measurements of cosmogenic neon isotopes in solar flare irradiated olivine grains from several carbonaceous chondrites (Hohenberg et al., 1990; see also Caffee et al., 1991). However, there are several problems with the solar particle irradiation scenario. These are: (i) use of arbitrary spectral parameters for the solar energetic particles to avoid co-production of nuclides for which no anomalous abundances have been found in meteoritic phases, (ii) requirement of very high energetic particle fluence, and (iii) mismatch with observational data for the short-lived isotopes (e.g., ^{26}Al and ^{53}Mn) by solar energetic particles. Inspite of the attempts made so far, a rigorous calculation of cosmogenic production of all the short-lived nuclides, including ^{41}Ca and the recently discovered ^{36}Cl (Murty et al., 1997) with appropriate cross section data is still lacking. In the present study, we have carried out detailed calculations for the production of

the short-lived nuclides, ^{26}Al, ^{41}Ca, ^{36}Cl and ^{53}Mn in CAI precursor material in the solar nebula by solar energetic particles to further investigate this problem. We have included in our calculations all the possible low-energy (< 100 MeV/amu) solar proton and alpha particle induced reactions in different target elements that can produce these radionuclides. The alpha to proton abundance ratio in solar energetic particles was taken as 0.1. The relevant reactions along with their reaction cross sections are shown in Fig. 5.3. The reaction cross sections for the production of ^{26}Al, ^{41}Ca and ^{53}Mn were taken from Ramaty et al. (1996). In the absence of measured reaction cross sections for ^{36}Cl production, we have estimated the same by considering equivalent reactions, based on compilation of reaction cross sections for Z = 20-40 (Lorenzen and Brune, 1974) and reaction cross section data for production of ^{26}Al, ^{41}Ca and ^{53}Mn (Ramaty et al., 1996). In particular, the reaction cross section for ^{33}S(α,p)^{36}Cl was based on compilation of cross sections from Lorenzen and Brune (1974); for the ^{34}S(α,pn)^{36}Cl reaction, equivalent reactions, ^{39}K(α,pn)^{41}Ca and ^{24}Mg(α,pn)^{26}Al were used and the ^{41}K(p,n)^{41}Ca reaction cross section was used for ^{36}S(p,n)^{36}Cl reaction. The equivalent reactions considered for ^{37}Cl(p,pn)^{36}Cl, are ^{54}Fe(p,pn)^{53}Fe, ^{42}Ca(p,pn)^{41}Ca and ^{27}Al(p,pn)^{26}Al, and for the reaction ^{39}K(p,3pn)^{36}Cl, the intermediate values of cross section from the reactions ^{44}Ca(p,p3n)^{41}Ca and ^{28}Si(p,2pn)^{26}Al were used. For ^{35}Cl(α,^{3}He)^{36}Cl, we used the reaction cross sections of ^{40}Ca(α,^{3}He)^{41}Ca. However, as the threshold for the former reaction is ~ 2.5 MeV/amu as compared to ~ 7 MeV/amu for the later, the reaction cross section for ^{36}Cl production were taken by scaling the energy from E to E/2.3.

The calculations for cosmogenic production of radionuclides were carried out by considering different spectral parameters for the solar energetic particles. These energetic particles that are associated with solar-flare events have a typical range in kinetic energy of 1-100 MeV/amu with their flux decreasing rapidly with increasing energy (Caffee et al., 1988). The solar particle energy spectrum is expressed either as a power law in kinetic energy, E, or as an exponential in rigidity R (momentum per unit charge):
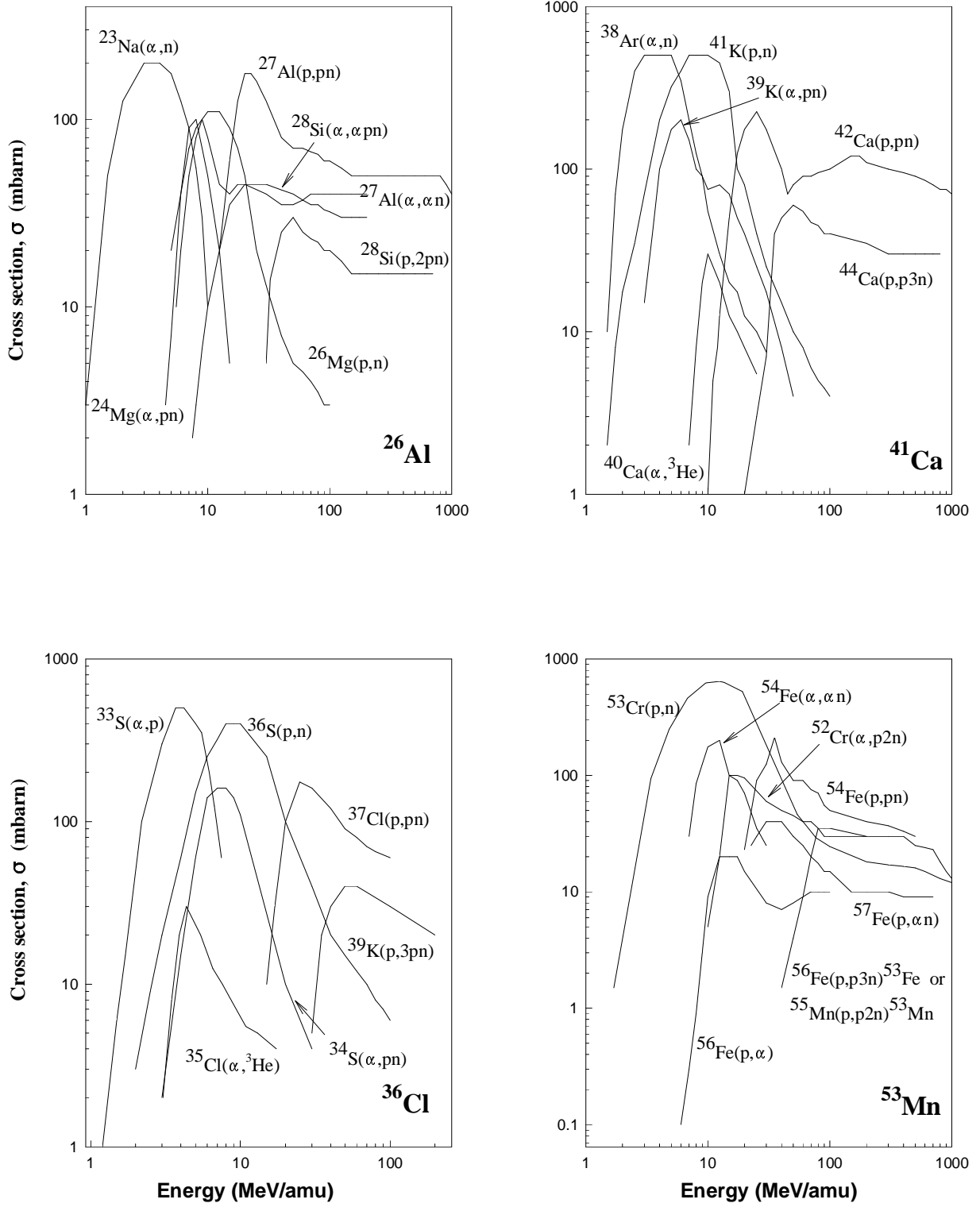
Figure 5.3: Nuclear reaction cross sections for production of short-lived nuclides, ^{26}Al, ^{41}Ca, ^{36}Cl and ^{53}Mn from various target nuclides.

108

$$\frac{dN}{dE} = \text{constant} \times E^{-\gamma} \tag{5.1}$$

or

$$\frac{dN}{dR} = \text{constant} \times e^{-\frac{R}{R_0}} \tag{5.2}$$

where γ is the power law exponent, and R_0, the characteristic rigidity, defining the spectral hardness. Typical values for γ and R_0 in contemparary solar flares range from 2 to 4, and 50 to 200 MV, respectively (Reedy and Arnold, 1972; Lal, 1972; Goswami et al., 1988). We have performed calculations for the above range in γ and R_0.

CAI-precursor grains present in the solar nebula were considered as the target material and we have assumed them to be of chondritic (CI) composition (Anders and Ebihara, 1982). A grain size in the range of ten microns to cm, following a number-size distribution of the type, $dn/dr \propto r^{-\beta}$, was chosen for the production calculations. Only ionization energy loss process has been considered for the low energy solar particles and appropriate range-energy relation was used to obtain the modified differential energy spectra at different depths within a grain. The production rates at various depths within grains of different sizes were calculated following the approach described by Lal (1972).

The production rates of the radionuclides, ^{26}Al, ^{41}Ca, ^{36}Cl and ^{53}Mn at different depths within grains of three different sizes are shown in Figures 5.4 to 5.7. The equilibrium production rates are expressed in terms of production per kilogram of material per minute (dpm/kg). Except for grains of radii less than 0.1 gm/cm^2, the production rates fall steeply with depth. Production rates for grain with radius 0.034 gm/cm^2 (radius $\sim 100\mu$m, density = 3.4 gm/cm^3) are almost uniform throughout the grain and are higher than those for larger grains. This is because of "effective" 4π irradiation in case of smaller grains as compared to "effective" 2π irradiation for the larger grains. The maximum contribution to the average production rate basically comes from the smaller

109
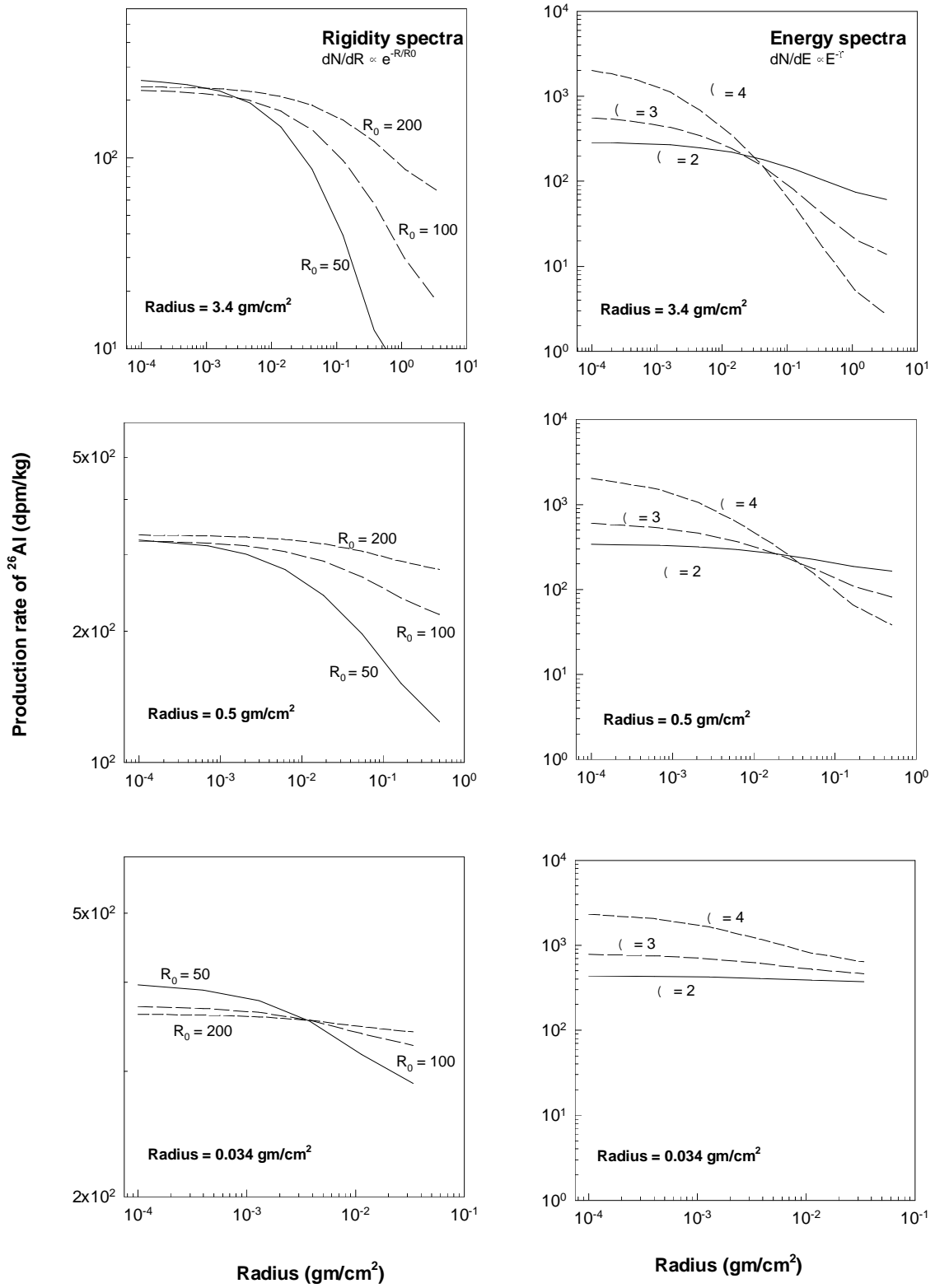
Figure 5.4: Production rate (dpm/kg) of the radionuclide, ^{26}Al as function of depth for grains of three different sizes. Energy and rigidity spectra with different γ and R_0 values, respectively, were used for the calculations.
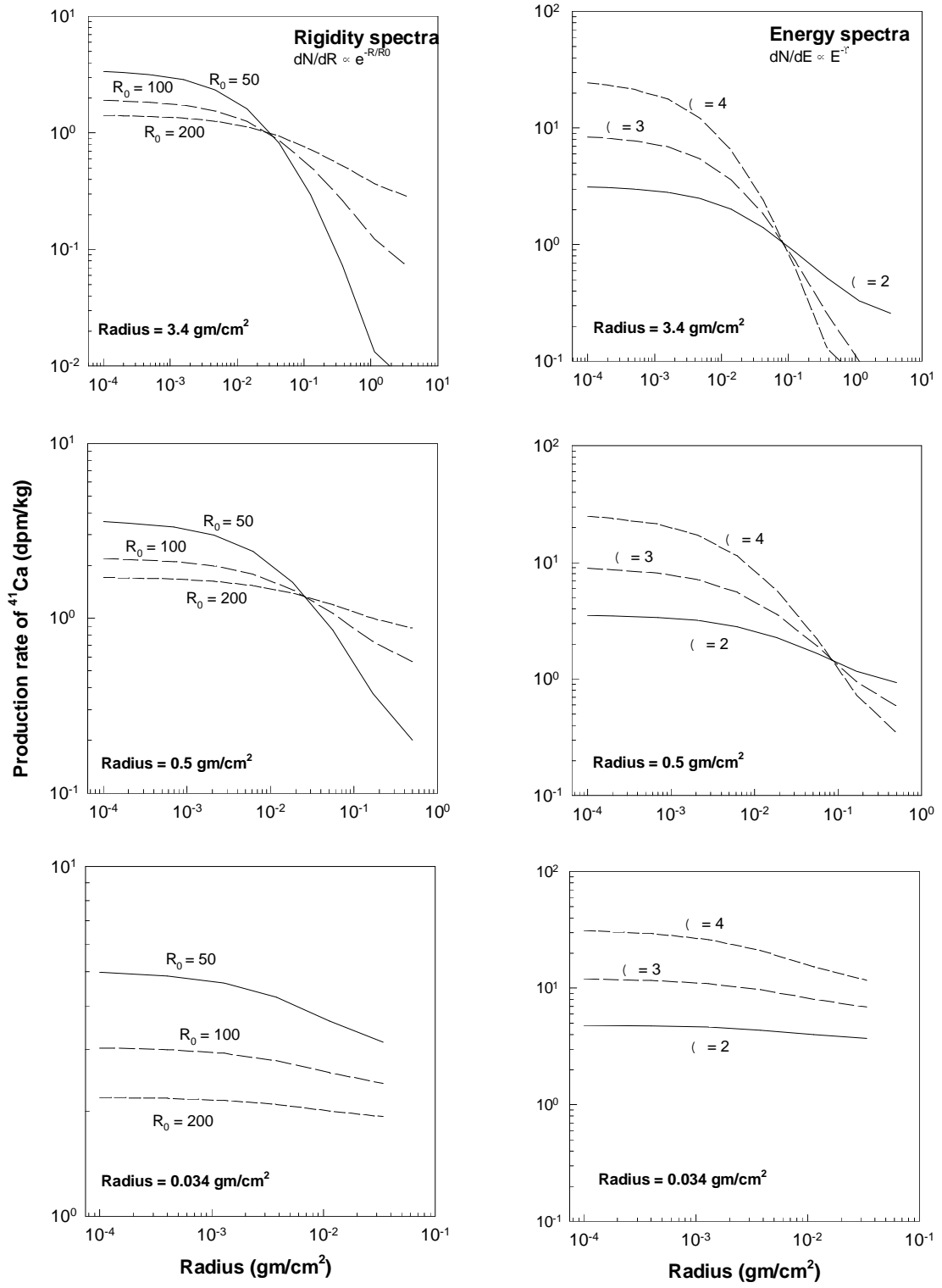
Figure 5.5: Production rate (dpm/kg) of the radionuclide, ^{41}Ca as function of depth for grains of three different sizes. Energy and rigidity spectra with different γ and R_0 values, respectively, were used for the calculations.

111
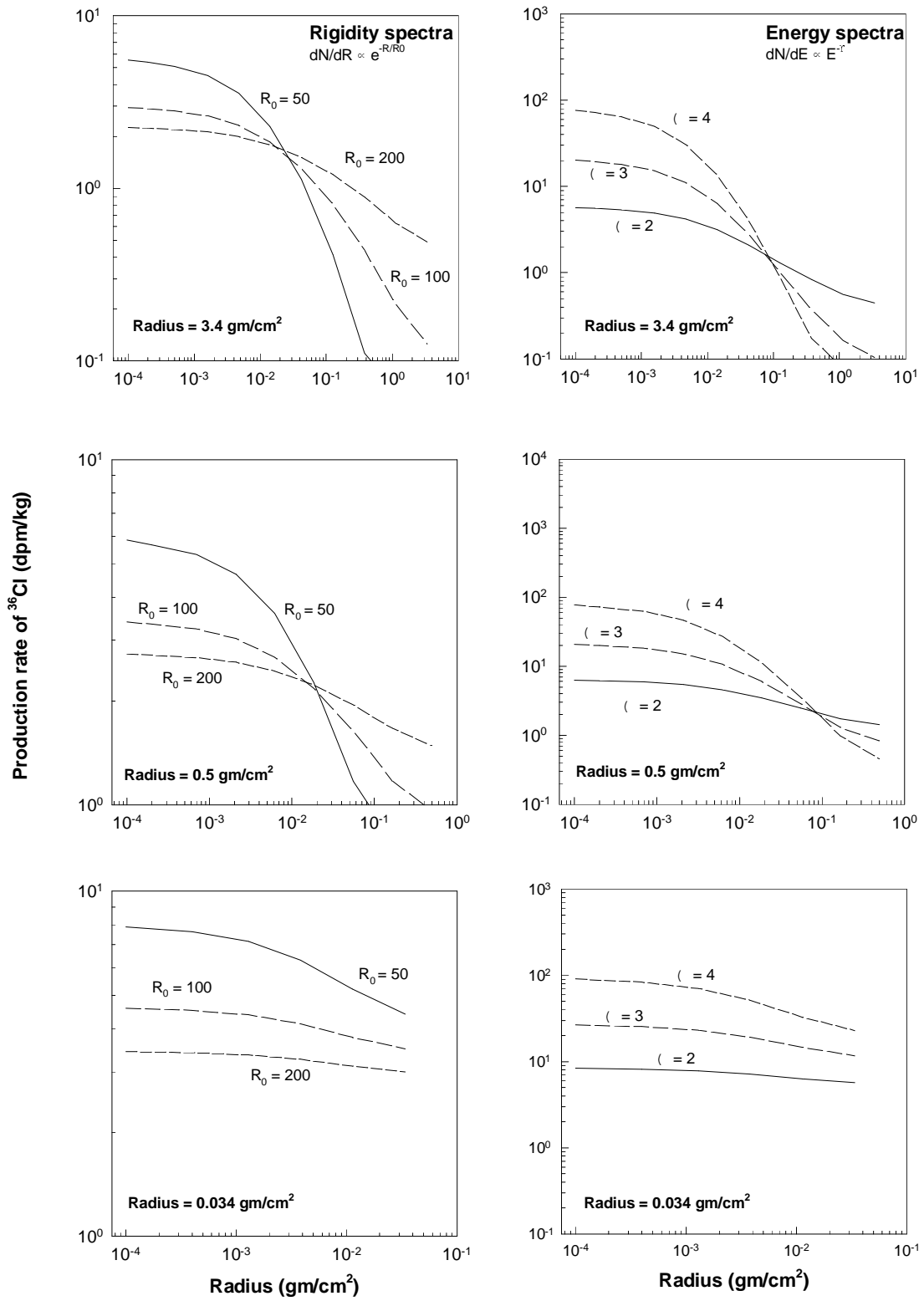
Figure 5.6: Production rate (dpm/kg) of the radionuclide, ^{36}Cl as function of depth for grains of three different sizes. Energy and rigidity spectra with different γ and R_0 values, respectively, were used for the calculations.

112
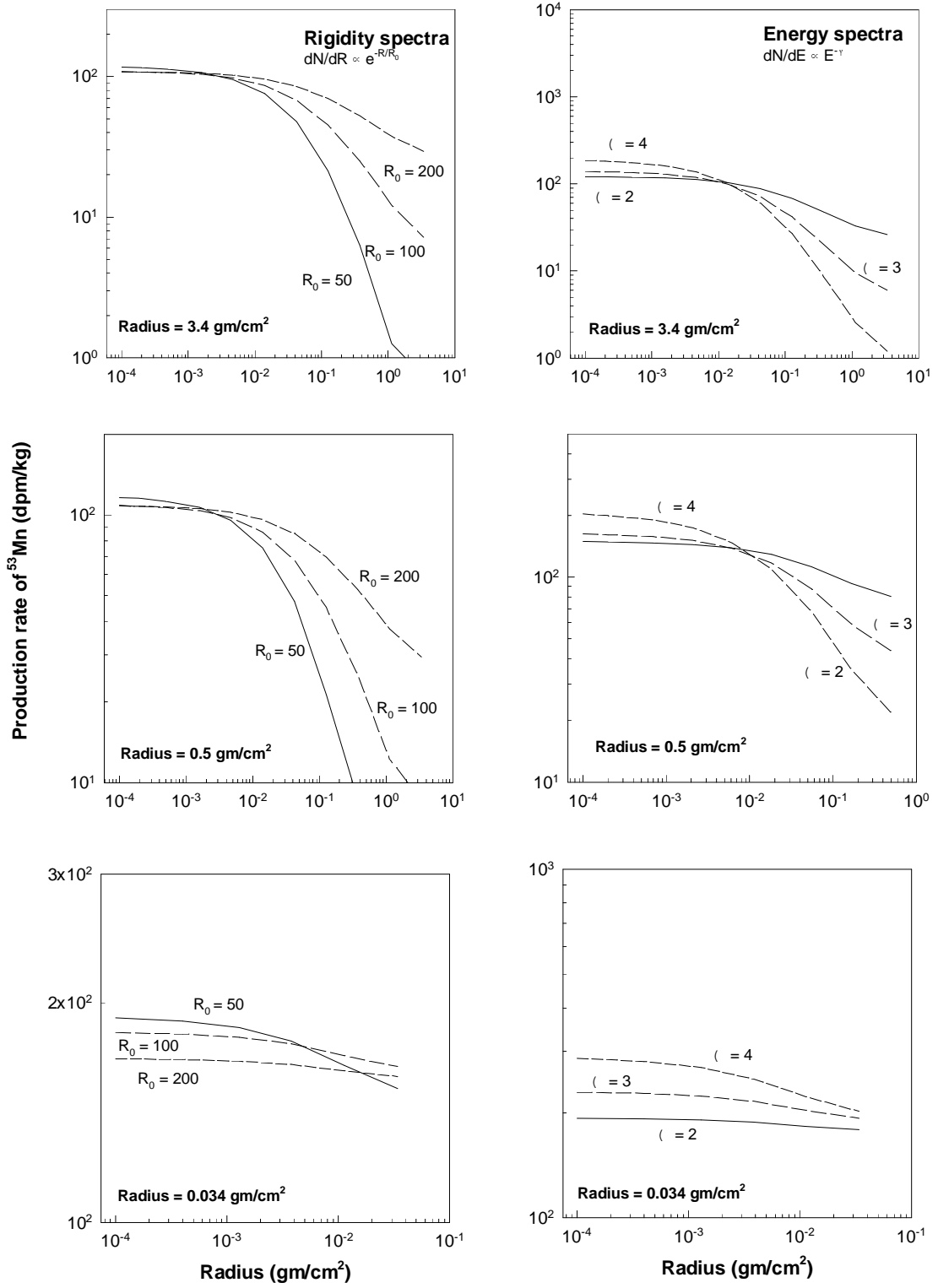
Figure 5.7: Production rate (dpm/kg) of the radionuclide, ^{53}Mn as function of depth for grains of three different sizes. Energy and rigidity spectra with different γ and R_0 values, respectively, were used for the calculations.

113

grains due to the power law distribution in grain size used by us.

The average production rates for single grains of different sizes with $\gamma = 3$ and $R_0 = 100$ MV are shown in Fig. 5.8a. These values were finally used to determine the average production rate for an ensemble of grains of different sizes following the grain size distribution, $dn/dr \propto r^{-\beta}$; with $\beta = 3$ and 4. The integration was carried over grain sizes in the range of 10 μm to 1 cm. The average production rates of the four radionuclides for $\gamma = 3$, $R_0 = 100$ MV, and $\beta = 3$ and 4 are shown in Fig. 5.8b.

The energetic particle flux required for production of the short-lived nuclides, ^{26}Al, ^{41}Ca, ^{36}Cl and ^{53}Mn at the required level to match their observed abundances in meteorite phases was estimated using the average production rates of these nuclides in grain ensemble of 10 μm - 1cm. The meteoritic abundances were estimated from the observed initial ratios of 5×10^{-5} for ^{26}Al/^{27}Al, 1.4×10^{-8} for ^{41}Ca/^{40}Ca and 10^{-6} for ^{36}Cl/^{35}Cl, respectively. In case of ^{53}Mn, two initial values, 4.4×10^{-5} (Birck and Allegre, 1985) and 3.6×10^{-6} (Lugmair et al., 1995) were used for initial ^{53}Mn/^{55}Mn. The energetic particle flux needed for production of the radionuclides are expressed in term of flux enhancement factor over the contemporary long-term, time averaged solar energetic proton flux of ~ 100 protons/cm^2/sec (Reedy and Marti, 1991) for E > 10 MeV/amu obtained from lunar sample data. The flux enhancement factors are shown in Fig. 5.9 as function of duration of irradiation by solar energetic particles.

The important results obtained from these calculations, that can be clearly seen from Fig. 5.9 are:

(1) Co-production of ^{26}Al along with any of the other radionuclides is not possible for any enhancement factor irradiation time combination. Production of ^{26}Al requires at least one order of magnitude higher flux compared to the other nuclides.

(2) Co-production of the nuclides, ^{41}Ca, ^{36}Cl and ^{53}Mn requires a flux enhancement
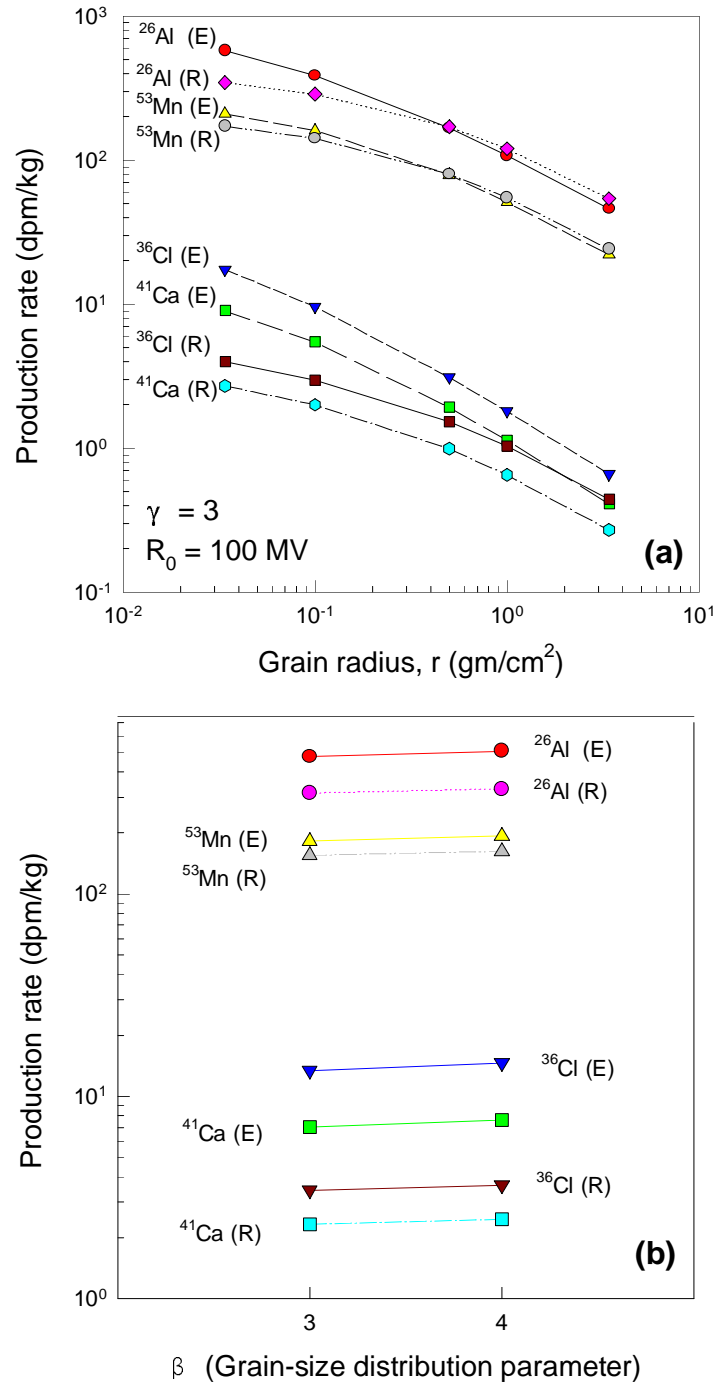
Figure 5.8: (a) Weighted-average production rates of the radionuclides, ^{26}Al, ^{41}Ca, ^{36}Cl and ^{53}Mn for grains of different sizes; E and R refer to calculations based on kinetic energy spectra with power law exponent γ, and the rigidity spectra with characteristic rigidity, R_0. (b) Average production rates in grain ensemble for different values of grain size distribution parameter β (dn/dr α r$^{-\beta}$).
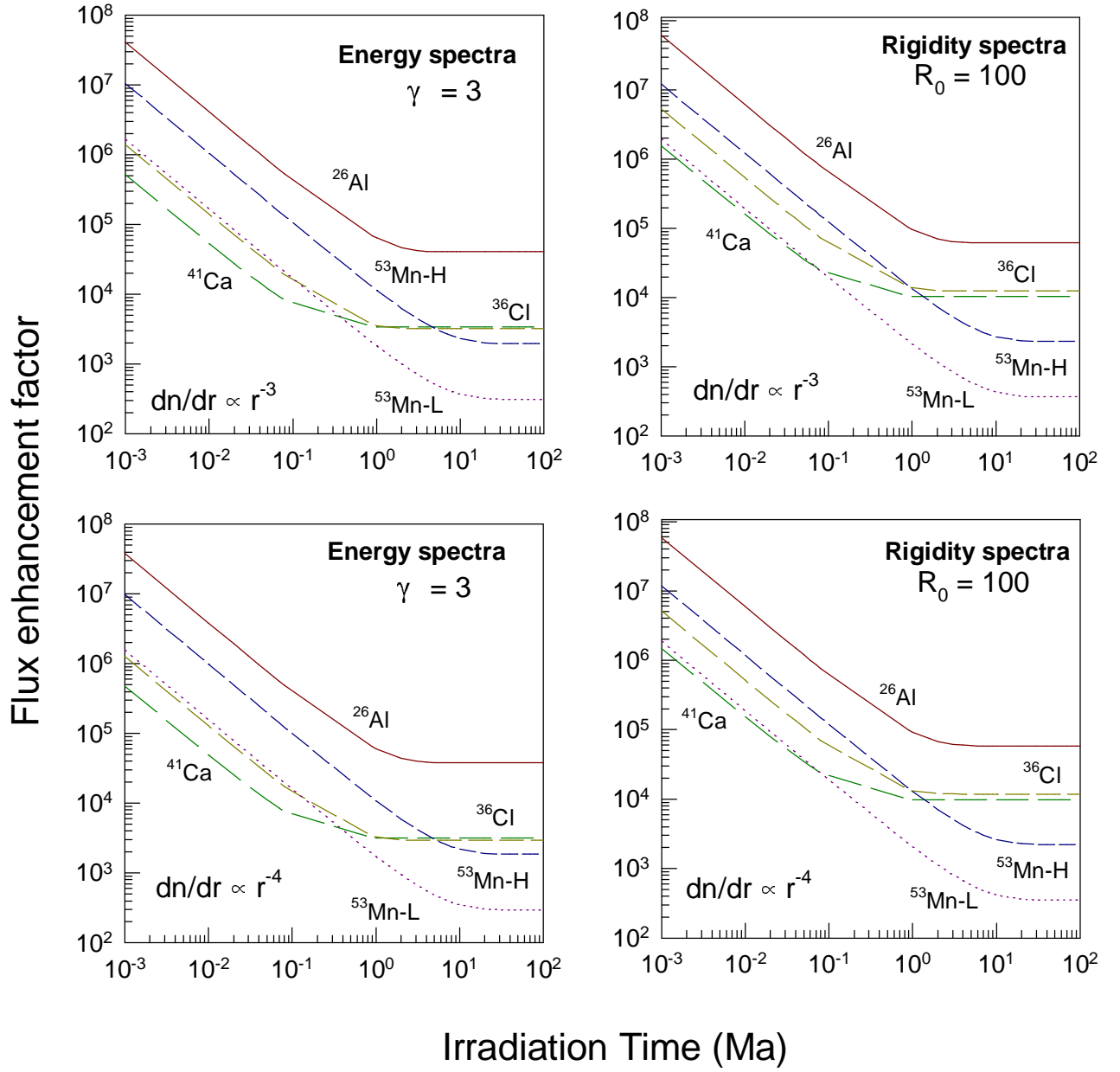
Figure 5.9: Flux enhancement factor required to produce the radionuclides to match their observed initial abundances in meteoritic phases.

of $\sim 10^4$ over the contemporary average flux even for irradiation times longer than a million year if we consider the higher initial ^{53}Mn/^{55}Mn value.

(3) For the lower value of 3.6×10^{-6} for initial ^{53}Mn/^{55}Mn (Lugmair et al., 1995), production of ^{53}Mn is possible even with a moderate flux enhancement of ~ 1000 for an irradiation time scale of ~ 1 Ma.

The above results coupled with our observation of correlated presence/absence of ^{41}Ca and ^{26}Al in individual refractory phases and inclusions from different meteorites, show that we can rule out the cosmogenic production of these radionuclides by solar energetic particles. The production of ^{26}Al to match meteoritic observation will over-produce ^{41}Ca. In addition, the inferred flux enhancement factor for production of ^{26}Al is orders of magnitude higher than that inferred by Hohenberg et al. (1990) from studies of solar flare irradiated olivine grains in CM chondrites and estimated indirectly from studies of T Tauri stars (Gahm, 1989) that also suggest flux enhancement factors of the order of 100-1000. Although it is difficult to rule out the possibility of a higher flux of solar energetic particles at the time of formation of CAI from their precursor components than at the time of irradiation of the olivine grains in CM chondrite, the problem of co-production of ^{41}Ca and ^{26}Al remains. We therefore do not favour the proposal that nuclear interactions by energetic particles from an active early Sun could be the cause for the observed excess of ^{41}K and ^{26}Mg in the refractory phases and inclusions found in the primitive meteorites. The possibility that ^{53}Mn present in the early solar system may be produced by solar energetic particles remain a viable suggestion if the lower value for initial ^{53}Mn/^{55}Mn is proven to be correct by future experiments.

Irradiation in the proto-solar cloud

The recent discovery of enhanced γ ray flux from OB star formation region in the Orion nebula (Bloemen et al., 1994) provides a direct measure of energy generation through

nuclear processes in star formation regions. The measured flux of the γ rays from nuclear deexcitation of ^{12}C and ^{16}O is hundred fold higher than previously predicted (Ramaty et al., 1979) and suggests enhanced abundances of low energy cosmic ray carbon, oxygen and other heavier ions in these regions. The sources of these particles inside the molecular cloud are not unambiguously known but they could be T Tauri stars and mass ejecta from stars or exploding supernovae. The possibility of production of different nuclides in the proto-solar cloud, within such a molecular cloud complex, by reactions induced by an enhanced flux of energetic ions and secondary neutrons has been proposed by several authors (Clayton, 1994; Marti and Lingenfelter, 1995; Clayton and Jin, 1995b; Ramaty et al., 1996). The detailed analysis carried out by Ramaty et al.(1996), who have considered production of both light isotopes of Li and B as well as the extinct nuclides, ^{26}Al, ^{41}Ca and ^{53}Mn, indicate that it may be possible to produce the required amount of ^{41}Ca to explain the initial ^{41}Ca/^{40}Ca in meteoritic phases, while ^{26}Al will be under-produced as in the case of solar particle irradiation, discussed in the last section. Unfortunately, Ramaty et al.(1996) assumed the initial ratios measured in the CAIs as representative values for the proto-solar nebula which are not correct (particularly in the case of ^{41}Ca having a short mean life), unless one assumes that production continued throughout the period of proto-solar cloud collapse and close up to the time of formation of the CAIs. The inability to coproduce the two short-lived nuclides, ^{41}Ca and ^{26}Al in their required amount also makes this model less attractive compared to the proposal of injection of material from stellar sources in which some of the extinct nuclides could be assumed to be cogenetic. Thus, injection of freshly synthesized material from specific stellar site(s) into the proto-solar clouds remain the most viable process for explaining the presence of the short-lived nuclides, and particularly ^{41}Ca and ^{26}Al, in the early solar system. In the following, we consider the scenario of injection of freshly synthesized ^{41}Ca and ^{26}Al to the solar nebula from specific stellar sources, and the constraint on time scales of processes that can be put from our observations.

5.3 Extinct Radionuclides and Time Scales of Early Solar System Processes

The presence of ^{41}Ca, ^{26}Al and several other short-lived now-extinct nuclides in the early solar system has been established from isotopic studies of suitable phases from primitive meteorites. These radionuclides can serve as useful chronometers of early solar system processes. In particular, if we attribute the presence of these nuclide to injection of freshly synthesized material from specific stellar source(s), we can estimate the value of Δ, the time interval between the injection of the short-lived nuclides to the solar nebula and the formation of some of the first solar system solids (CAIs) in which their decay products have been observed. Obviously the radionuclide with the shortest meanlife will provide the most stringent constraint on the value of Δ. Prior to our work (Srinivasan et al., 1994, 1996), ^{26}Al ($\tau \sim 1$Ma) was the shortest lived radionuclide whose presence in the early solar system was conclusively established. We have now shown that ^{41}Ca, that has a much shorter meanlife than ^{26}Al, was also present in the early solar system.

Several stellar sources like novae, supernovae, Wolf-Rayet and asymptotic giant branch (AGB) stars have been proposed as plausible candidates for production and late injection of freshly synthesized matter containing these radionuclides to the solar nebula. Cameron (1993) reviewed the plausible stellar sources of several short-lived nuclides that were present in the early solar system.

In recent times, efforts have been made to identify suitable stellar source(s) where several of these short-lived nuclides are co-produced and are then added to the solar nebula in a manner that can lead to their observed abundances in the early solar system objects (CAIs). The case for a thermally pulsing asymptotic giant branch (TP-AGB) star as a source of several of the short-lived nuclides has been investigated in some detail (Wasserburg et al., 1994). The production of ^{41}Ca via neutron capture in the He shell of

a low-mass TP-AGB star has also been investigated recently (Wasserburg et al., 1995), and it appears to be a very plausible candidate for explaining the presence of the now-extinct nuclides, ^{41}Ca, ^{26}Al, ^{60}Fe and ^{107}Pd in the early solar system. Production of ^{41}Ca in supernovae had been investigated earlier (Bodansky et al., 1968; Woosley et al., 1973) and the Ca isotope production rates in supernovae have been updated recently (Weaver and Woosley, 1993, Woosley and Weaver, 1995). Cameron et al. (1995) suggested a supernova as a plausible source for several of the short-lived nuclides present in the early solar system and have sought to revive the proposal of supernova trigger for the formation of the solar system (Cameron and Turan, 1977). As our data suggest a correlated presence of ^{41}Ca and ^{26}Al in refractory phases, we now consider the constraint that we can place on the time interval Δ as well as on the plausible stellar site(s) where these two short-lived nuclides could have been produced before being injected into the solar nebula. Obviously we need to know the production ratios (P) of (^{26}Al/^{27}Al) and (^{41}Ca/^{40}Ca) in the various stellar sites to carry out this exercise. The estimated P(^{26}Al/^{27}Al) values are (see also Clayton and Leising, 1987) :

(i) explosive nucleosynthesis in supernovae; $P \sim 4 \times 10^{-3}$ to $\sim 2 \times 10^{-2}$ (Woosley and Weaver, 1980, 1995),

(ii) hydrostatic carbon burning in massive stars; $P \sim 10^{-3}$ (Arnett and Wefel, 1978),

(iii) high temperature H-burning in novae and asymptotic giant branch stars; $P \sim 0.1$ to 20 (Hillebrandt and Theileman, 1982, Cameron, 1985, Wiescher et al., 1986; Wasserburg et al., 1994),

(iv) Wolf-Rayet star (core H-burning): P (ejecta) ~ 0.05 (Dearborn and Blake, 1985; Walter and Maeder, 1989).

While the production ratio of (^{26}Al/^{27}Al) varies over a wide range ($\sim 10^{-3}$ to ~ 20), the

situation in the case of ^{41}Ca, is much better. The nucleosynthetic processes that have been considered for production of ^{41}Ca and corresponding P(^{41}Ca/^{40}Ca) are:

(i) explosive oxygen burning; P $\sim$ 1.5 $\times$ 10^{-3} (Woosley et al., 1973),

(ii) explosive silicon burning; P $\sim$ 10^{-3} (Bodansky et al., 1968).

(iii) explosive supernovae nucleosynthesis; P $\sim$ (0.6-2.8) $\times$ 10^{-3} (Weaver and Woosely, 1993; Woosley and Weaver, 1995)

(iv) nucleosynthesis in TP-AGB stars; P $\sim$ 1.0 $\times$ 10^{-2} (Wasserburg et al., 1995)

(v) Wolf-Rayet stars (core He-burning); P(ejecta) $\sim$ 3 $\times$ 10^{-3} (Dearborn and Blake, 1988).

The production ratio for ^{41}Ca is thus more tightly constrained than that of ^{26}Al and ranges from $\sim$ 10^{-3} to 10^{-2}.

It is possible to obtain the value of Δ based on the theoretically estimated production ratio and measured initial ratio for any one pair of these isotopes, if we have *a priori* knowledge of the dilution factor, i.e., the amount of dilution of the freshly injected material containing the radionuclide (^{41}Ca or ^{26}Al) and its stable counterpart (^{40}Ca or ^{27}Al), with the pre-existing material in the proto-solar cloud containing only the stable nuclides and devoid of the short-lived species. Unfortunatly, there is no simple way of rigorously estimating this dilution factor and one can only obtain approximate values using meteorite data for the somewhat longer-lived isotopes ^{107}Pd ($\tau \sim$ 10Ma) and ^{129}I ($\tau \sim$ 23Ma) (see, e.g., Cameron, 1985; Cameron et al., 1993; Wasserburg et al., 1994), and assuming that they were also introduced into the solar nebula by the same event.

We can circumvent the difficulty of estimating the dilution factor and derive a self consistent value of Δ by combining data for two short-lived nuclides that were present in

the early solar system and were injected to the solar nebula from the same stellar source. The correlated observation of excess ^{41}K and ^{26}Mg in refractory phases and CAIs makes ^{41}Ca and ^{26}Al a suitable pair for such an analysis and we can consider several sources (supernova, TP-AGB star and Wolf-Rayet star) as being responsible for injecting freshly synthesized ^{26}Al and ^{41}Ca to the solar nebula. If we assume that the dilution factor is similar for both the nuclides, we get the following expression for Δ:

$$\Delta = -\frac{1}{\lambda_i - \lambda_j} \cdot ln \left[\frac{M_i}{P_i} \cdot \frac{P_j}{M_j} \right] \tag{5.3}$$

where P_i and P_j refer to stellar production ratios, M_i and M_j refer to measured ratios in CAIs, and λ_i and λ_j refer to the decay constants of the two short-lived nuclides. Obviously, one can use the value of Δ, obtained from a given (P_i, P_j) combination, specific to a particular stellar source, to infer a self consistent value for the dilution factor. Using the measured initial ratios (M) of 5×10^{-5} and 1.4×10^{-8} for (^{26}Al/^{27}Al) and (^{41}Ca/^{40}Ca), respectively, and the production ratios (P) noted earlier, we obtain the following solution for different stellar sources:

(i) **Supernova:** $\Delta \sim 0.8$ to 1.4 Ma; D (Dilution factor) ~ 180 to 20,

(ii) **TP-AGB star:** $\Delta \sim 0.6$ Ma; D $\sim 10,000$, and

(iii) **Wolf Rayet star:** $\Delta \sim 1$ Ma; D ~ 400.

It should be noted that both in the case of TP-AGB and Wolf-Rayet star the production of ^{26}Al and ^{41}Ca takes place in different regions of the evolving star and over extended periods. ^{26}Al is synthesized during H-shell burning (TP-AGB)/core H-burning(WR), and ^{41}Ca is synthesized during He-shell burning(TP-AGB)/core He-burning(WR). It is therefore necessary to take into account the ratio of nucleosynthetic products from these two source regions that finally reach the outer envelope and get

122

ejected while evaluating the value of Δ. This ratio is close to unity (0.7 to 2) for TP-AGB star (Wasserburg et al., 1994). In the case of Wolf-Rayet stars we have used the time averaged values for the abundance ratios of these nuclides in the ejected material (Dearborn and Blake, 1985, 1988). As already noted, the effective production of ^{41}Ca in TP-AGB star would also be somewhat lower than the values noted above as its production persists over a period, comparable to its mean life, and one has to take into account the decay of ^{41}Ca during this duration (Wasserburg et al., 1995).

Although the Δ values deduced above cluster around a narrow range (0.6 to 1.4Ma), irrespective of the stellar source, the corresponding dilution factor varies over an extremely wide range (20 to 10,000). For example, if we consider a TP-AGB star as the source for ^{41}Ca and ^{26}Al in the early solar system, this event need to supply only ~ 0.01 percent of the stable nuclide component in the solar system, which appears quite reasonable. Such a star can contaminate about 100 M$_\odot$ of the molecular cloud with its ejecta in the form of AGB wind/planetary nebula during the final stages of its evolution. Although the probability of such an event taking place during the life time of a molecular cloud is rather low because of the longer time scale for evolution of AGB stars (few billion years) compared to the typical life time of molecular clouds (few tens of million year), the possibility of an AGB association with a molecular cloud cannot be ruled out. Based on observational data, the probability of such an association has been estimated to be ~ 1 % in a million year (Kastner and Myers, 1994); and over the life time of a molecular cloud, this probability could be much higher. A close encounter between an AGB star and the proto-solar cloud could have resulted in injection of the radionuclides, ^{41}Ca and ^{26}Al into the proto-solar cloud and might have also triggered the collapse of the proto-solar cloud (see e.g., Cameron, 1993).

On the other hand, if we take supernova as a plausible source, the same event need to supply more than one percent of the stable nuclides in the solar system, and

in particular those of Mg, Al, K and Ca. Cameron et al.(1995) have recently suggested that freshly synthesized supernova material will get diluted to different extent during the 'post-explosion fall back' event, leading to an effectively higher production of ^{26}Al compared to the other short-lived nuclides. In fact they concluded that supernova associated with a massive star, initially going through a Wolf-Rayet stage, could be a plausible source for several of the observed short-lived nuclides, including ^{41}Ca and ^{26}Al, in the early solar system. In addition, such an event taking place even at a distance of 2-10 parsec from the proto-solar cloud could in principle trigger the collapse of the proto-solar cloud. An added advantage of considering a supernova as a source is its capability to synthesize the short-lived nuclide ^{53}Mn that was also present in the early solar system (Birck and Allegre, 1985; Lugmair et al., 1995) and which cannot be synthesized in TP-AGB stars.

Irrespective of the problem of identification of the exact stellar source of the freshly synthesized ^{26}Al and ^{41}Ca, the presence of ^{41}Ca in the early solar system, and the observed correlation of ^{26}Al and ^{41}Ca in refractory phases and CAIs have tightly constrained the time interval Δ between the last injection of freshly synthesized matter to the solar nebula and the formation of the first solar system solids (CAIs) to < 1Ma with a plausible value of ~ 0.6Ma. The relatively small value of Δ obtained by us is not inconsistent with the observation of the extinct nuclide ^{60}Fe ($\tau \sim 2.2$Ma) in differentiated meteorites (Shukolyukov and Lugmair, 1993a, b; Lugmair et al., 1995) which suggest that the time interval between the isolation of the solar nebula and the formation of large ($\gg$km-sized) objects and their subsequent heating, melting and recrystallization is < 6 Ma (Lugmair et al., 1995). It should be noted that the small value of Δ also places a very strong constraint on the dynamical evolution of the solar system, as it also provides the *upper limit* on the time scale for the collapse of the proto-solar cloud to form the Sun. If we assume a "free-fall" time scale for collapse, the deduced value of < 1 Ma for Δ suggests a rather dense proto-solar cloud with $n_H \sim 10^4$ cm^{-3}, from which

the Sun and the solar system have evolved.

Chapter 6

Heat Source for Early Thermal Processing of Meteorite Parent Bodies: The case for ^{26}Al

In this chapter, the implications of the results obtained from the measurements of Mg isotopic composition in igneous, non-refractory phases from different chondritic meteorites are discussed to assess the plausible role of ^{26}Al as a heat source for the early thermal metamorphism/melting of meteorite parent bodies. Presence of live ^{26}Al in sufficient amount at the time of formation of these non-refractory phases, will provide evidence for ^{26}Al as a primary heat source for thermal processing of meteorite parent bodies. In order to interpret the results obtained in this study, a quantitative discussion on the magnitude of heat production in meteorite parent bodies as function of their size and initial ^{26}Al abundance is presented.

6.1 Heating of Meteorite Parent Bodies by ^{26}Al: Numerical Estimates

The magnitude of thermal processing in a meteorite parent body due to radioactive heating by ^{26}Al depends on the initial abundance of ^{26}Al and the size of the body. Here we estimate the abundance of initial ^{26}Al (relative to its stable counterpart ^{27}Al) required to induce varying dergrees of thermal metamorphism and/or melting of planetesimals that acted as meteorite parent bodies. This is based on the results obtained by solving the heat conduction equation (6.1) for a sphere with an exponentially decaying heat source term.

$$\frac{1}{\mathcal{K}}\frac{\partial T}{\partial t} = \frac{\partial^2 T}{\partial r^2} + \frac{2}{r}\frac{\partial T}{\partial r} + \frac{Q\rho}{k}e^{-\lambda t} \tag{6.1}$$

where, $\mathcal{K} = \dfrac{k}{\rho c}$ is the thermal diffusivity, with k and ρ, the thermal conductivity and specific heat, respectively. Q is the heat generation rate and λ is the decay constant of radionuclide.

The heat conduction equation was solved numerically by using finite difference method with non-radiative boundary condition. Temperature profiles inside meteorite parent bodies of chondritic composition and of varying sizes and initial ^{26}Al/^{27}Al were calculated (Fig. 6.1 to 6.3). The calculations were carried out by taking into account the non-linear dependence of thermal diffusivity and specific heat on temperature (Yomogida and Matsui, 1983). In the finite difference approach, temperature was estimated at each step of the calculation by using the values of thermal diffusivity and specific heat at that time and space coordinates.

The maximium central temperature attained in a meteorite parent body as a function of its size and initial abundance of ^{26}Al is shown in Fig. 6.1a. The results obtained from these calculations differ significantly from those obtained by taking temperature independent thermal diffusivity and specific heat (Fig 6.1b), and we consider here the temperature dependent solutions. The minimum value of initial ^{26}Al/^{27}Al (assuming a chondritic abundance for ^{27}Al) required to induce varying degrees of thermal metamorphism seen in ordinary chondrites (T $\sim$ 400°-950°C) near the central region of a parent body, is $\sim$ 4 - 9 $\times$ 10^{-6}, whereas, an initial value of $\geq$ 1 $\times$ 10^{-5} is required to initiate melting (T $\geq$ 1000°C) in the central region of the body, if the radius is greater than 30 km. For radius greater than 30km, the maximum temperature attained in the central region of the body is independent of its size.

The temperature-time profile for a chondritic body of radius 100 km for an initial ^{26}Al/^{27}Al of 1 $\times$ 10^{-5} is shown in Fig. 6.2a. As can be noted from the figure, such a body will be heated to temperature greater than 1000°C (except for the outer 20 km layer) that can result in partial melting of the object. However, for lower initial ^{26}Al/^{27}Al or for bodies of smaller radius ($\leq$ 40km), the temperature may not be sufficient for melting, even though it could be sufficient to initiate thermal metamorphism. For example, only the core region of a 40 km chondritic body with an initial ^{26}Al/^{27}Al of 1 $\times$ 10^{-5} (similar to the case just considered) will be heated to a temperature of $\sim$ 1000°C while the outer 20 km of the object will experience temperature $\leq$900°C (Fig. 6.2b). Even for a large object of radius 100 km with low initial ^{26}Al/^{27}Al of 8 $\times$ 10^{-6}, only the central region will be heated to temperature greater than 600°C for 2 to 5 Ma (Fig. 6.3). Obviously, these temperatures are insufficient for melting of silicates, but they can cause varying degrees of thermal metamorphism generally observed in chondritic meteorites. Thus, in general, initial ^{26}Al/^{27}Al of $\geq$ 4 $\times$ 10^{-6} is needed for inducing thermal metamorphism in a chondritic parent body while an initial ratio of $>$ 10^{-5} is needed to induce melting of the body.
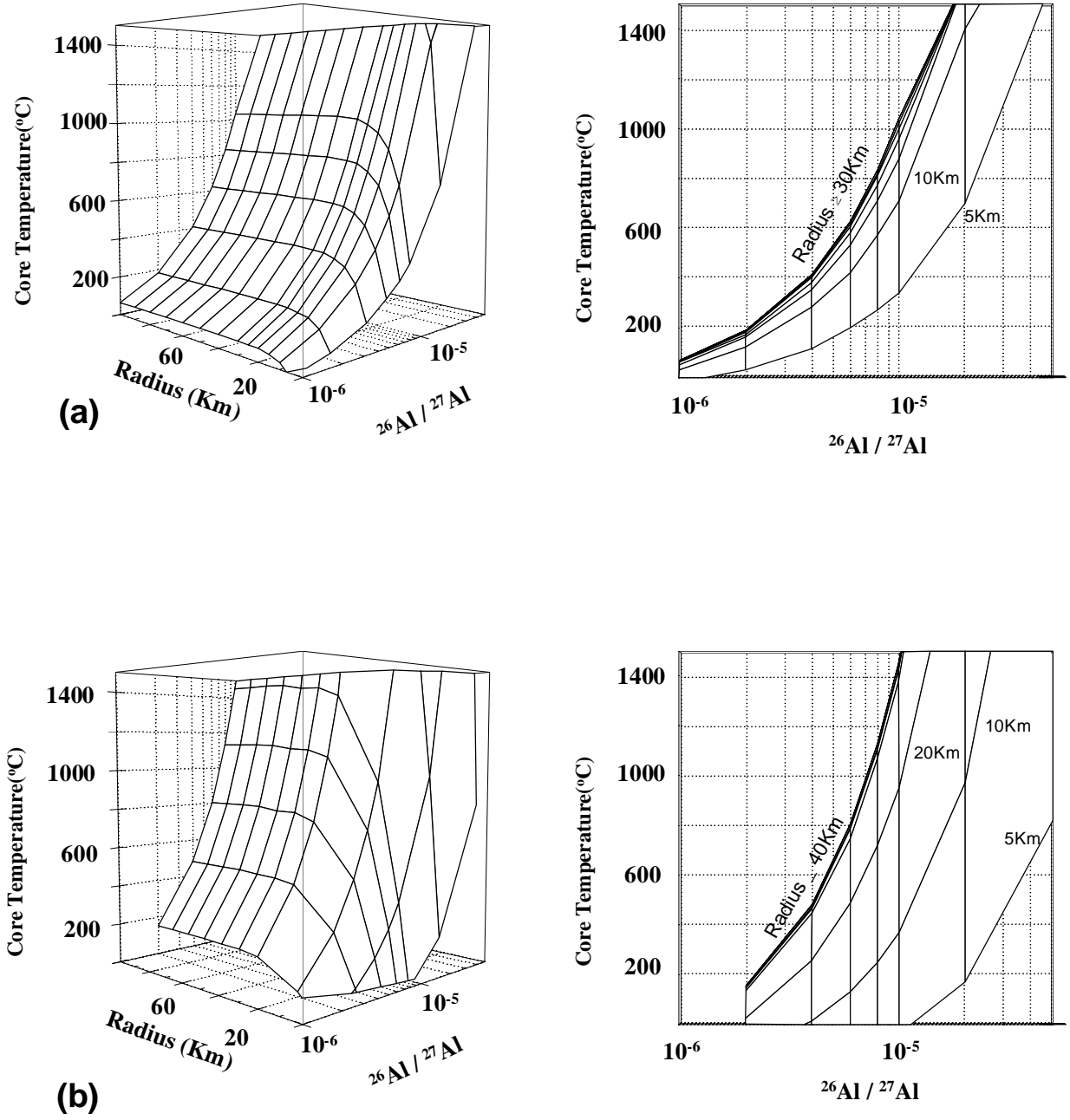
Figure 6.1: Maximum central temperature attained in meteorite parent body as function of its size and initial abundance of ^{26}Al assuming temperature dependent thermal diffusivity (κ) and specific heat (Fig. a) and constant thermal diffusivity ($\kappa \sim 0.007$ cm^2/s; Fig. b).

129
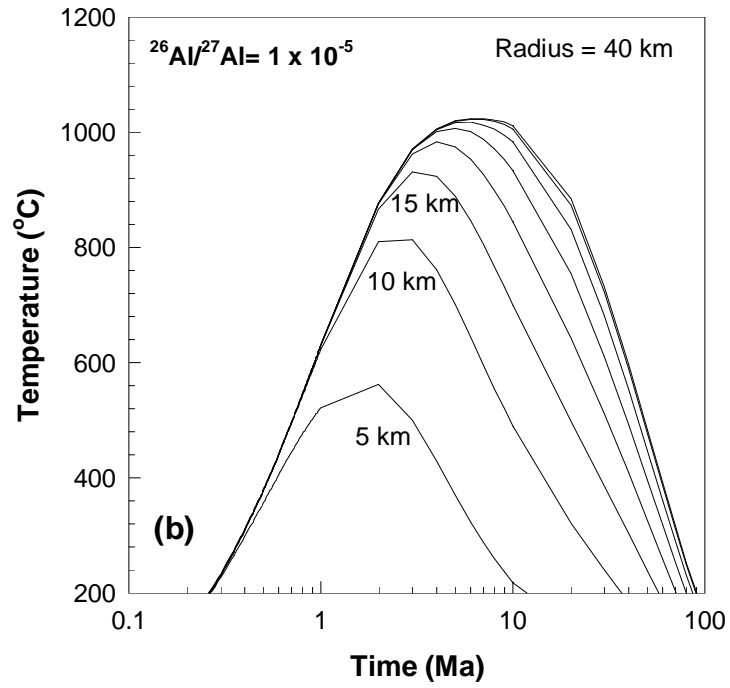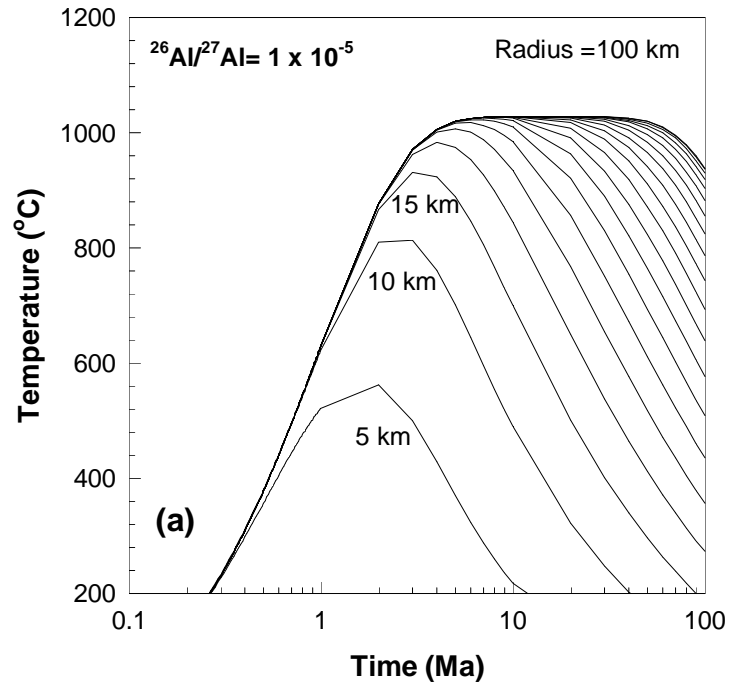
Figure 6.2: Temperature-time profile at different depths from surface for a chondritic body of radius 100 km (Fig. 6.2a) and 40 km (Fig. 6.2b), for initial $^{26}\text{Al}/^{27}\text{Al} = 1 \times 10^{-5}$.
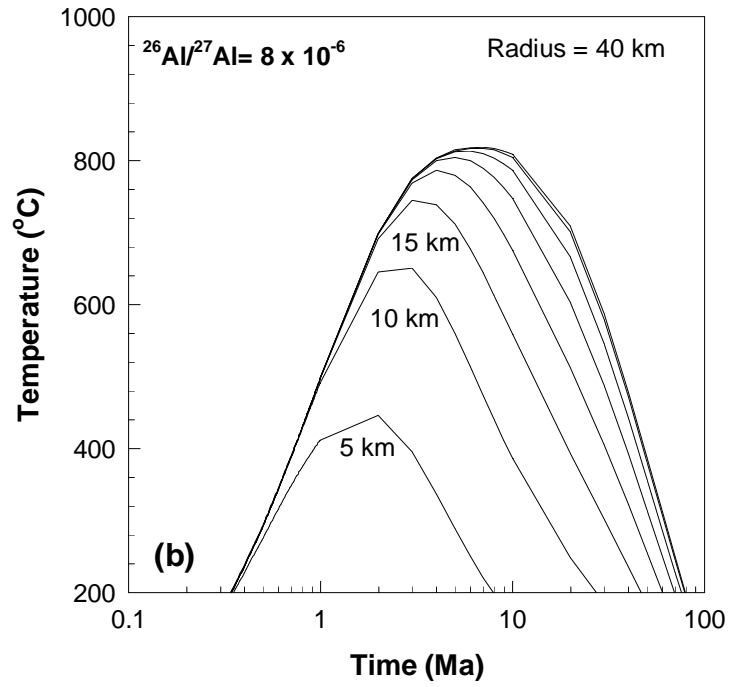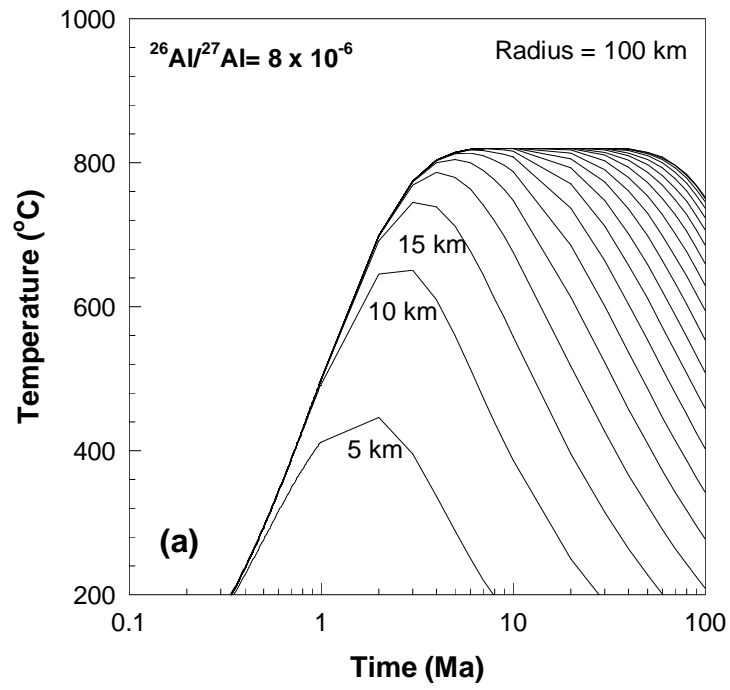
Figure 6.3: Temperature-time profile at different depths from surface for a chondritic body of radius 100 km (Fig. 6.3a) and 40 km (Fig. 6.3b), for initial $^{26}Al/^{27}Al = 8 \times 10^{-6}$.

6.2 ^{26}Al as a Heat Source: Meteoritic Evidence

The results obtained from the magnesium isotopic studies of plagioclase phases of igneous inclusions from several chondrites (Fig. 6.4) indicate absence of excess ^{26}Mg in most of the analyzed phases except for a marginal evidence in a few cases. These include an Al-rich phase in the silica bearing inclusion from the Dengli chondrite, a plagioclase from Tsarev, and two anorthite grains from the Kaidun meteorite. While the experimental uncertainities of the measured initial values in the first two cases are rather large and an excess in ^{26}Mg cannot be established conclusively, the data for the two anorthite grains from Kaidun clearly show an excess. However, these anorthite grains, hand-picked from this multi-component meteorite breccia, may not be representative products of large scale thermal processing and could be fragments of Ca-Al-rich inclusions (CAIs) present in the CM component of this meteorite. As already noted in the introduction, there is abundant evidence for ^{26}Mg excess in CAIs that are believed to be some of the first solids to form in the solar system. In addition, not all of the anorthite grains analyzed from Kaidun show ^{26}Mg excess. Thus, we at best have a few grains with an upper limit of 1×10^{-6} for initial ^{26}Al/^{27}Al and the bulk of the analyzed grains do not show any detectable ^{26}Al at the time of their formation. Our data therefore do not provide definitive evidence for the presence of residual ^{26}Al at the time of formation of the igneous, non-refractory components from the different chondritic meteorites analyzed by us.

Earlier efforts by Hutcheon et al. (1994) and Hutcheon and Jones (1995) to detect excess ^{26}Mg in Al-rich phases of chondrules and igneous inclusions also yielded negative results. However, Russel et al. (1996) have recently reported observation of ^{26}Mg excess in chondrules from the chondritic meteorites, Inman and Chainpur, with an inferred initial ^{26}Al/^{27}Al values of $(9.4 \pm 6.3) \times 10^{-6}$ and $(7.9 \pm 2.1) \times 10^{-6}$, respectively. Chondrules are believed to be products of rapid crystallization of melt

132
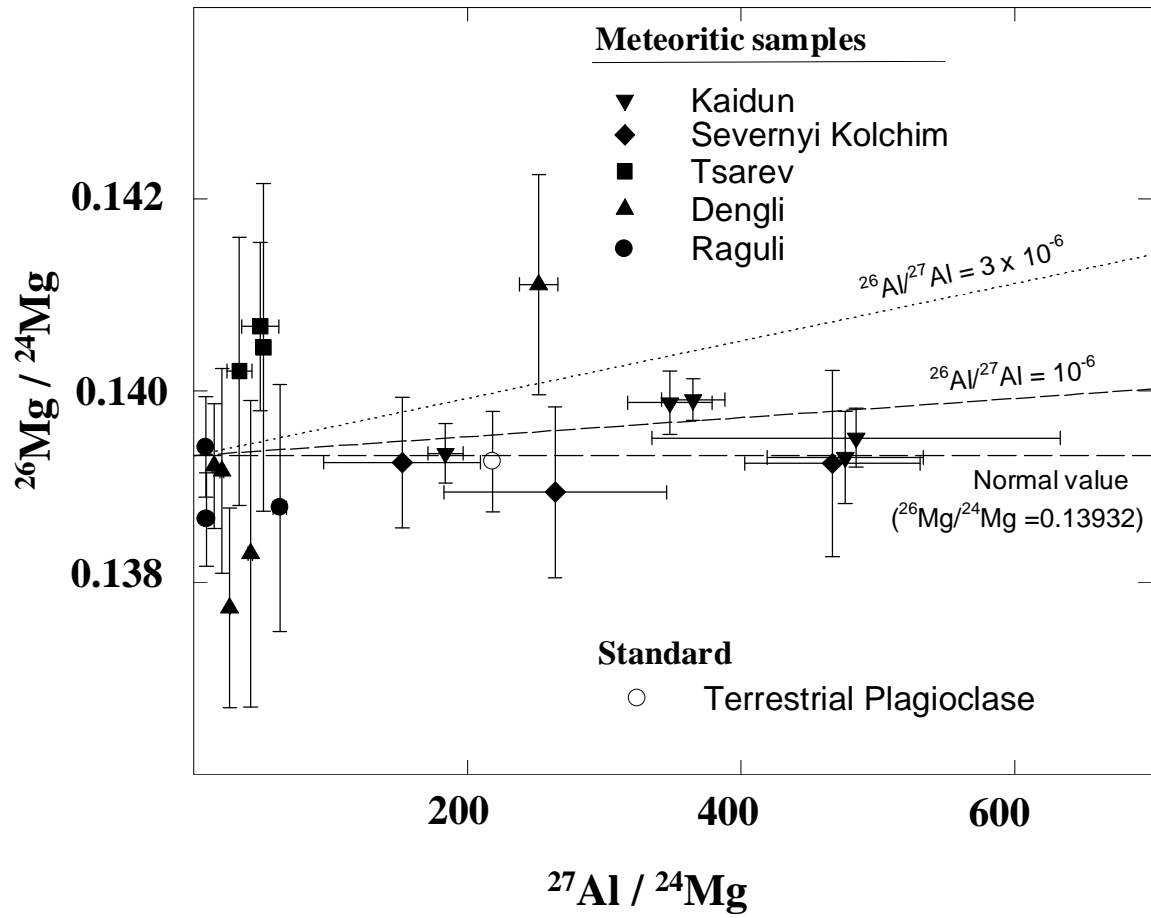
Figure 6.4: Mg-Al isotopic systematics in plagioclase phases from igneous, non-refractory inclusions of chondritic meteorites.

droplets produced in a nebular environment and most probably formed after the CAIs, but before the meteorite parent bodies. One would therefore expect ^{26}Mg excess in chondrules, if the distribution of ^{26}Al was widespread in the solar nebula, and the initial ^{26}Al in chondrule could be an upper limit on the initial abundance of this nuclide at the time of formation of meteorite parent bodies. In the following we consider several possible alternatives that may explain the negative results obtained by us.

1. The time scale for formation of the analyzed igneous, non-refractory phases were much longer (several Ma) and magnesium isotopic exchange between the analyzed Mg-poor (Al-rich) phases with co-existing Mg-rich phases was pervasive during this protracted period. Thus the closure of Mg-Al isotopic system in the analyzed objects took place at a time when residual ^{26}Al was extremely small, leading to a barely detectable ^{26}Mg excess. For example, a solar system (CAI) initial ^{26}Al/^{27}Al of 5×10^{-5} would decrease to less than 1×10^{-6} within 4 Ma which is difficult to detect for phases with Al/Mg ratio of less than a few hundred, typical of the plagiclase grains analyzed by us.

2. The analyzed phases experienced Mg isotopic redistribution and/or exchange with a reservoir of normal isotopic composition during their evolution in the meteorite parent body at a later time. The lower ^{26}Al/^{27}Al found in many of the petrographically altered CAIs compared to the generally accepted solar system initial value of 5×10^{-5}, characteristic of petrographically unaltered CAIs, has been attributed to such exchange/redistribution of Mg isotopes during the processes leading to the observed petrographic alteration (e.g., Podosek et al., 1991; Goswami et al., 1994; MacPherson et al., 1992, 1995). Thus, it is possible that the Al-rich silicate phases analyzed by us have undergone secondary alterations following their formation resulting in Mg-isotopic reequilibration to the observed normal values. Such an exchange/redistribution is possible if the analyzed phases were derived via recrystallization of Al-rich glassy material during a late stage thermal event in a meteorite parent body (e.g., McSween and Grimm

1994).

3. ^{26}Al was not the primary heat source for early melting of planetesimals. If true, this points towards the need for quantitative study of other physical processes, e.g., induction heating of planetesimals by strong protosolar wind from the active early Sun (Herbert et al., 1991; Wood and Pellas, 1991), proposed in this regard.

An extended time scale of several million years for the formation of chondrules following CAI formation has been favored by several authors to explain the absence/low abundance of ^{26}Mg excess in chondrules from low metamorphic grade chondrites (Hutcheon et al., 1994; Hutcheon and Jones, 1995; Russell et al., 1996). As the chondrules were formed prior to the formation of meteorite parent bodies, their formation time scale can be taken as lower limit for the accretion time scale of meteorite parent bodies. Thus time scale for accretion of planetesimals appears to vary over ~ 2.5 - 5 Ma. The initial ^{26}Al/^{27}Al will be $\sim 5 \times 10^{-6}$ in the first case, which can induce thermal metamorphism in meteorite parent body, while the longer time scale indicate initial ^{26}Al/^{27}Al of $< 10^{-6}$, not sufficient to cause thermal metamorphism.

The duration of thermal metamorphism/melting in meteorite parent bodies is also an important factor that may result in the observed absence of ^{26}Mg excess in the analyzed phases. If we consider an initial value of 1×10^{-5} for ^{26}Al/^{27}Al at the time of formation (accretion time ~ 1.6 Ma) of a 100 km planetesimal, the central 70 - 80 km of the body will be raised to temperature $> 1000^{o}$C in 3 Ma (Fig. 6.2a). The partial melt produced as a result of this heating will have an initial ^{26}Al/^{27}Al value of $< 1 \times 10^{-6}$ and only if the melt cools quickly, there is a chance of detecting excess in ^{26}Mg. However, on the basis of cooling rates inferred for the central 80 km region of such a planetesimal (Fig. 6.2a), the cooling-off rate appears to be rather slow and we need to invoke other physical processes for extraction of the melt from the interior, e.g., impact triggered extraction of melt (Scott et al., 1989) to see preserved records of ^{26}Al

in the recrystallized phases. Thus, even if ^{26}Al was the primary heat source for thermal processing of meteorite parent bodies, a delayed Mg-Al closure of igneous, non-refractory inclusions could have resulted in absence of ^{26}Mg excess in the phases analyzed by us.

In summary, no definite evidence for the presence of residual ^{26}Al at the time of formation of igneous components from several chondritic meteorites have been found to support the case of this short-lived nuclide as the primary heat source for the early melting of planetesimals. The absence of ^{26}Mg excess in most of the analyzed objects may be attributed to an extended period (> 5 Ma) of formation and thermal processing of meteorite parent bodies. A strong case for ^{26}Al as the heat source for early thermal processing of planetesimals remains inconclusive.

Chapter 7

Summary and Conclusions

The main emphasis in this thesis work was to look for the widespread presence of ^{41}Ca in refractory phases from different meteorites in the early solar system, and to infer its relation with the presence/absence of ^{26}Al in these phases. Because of their short mean lives, these two nuclides can put very stringent constrain on the time scale for the formation of the Sun and the earliest solar system solids. In addition, we have analyzed several igneous, non-refractory phases from various chondrites to look for the presence of ^{26}Al. One time presence of ^{26}Al in these phases will support the role of this radionuclide as a potential heat source for the thermal processing of the meteorite parent bodies. The most important results obtained from these studies are:

(1) The one time presence of ^{41}Ca was found in refractory phases from the three meteorites, Murchison, Allende and Efremovka. An initial value of $(1.38 \pm 0.13) \times 10^{-8}$ for ^{41}Ca/^{40}Ca at the time of formation of these refractory phases has been established from our data.

(2) We have shown for the first time correlated presence/absence of the two short-lived nuclides, ^{41}Ca and ^{26}Al, based on the study of individual refractory phase (hibonite) from Murchison, Allende and Efremovka meteorites. They were found

to be either present with their characteristic initial values of $\sim 1.4 \times 10^{-8}$ for ^{41}Ca/^{40}Ca and $\sim 5 \times 10^{-5}$ for ^{26}Al/^{27}Al or absent/occur in extremely low abundances.

(3) The search for the one time presence of ^{26}Al in igneous, non-refractory phases from several chondrites did not yield any positive evidence for its role as a heat source for thermal processing of meteorite parent bodies.

The widespread presence of ^{41}Ca in the region of formation of refractory phases found in the three meteorites, Murchison, Allende and Efremovka puts a stringent limit on the time scale for the collapse of proto-solar cloud to form the Sun and some of the first solar system solids, represented by these refractory phases. In addition, the correlated presence of the two short-lived nuclides, ^{41}Ca and ^{26}Al suggests that they are co-genetic. This allowed us to infer their most plausible source(s) from among the various sources proposed so far. "Fossil" origin (via stardust) of ^{41}Ca as well as its cosmogenic origin due to interactions of secondary neutrons during cosmic ray exposures of meteorites in the interplanetary space can be ruled out. Production of ^{41}Ca and ^{26}Al in the nebula by energetic particle irradiation from an active early Sun or by energetic heavy ions from stellar sources in the proto-solar cloud also seems to be unlikely. Our detailed calculations of production of the radionuclides, ^{41}Ca, ^{26}Al, ^{36}Cl and ^{53}Mn by solar energetic particles show that co-production of ^{26}Al and other radionuclides is not possible as the former requires more than an order of magnitude higher energetic particle flux compared to the rest, if we wish to match the meteoritic observations. In addition, the inferred enhancement factors of 10^4 to 10^5 for energetic particle flux from the active early Sun required for production of the radionuclides in their requisite amounts is also orders of magnitude higher than the enhancement factor inferred from studies of cosmogenic records in olivine grains in CM chondrites that were exposed to solar flare irradiation from an early Sun. We, therefore, rule out cosmogenic production of ^{41}Ca

and ^{26}Al, and injection of freshly synthesized material from specific stellar site(s) into the proto-solar cloud remains the most viable mechanism for explaining their presence in the early solar system. Among the various stellar sources, theoretical calculations for the production of short-lived nuclides in an AGB star, Wolf-Rayet star and supernova have been worked out in details. Based on the production rates of ^{26}Al and ^{41}Ca, the time interval between the synthesis of these nuclides in specific stellar site(s) and the formation of some of the earliest solar system solids (where the presence of these radionuclides have been found) turns out to be ~ 1 Ma. This would be the upper limit for the formation time scale of the Sun via the collapse of the proto-solar cloud. Among the three stellar sources that have been proposed as the source of these two radionuclides an AGB star seems to be a more plausible source.

The present effort to look for the presence of 'live' ^{26}Al at the time of formation of igneous, non-refractory phases from various chondrites belonging to different groups did not provide positive evidence for the role of ^{26}Al as a heat source for thermal processing of meteorite parent bodies. The absence of signatures of 'live' ^{26}Al in these phases combined with the results of our model calculations for heat generation by ^{26}Al in meteorite parent bodies suggest an extended period (> 5 Ma) of evolution, after which the closure of Mg-Al isotopic system took place in the analyzed phases. This could mean that formation and/or thermal processing of meteorite parent bodies occured over this time scale. The possibility that ^{26}Al is not the primary source for thermal processing of meteorite parent bodies cannot be ruled out completely.

7.1   Scope of future work

Short-lived nuclides present in the early solar system have played a major role as chronometers of various processes that occured during the formation of the solar system.

These processes include the collapse of the proto-solar cloud to form the Sun, condensation of the earliest formed solar system grains, formation and subsequent thermal metamorphism and differentiation of planetesimals, and the formation of Earth's core and origin of the Moon. The present study mainly addresses the problem of plausible source(s) of the short-lived nuclides and the time scale for the formation of some of the first solar system solids. An attempt has also been made to obtain evidence for the role of the short-lived nuclides as heat source for early thermal processing of meteorite parent bodies. Several aspects of these studies that need further attention are briefly outlined below.

(1) In the present study, a limited number of refractory phases from primitive meteorites were analyzed to look for correlated presence of the radionuclides, ^{26}Al and ^{41}Ca. The initial ^{41}Ca/^{40}Ca values for the refractory phases from three different meteorites, Allende, Efremovka and Murchison are nearly the same, within our experimental uncertainties, indicating that all of them formed within a very short time span of < 0.1 Ma. All these analyzed phases also have initial ^{26}Al/^{27}Al values close to the canonical value of 5×10^{-5}. To put the observed correlation between ^{41}Ca and ^{26}Al on a firm footing it will be extremely useful to analyze refractory phases with well defined Mg-Al isotopic systematics, but with lower initial ^{26}Al/^{27}Al of $\leq 3 \times 10^{-5}$, where ^{41}Ca will be below detection limit.

(2) The time scale of < 1Ma, with a plausible value of 0.6 Ma, inferred by us for the formation of the earliest solar system grains can be considered as the upper limit of time scale for the formation of the Sun. This imposes important constraints on the theoretical models for the formation of the solar system, and also for stars of about 1 M$_\odot$. For example, the time scale of 0.6 Ma would imply a rather dense proto-solar cloud with density $n_H \sim 10^4$/cc, even if we consider free-fall time for collapse. The dynamical plausibility of injection of freshly synthesized material

140

via AGB-wind or supernova ejecta into such a dense cloud need to be worked out. The various aspects of the formation of the solar system, e.g., the dynamics of the proto-solar cloud collapse, the evolution of solar nebula and the formation of the earliest solar system solids also need to be reviewed in the light of present results.

(3) The presence of the short-lived nuclides, ^{41}Ca in the early solar system, strongly suggest the possible presence of the radionuclide ^{36}Cl ($\tau \sim 0.43$ Ma) as well. Excess in ^{36}Ar has been observed recently in Efremovka meteorite by Murty et al. (1997), which they attribute to the presence of ^{36}Cl in the early solar system. They have also suggested a time scale of ~ 1Ma for the formation of some of the first silicate grains in the solar nebula which is consistent with the time scale for the formation of CAI deduced by us. Further experiments are needed to confirm the observation made by Murty et al. (1997), and in particular, to establish a correlation between the observed excess of ^{36}Ar and the content of Cl (the parent element) in the samples. The absence of measured cross sections for ^{36}Cl production also need further attention.

Another important radionuclide whose presence in the early solar system has been found is ^{182}Hf (Harper et al., 1991; Lee and Halliday, 1996). ^{182}Hf decays to ^{182}W with a mean life of 13 Ma. Because of the different chemical properties of hafnium (Hf) and tungsten (W), Hf being a lithophile element, whereas, tungsten (W) being a moderately siderophile element, the Hf radionuclide can be used as a chronometer for iron-silicate differentiation in planetesimals. The recent study of Lee and Halliday (1996) suggests that the iron meteorites formed within a few million years following the formation of the chondritic meteorites. Attempts have also been made to determine the time scale for the formation of the Earth's core and the origin of Moon (Lee and Halliday, 1995). More work on this new chronometer that can bridge the gap between ^{53}Mn and ^{129}I will be very useful.

The possibility that an AGB star could be the source of several of the s-process

141

nuclides like ^{41}Ca, ^{60}Fe and ^{107}Pd (Wasserburg et al., 1994, 1995) also indicates the possibility of excess in ^{99}Ru in early solar system phases from the decay of the short-lived nuclide, ^{99}Tc ($\tau \sim 0.29$ Ma). ^{99}Tc is an important nuclide because it is a characteristic s-process product that has been observed directly in atmospheres of red-giants going through the AGB phase. An indications of ^{99}Ru excess in sample of the carbonaceous chondrite Maralinga was reported by Yin et al. (1992); however, firm evidence for the one time presence of ^{99}Tc is still awaited. If detected, it may play a key role in establishing AGB star as the source of most of the short-lived nuclides present in the early solar system.

(4) Initial abundance of ^{53}Mn at the time of CAI formation needs to be re-assesed. At present, we have two initial values for ^{53}Mn/^{55}Mn, 4.4×10^{-5} (Birck and Allegre, 1985), based on measurements of CAI and bulk samples of primitive meteorites, and 3.6×10^{-6} (Lugmair et al., 1995) measured in Eucrites, which would imply a back extrapolated value of $\sim 7 \times 10^{-6}$ for CAIs. As discussed in chapter 5, if the lower value of initial ^{53}Mn/^{55}Mn is correct, production of ^{53}Mn in the early solar system by solar particle irradiation appears to be plausible as it requires only a moderate flux enhancement factor of ~ 1000 from an active early Sun for an irradiation time of ~ 1 Ma. In addition, ^{53}Mn is also a key nuclide as it can be produced only during supernova nucleosynthesis. Thus, if ^{53}Mn present in the early solar system has to be attributed to a stellar source, we definitely need contribution from a supernova to the proto-solar cloud even though a TP-AGB star appears to be the most plausible source for the short-lived nuclides, ^{41}Ca, ^{26}Al, ^{60}Fe and ^{107}Pd (Wasserburg et al., 1994, 1995).

(5) Regarding the role of ^{26}Al as a potential heat source for thermal processing of meteorite parent bodies, additional well documented non-refractory samples from meteorites need to be analyzed. In this respect, the absolute/relative age determination of these phases using other chronometer would be quite useful in calibrating

142

the ^{26}Al systematics.

Eventhough ^{26}Al appears to be the most likely heat source for thermal processing and differentiation of meteorite parent bodies, the absence of concrete experimental evidence to support this possiblity points towards the need for more indepth study of other suggested heat sources, e.g., induction heating of meteorite parent bodies by strong solar wind from an active (T Tauri) early Sun.

References

Allen J. M., Grossmann L., Lee T. and Wasserburg G. J. (1980) Mineralogy and petrography of HAL, an isotopically-unusual Allende inclusion. *Geochim. Cosmochim. Acta.* **44**, 685-699.

Amari S., Lewis R. S. and Anders E. (1994) Interstellar grains in meteorites: 1. Isolation of SiC, graphite, and diamond: Size distributions of SiC and graphite. *Geochim. Cosmochim. Acta.* **58**, 459-470.

Amari S., Zinner E., and Lewis R. S. (1995) Calcium-41 in circumstellar graphite from supernovae. *Meteoritics* **30**, 480.

Andersen C. A. and Hinthorne J. R. (1972) Ion microprobe mass analyzer. *Science* **175**, 853-860.

Anders E. and Ebihara M. (1982) Solar-system abundances of the elements. *Geochim. Cosmochim. Acta.* **46**, 2363-2380.

Armstrong J. T., Hutcheon I. D. and Wasserburg G. J. (1984) Disturbed Mg isotopic systematics in Allende CAI. *Lunar Planet. Sci.* **XV**, 15-16.

Arnett D. and Wefel J. P. (1978) [26]Al production from a stellar evolutionary sequence. *Astrophys J. Lett.* **224**, L139-L142.

Audoze J., Bibring J. P., Dran J. C., Maurette M., and Walker R. M. (1976) Heavily irradiated grains and neon isotope anomalies in carbonaceous chondrites. *Astrophys. J. Lett.* **206**, L185-L189.

Begemann F. and Stegmann W. (1976) Implications from the absence of a [41]K anomaly in an Allende inclusion. *Nature* **259**, 549-550.

Benninghoven A., Rüdernauer F. G. and Werner H. W. (1987) *Secondary Ion Mass Spectrometry: Basis concepts, Instrumental aspects, applications and Trends* (John Wiley and sons).

Bernius M. T., Hutcheon I. D., and Wasserburg G. J. (1991) Search for evidence of [26]Al in meteorites that are planetary differentiates. *Lunar and Planet. Science* **XXII**, 93-94.

Birck J. -L and Allègre C. J. (1985) Evidence for the presence of [53]Mn in the early solar system. *Geophys. Res. Lett.* **12**, 745-748.

Bloemen H., Wijnands R., Bennet K., Diehl R., Hermsen W., Lichti G., Morris D., Ryan J., Schönfelder V., Strong A. W., Swanenburg B. N., De Vries

C., and Winkler C. (1994) COMPTEL observations of the Orion complex: Evidence for cosmic-ray induced gamma ray lines. *Astron. Astrophys.* **281**, L5-L8.

Bodansky D., Clayton D. D., and Fowler W. A. (1968) Nuclear quasi-equilibrium during silicon burning. *Astrophys. J. Suppl.* **16**, 299-371.

Caffee M. W., Goswami J. N., Hohenberg C. M., Marti K. and Reedy R. C. (1988) Irradiation records in meteorites. In *Meteorites and the early solar system*, eds. Kerridge J. F. and Matthews M. S., (Tucson: The Univ. of Arizona Press), 205-245.

Caffee M. W., Hohenberg C. M., Nichols R. H. Jr., Olinger C. T., Wieler R., Pedroni A., Signer P., Swindle T. D., and Goswami J. N. (1991) Do meteorites contain irradiation records from exposure to an enhanced-activity sun ? In *The sun in time*, eds. C. P. Sonett et al. (Tucson: The Univ. of Arizona Press), 413-425.

Caillet C., MacPherson G. J. and Zinner E. K. (1993) Petrologic and Al-Mg isotopic clues to the accretion of two inclusions onto the Leoville parent body: One was hot, the other wasn't. *Geochim. Cosmochim. Acta.* **57**, 4725-4743.

Cameron A. G. W. (1985) Formation and evolution of the primitive solar nebula. In *Protostars and Planets II*, eds. Black D. C. and Matthews M. S. (Tucson: The Univ. of Arizona Press), 1073-1099.

Cameron A. G. W. (1993) Nucleosynthesis and star formation. In *Protostars and Planets III*, eds. E. H. Levy et al. (Tucson: The Univ. of Arizona Press), 47-73.

Cameron A. G. W. and Truran J. W. (1977) The supernova trigger for the formation of the solar system. *Icarus* **30**, 447-461.

Cameron A. G. W., Thielemann F. -K., and Cowan J. J. (1993) s- and r- process contributions to extinct radioactivities. *Phys. Rept.* **227**, 283-291.

Cameron A. G. W., Hoflich P., Myers P. C., and Clayton D. D. (1995) Massive supernova, Orion gamma rays and the formation of the solar system. *Astrophys. J. Lett.*, **447**, L53-L57.

Catanzaro E. J., Murphy T. J., Garner E. L., and Shields W. R. (1966) Absolute isotopic abundance ratios and atomic weights of magnesium. *J. Res. Nat. Bur. Stand.*, **70a**, 453-458.

145

Chen J. H. and Wasserburg G. J. (1981) The isotopic composition of uranium and lead in Allende inclusions and meteoritic phosphates. *Earth and Planet. Science Lett.*, **52**, 1-15.

Clayton D. D. (1977) Interstellar potassium and argon. *Earth Planet. Sci. Lett.* **36**, 381-390.

Clayton D. D. (1982) Cosmic chemical memory: A new Astronomy. *Quat. J. of Roy. Ast. Soc.* **23**, 174-212.

Clayton D. D. (1986) Interstellar fossil ^{26}Mg and its possible relationship to excess meteoritic ^{26}Mg. *Astrophys. J.* **310**, 490-498.

Clayton D. D. (1988) Stellar nucleosynthesis and chemical evolution of the solar neighborhood. In *Meteorites and the early solar system*, eds. Kerridge J. F. and Matthews M. S. (Tucson: The Univ. of Arizona Press), 1021-1062.

Clayton D. D. (1994) Production of ^{26}Al and other extinct radionuclides by low-energy heavy cosmic rays in molecular clouds. *Nature* **368**, 222-224.

Clayton D. D. and Leising M. D. (1987) ^{26}Al in the interstellar medium. *Phys. Rept.* **144**, 1-50.

Clayton D. D. and Jin L. (1995a) A new interpretation of ^{26}Al in meteoritic inclusions.*Astrophys. J. Lett.* **451**, L87-L91.

Clayton D. D. and Jin L. (1995b) Gamma rays, cosmic rays, and extinct radioactivity in molecular cloud. *Astrophys. J.* **451**, 681-699.

Clayton D. D., Dwek E., and Woosley S. E. (1977) Isotopic anomalies and proton irradiation in the early solar system. *Astrophys. J.* **214**, 300-315.

Clayton R. N. (1993) Oxygen isotopes in meteorites. *Ann. Rev. Earth Planet. Sci.* **21**, 115-149.

Curien H., Guillemin C., Orcel J. and Sternberg M. (1956) La Hibonite, nouvelle especeminerale. *Compt. Rend.* **242**, 2845-2847.

Dearborn D. S. P. and Blake J. B. (1985) On the source of the ^{26}Al observed in the interstellar medium. *Astrophys. J. Lett.* **288**, L21-L24.

Dearborn D. S. P. and Blake J. B. (1988) Possible contributions by Wolf-Rayet stars to the protosolar nebula: Extinct radioactivities, or grains of truth from Wolf-Rayet stars? *Astrophys. J.* **332**, 305-312.

Fahey A. J., Goswami J. N., McKeegan K. D. and Zinner E. K. (1987) ^{26}Al, ^{244}Pu, ^{50}Ti, REE, and trace element abundances in hibonite grains from CM and CV meteorites. *Geochim. Cosmochim. Acta* **51**, 329-350.

Feigelson E. D., Giampapa M. S. and Vrba F. J. (1991) Magnetic activity in pre-main-sequence stars. In *The Sun in Time*, eds. C. P. Sonett et al. (Tucson: The Univ. of Arizona Press), 658-681.

Fireman E. L. and Göbel R. (1970) Argon 37 and Argon 39 in recently fallen meteorites and cosmic ray variations. *J. Geophys. Res.* **75**, 2115-2124.

Fowler W. A., Greenstein J. H., and Hoyle F. (1962) Nucleosynthesis during the early history of the solar system. *Geophys. J. Roy. Astron. Soc.* **6**, 148-220.

Gahm G. F. (1989) Some aspects of T Tauri variability. In *Formation and evolution of low mass stars*, eds. Dupree A. K. and Lago M. T. V. T., (Dordrecht: Kluwer), 295-304.

Garner E. L., Murphy T. J., Gramlich J. W., Paulsen P. J., and Barnes I. L. (1975). Absolute isotopic abundance ratios and the atomic weight of a reference sample of potassium. *Jour. Res. NBS* **79A**, 713-725.

Göbel R., Begemann F., and Ott U. (1982) On neutron-induced and other noble gases in Allende inclusions. *Geochim. Cosmochim. Acta* **46**, 1777-1792.

Göpel C., Manhès G., and Allègre C. J. (1989) U-Pb study of phosphates in chondrites. *Meteoritics*, **24**, 270-271.

Göpel C., Manhès G. and Allègre C. J. (1991) Constraints on the time of accretion and thermal evolution of chondrite parent bodies by precise U-Pb dating of phosphates. *Meteoritics* **26**, 338.

Goswami J. N. and Srinivasan G. (1994) Isotopic analysis of early solar system objects by an ion microprobe: Parametric studies and initial results. *Proc. Ind. Acad. Sci. (EPS)* **103**, 57-82.

Goswami J.N., McGuire R. E., Reedy R. C., Lal D. and Jha R. (1988) Solar flare protons and alpha particles during the last three solar cycles. *J. Geophys. Res.* **93**, 7195-7205.

Goswami J. N., Srinivasan G., and Ulyanov A. A (1994) Ion microprobe studies of Efremovka CAIs: I. Magnesium isotope composition. *Geochim. Cosmochimica. Acta* **58**, 431-447.

Grossman J. N., Rubin A. E., Nagahara H. and King E. A. (1988) Properties of chondrules. In *Meteorites and the early solar system*, eds. Kerridge J. F. and Matthews M. S. (Tucson: The Univ. of Arizona Press), 619-659.

Grossman L. (1972) Condensation in the primitive solar nebula. *Geochim. Cosmochim. Acta* **36**, 597-619.

147

Grossman L. (1980) Refractory inclusions in the Allende meteorite. *Ann. Rev. Earth Planet. Sci.* **8**, 559-608.

Grossman L. and Clark S.P., Jr (1973) High-temperature condensates in chondrites and the environment in which they formed. *Geochim. Cosmochim. Acta* **37**, 635-649.

Harper C. L., Völkening J. and Heumann K. G. (1991) ^{182}Hf-^{182}W: New cosmochronometric constraints on terrestrial accretion, core formation, the astrophysical site of the r-process, and the origin of the solar system. *Lunar Planet. Sci.* **XXII**, 515-516.

Hashimoto, A., Hinton R. W., Davis A. M. Grossman L., Mayeda T. K., and Clayton R. N. (1986) A hibonite-rich Murchison inclusion with anomalous Oxygen isotopic composition. *Lunar Planet. Sci.* **XVII**, 317-318.

Herbert F. (1989) Primordial electrical induction heating of Asteroids. *Icarus* **78**, 402-410.

Herbert F., Sonett C. P. and Gaffey M. J. (1991) Protoplanetary thermal metamorphism: The hypthosis of electromagnetic induction in the protosolar wind. In *The Sun in Time*, eds. C. P. Sonett et al. (Tucson: The Univ. of Arizona Press), 710-739.

Herzog G. F. (1972) Relation between solar and planetary neon in carbonaceous chondrites. *J. Geophys. Res.* **77**, 6219-6225.

Hewins R. H. and Newsom H. E. (1988) Igneous activity in the early solar system. In *Meteorites and the early solar system* eds. Kerridge J F and Matthews M S (Tucson: The Univ. of Arizona Press), 73-101.

Heymann D. and Dziczkaniec M. (1976) Early irradiation of matter in the solar system: Magnesium (proton, neutron) scheme. *Science* **191**, 79-81.

Heymann D., Dziczkaniec M., Walker A., Huss G., and Morgan J. A. (1978) Effects of proton irradiation on a gas phase in which condensation take place. I. negative ^{26}Mg anomalies and ^{26}Al. *Astrophys. J.* **225**, 1030-1044.

Hillebrandt W. and Thielemann F.-K. (1982) Nucleosynthesis in novae: a source of Ne-E and ^{26}Al ? *Astrophys. J.* **255**, 617-623.

Hohenberg C. M., Nichols R. H. Jr., Olinger C. T., and Goswami J. N. (1990) Cosmogenic neon from individual grains of CM meteorites: Extremely long pre-compaction exposure histories or an enhanced early flux. *Geochim. Cosmochim. Acta* **54**, 2133-2140.

Humayun M. and Clayton R. N. (1995) Precise determination of isotopic composition of potassium: Application to terrestrial rocks and lunar soils. *Geochim. Cosmochim. Acta* **59**, 2115-2130.

Huneke J. C., Armstrong J. T., and Wasserburg G. J. (1981) ^{41}K and ^{26}Al in Allende inclusions and a hint of ^{41}Ca in the early solar system. *Lunar Planet. Sci.* **XII**, 482-484.

Hutcheon I. D. and Hutchison R. (1989) Evidence from the Semarkona ordinary chondrite for ^{26}Al heating of small planets. *Nature*, **337**, 238-241.

Hutcheon I. D. and Jones R. H. (1995) The ^{26}Al-^{26}Mg record of chondrules: Clues to nebular chronology. *Lunar and Planet. Science*, **XXVI**, 647-648.

Hutcheon I. D., Armstrong J. T., and Wasserburg G. J. (1984) Excess ^{41}K in Allende CAI: A hint reexamined. *Meteoritics* **19**, 243-244.

Hutcheon I. D., Bar-Matthews M., Tanaka T., MacPherson G. J., Grossman L. and Kawabe L. I. (1980) A Mg isotope study of hibonite-bearing Murchison inclusions. *Meteoritics* **15**, 306-307.

Hutcheon I. D., Huss G. R. and Wasserburg G. J. (1994) A search for ^{26}Al in chondrites: Chondrules formation time scale. *Lunar and Planet. Science*, **XXV**, 587-588.

Iben Icko, Jr. (1985) Nucleosynthesis in low and intermediate mass stars on the Asymptotic Giant branch. In *Nucleosynthesis: Challenges and new developments*, eds. Arnett W. D. and Truran J. W., 272-291.

Iben Icko, Jr. and Renzini A. (1983) Asymptotic giant branch evolution and beyond. *Ann. Rev. Astron. Astrophys.* **21**, 271-342.

Ivanov A. V. (1989) The Kaidun meteorite: Composition and history. *Geochem. International*, **26**, 84-91.

Ivanova M. A. and Krot A. N. (1994) Chromite chondrules and inclusions in ordinary chondrites. *Geochemistry International*, **31**, no. 12, 19-35.

Ivanova M. A., Zaslavskay N. I., and Kononkova N. N. 1992 The Dengli H3 complex breccia: A (1976) find from the Karakoom desert. *Meteoritics*, **27**, 463-464.

Ivanova M. A., Assonov S. S., Kononkova N. N., and Shukolyukov Yu A. (1993) The Dengli(H3.8) complex breccia: Petrological and isotopic studies. *Meteoritics*, **28**, 371.

Jeffery P. M. and Reynolds J. H. (1961) Origin of excess Xe^{129} in stone meteorites. *J. Geophys. Res.* **66**, 3582-3583.

Kaiser T. and Wasserburg G. J. (1983) The isotopic composition and concentration of Ag in iron meteorites and the origin of exotic silver. *Geochim. Cosmochim. Acta* **47**, 43-58.

Käppeler F., Gallino R., Busso M., Picchio G. and Raiteri C. M. (1990) s-Process nucleosynthesis: Classical approach and asymptotic giant branch models for low mass stars. *Astrophys. J.* **354**, 630-643.

Kastner J. H. and Myers P. C. (1994) An observational estimate of the probability of encounters between mass-losing evolved stars and molecular clouds. *Astrophys. J.* **421**, 605-614.

Kelly W. R. and Wasserburg G. J. (1978) Evidence for the existence of ^{107}Pd in the early solar system. *Geophys. Res. Lett.* **5**, 1079-1082.

Kennedy A. K., Hutchison R., Hutcheon I. D. and Agrell S. O. (1992) A unique high Mn/Fe microgabbro in the Parnallee (LL3) ordinary chondrite: Nebular mixture or planetary differentiate from a prevously unrecognized planetary body. *Earth and Planet. Science Lett.*, **113**, 191-205.

Krot A. N. and Ivanova M. A. (1992) Cr-rich chondrules and inclusions in ordinary chondrite. *Lunar and Planet. Science*, **XXIII**, 729-730.

Krot A. N., Mitreikina O. B., Ivanova M. A., Stroganov I. A. and Zinovyeva N. G. (1992) Chromite chondrules from the ordinary chondrite Raguli(H3-4) and Cullison(H4): Mineralogy and chemistry. *Lunar and Planet. Science*, **XXIII**, 733-734.

Lal D. (1972) Hard roch cosmic ray archaeology. *Space Sci. Rev.* **14**, 3-102.

Lattanzio J. C. (1995) Evolution and mixing in low and intermediate mass stars. In *Nuclei in the cosmos III*, eds. M. Busso et al., AIP press, 353-364.

Lee Der-Chuen and Halliday A. N. (1995) Hafnium-tungsten chronometry and the timing of terrestrial core formation. *Nature* **378**, 771-774.

Lee Der-Chuen and Halliday A. N. (1996) Hf-W isotopic evidence for rapid accretion and differentiation in the early solar system. *Science* **274**, 1876-1879.

Lee T. (1978) A local proton irradiation model for isotopic anomalies in the solar system. *Astrophys. J.* **219**, 217-226.

Lee T. (1988) Implications of isotopic anomalies for nucleosynthesis. In *Meteorites and the early solar system*, eds. Kerridge J. F. and Matthews M. S.

(Tucson: The Univ. of Arizona Press), 1063-1089.

Lee T., Mayeda T. K. and Clayton R.N. (1980) Oxygen isotopic anomalies in Allende inclusion HAL. *Geophys. Res. Lett.* **7**, 493-496.

Lee T., Papanastassiou D. A., and Wasserburg G. J. (1976) Demonstration of ^{26}Mg excess in Allende and evidence for ^{26}Al. *Geophys. Res. Lett.* **3**, 109-112.

Lee T., Russell W. A. and Waserburg G. J. (1979) Calcium isotopic anomalies and the lack of aluminum-26 in an unusual Allende inclusion. *Astrophys. J. Lett.* **228**, L93-98.

Lorenzen J. and Brune D. (1974) Excitation functions for the charged-particle-induced nuclear reactions in light elements at low projectile energies. In *Handbook on Nuclear Activation Cross-sections, Technical reports series No. 156* (International atomic energy agency, Vienna), 325-473.

Lugmair G. W. and Galer S. J. G. (1992) Age and isotopic relations among the angrites Lewis Cliff 86010 and Angra dos Reis. *Geochim. Cosmochim. Acta* **56**, 1673-1694.

Lugmair G. W., Shukolyukov A., and MacIsaac Ch. (1995) The abundance of ^{60}Fe in the early solar system. In *Nuclei in the cosmos III*, eds. M. Busso et al., AIP press, 591-594.

MacPherson G. J. and Davis A. M. (1993) A petrologic and ion microprobe study of a Vigarano Type B refractory inclusion: Evolution by multiple stages of alteration and melting. *Geochim. Cosmochim. Acta* **57**, 231-243.

MacPherson G. J., Bar-Matthews M., Tanka T., Olsen E. and Grossman L. (1983) Refractory inclusions in Murchison meteorite. *Geochim. Cosmochim. Acta* **47**, 823-839.

MacPherson G. J., Davis A. M. and Zinner E. K. (1992) Distribution of ^{26}Al in the early solar system - A reappraisal. *Meteoritics* **27**, 253-254.

MacPherson G. J., Davis A. M. and Zinner E. K. (1995) The distribution of aluminum-26 in the early solar system - A reappraisal. *Meteoritics* **30**, 365-386.

MacPherson G. J., Hinton R. W. and Davis A. M. (1986) Petrology, chemistry and magnesium isotope systematics of a unique Allende inclusion. *Meteoritics* **21**, 439-440.

MacPherson G. J., Wark D. A. and Armstrong J. T. (1988) Primitive material surviving in chondrites: Refractory inclusions. In *Meteorites and the early*

solar system, eds. Kerridge J. F. and Matthews M. S. (Tucson: The Univ. of Arizona Press), 746-807.

Maeder A. (1983) Evolution of chemical abundances in massive stars. *Astron. Astrophys.* **120**, 113-129.

Manhès G., Göpel C. and Allègre C. J. (1987) High resolution chronology of the early solar system based on lead isotopes. *Meteoritics*, **22**, 453.

Manhès G., Göpel C. and Allègre C. J. (1988) Systematique U-Pb dans les inclusions refractaries d'Allende: le plus vieuse materiau solaire. *C. R. ATP Plaètol.* 323-327.

Marti K. and Lingenfelter R. E. (1995) The Orion phenomenon: Particle fluences in the solar nebula. In *Nuclei in the cosmos III*, eds. M. Busso et al., AIP press, 549-552.

Mazor E., Heymann D., and Anders E. (1970) Noble gases in carbonaceous chondrites. *Geochim. Cosmochim. Acta* **34**, 781-824.

McSween H. Y. and Grimm R. E. (1994) ^{26}Al as an asteroidal heat source? *Meteoritics*, **29**, 500-501.

McSween H. Y., Sears D. W. G. and Dodd R. T. (1988) Thermal metamorphism. In *Meteorites and the early solar system*, eds. Kerridge J. F. and Matthews M. S. (Tucson: The Univ. of Arizona Press), 102-113.

Meeker G. P., Wasserburg G. J. and Armstrong J. T. (1983) Replacement textures in CAI and implications regarding planetary metamorphism. *Geochim. Cosmochim. Acta* **47**, 707-721.

Migdisova L. F., Yaroshevsky A. A. and Kononkova N. N. (1992) The inclusion in the L-chondrite Tsarev: New type of basaltic matter in the solar system. *Lunar and Planet. Science*, **XXIII**, 909-910.

Migdisova L. F., Yaroshevsky A. A., Nazarov M. A. and Kononkova N. N. (1994) Textural and mineralogical heterogeneity of silicate inclusions in Tsarev chondrites. *Lunar and Planet. Science*, **XXV**, 905-906.

Murty S. V. S., Goswami J. N. and Shukolyukov Yu. A. (1996) Excess ^{36}Ar in the Efremovka meteorite: A strong hint for the presence of ^{36}Cl in the early solar system. *Astrophys. J. Lett.* **475**, L65-L68.

Murty S. V. S., Nizhiizumi K., and Goswami J. N. (1996) Cosmogenic records in Efremovka CV3 meteorite *Lunar Planet. Sci.* **XXVII**, 923-924.

Murty S. V. S., Shukolyukov Yu. A., and Goswami J. N. (1995) Excess Argon-36 in the Efremovka meteorite: Evidence for live Chlorine-36 in the early solar system ? *Meteoritics* **30**, 555.

Nazarov M. A., Brandstätter F. and Kurat G. (1993) Igenous rock from Severnyi Kolchim (H3) chondrite : Nebular origin. *Lunar and Planet. Science*, **XXIV**, 1055-1056.

Nazarov M. A., Ulyanov A. A., Korina M. I., and Kolesov G. M. (1982) Efremovka CAI's: Major and Trace Element Chemistry. *Lunar Planet. Sci.* **XIII**, 584-585.

Nazarov M. A., Korina M. I., Ulyanov A. A., Kolesov G. M., and Sherbovsky E. Ya. (1984) Minerology, petrology and chemical composition of Ca and Al-rich inclusions of Efremovka meteorite. (In Russian) *Meteoritika* **43**, 49-66.

Podosek F. A. and Swindle T. D. (1988) Extinct radionuclides.In *Meteorites and the early solar system*, eds. Kerridge J. F. and Matthews M. S. (Tucson: The Univ. of Arizona Press), 1093-1113.

Podosek F. A., Zinner E. K., MacPherson G. J., Lundberg L. L., Brannon J. C. and Fahey A. J. (1991) Correlated study of initial ^{87}Sr/^{86}Sr and Al-Mg isotopic systematics and petrologic properties in a suite of refractory inclusions from the Allende meteorite. *Geochim. Cosmochim. Acta* **55**, 1083-1110.

Ramaty R., Kozlovsky B., and Lingenfetler R. E. (1979) Nuclear gamma-rays from energetic particle interactions. *Astrophys. J. (Suppl.)* **40**, 487-526.

Ramaty R., Kozlovsky B., and Lingenfelter R. E. (1996) Light isotopes, extinct radioisotopes and gamma ray lines from low energy cosmic ray interactions. *Astrophys. J.* **456**, 525-540.

Reedy R. C. and Arnold J. R. (1972) Interaction of solar and galactic cosmic-ray particles with the moon. *J. Geophys. Res.* **77**, 537-555.

Reedy R. C. and Marti K. (1991) Solar-cosmic-ray fluxes during the last ten million years. In *The Sun in Time*, eds. C. P. Sonett et al. (Tucson: The Univ. of Arizona Press), 260-287.

Rowe M. W. and Kuroda P. K. (1965) Fissiogenic xenon from the Pasamonte meteorite. *J. Geophys. Res.* **70**, 709-714.

Russell S. S., Srinivasan G., Huss G. R., Wasserburg G. J. and MacPherson G. J. (1996) Evidence for widespread ^{26}Al in the solar nebula and constraints for nebula time scales. *Science* **273**, 757-762.

Sahijpal S., Goswami J. N., Kashkarov L. L., Korotkova N. N. and Nazarov M. A. (1994) Search for ^{26}Mg isotopic anomaly in unequilibrated chondrites and unique meteorites. *Lunar and Planet. Science*, **XXV**, 1185-1186.

Sahijpal S., Ivanova M. A., Kashkarov L. L., Korotkova N. N., Migdisova L. F., Nazarov M. A. and Goswami J. N. (1995) ^{26}Al as a heat source for early melting of planetesimals: Results from isotopic studies of meteorites. *Proc. Indian Acad. Sci. (Earth Planet. Sci.)* **104** No. 4, 555-567.

Schramm D. N., Tera F. and Wasserburg G. J. (1970) The isotopic abundance of ^{26}Mg and limits on ^{26}Al in the early solar system. *Earth and Planet. Science Lett.*, **10**, 44-59.

Scott E. R. D., Taylor G. J., Newsom H. E., Herbert F., Zolensky M. and Kerridge J. F. (1989) Chemical, thermal and impact processing of asteroids. In *Asteroids II*, eds. R. P. Binzel et al. (Tucson: The Univ. of Arizona Press), 701-739.

Shimizu N. and Hart S. R. (1982a) Applications of the ion microprobe to geochemistry and cosmochemistry. *Ann. Rev. Earth Planet. Sci.* **10**, 483-526.

Shimizu N. and Hart S. R. (1982b) Isotope fractionation in secondary ion mass spectrometry. *J. Appl. Phys.* **53**, 1303-1311.

Shimizu N., Semet M. P., Allègre C. J. (1978) Geochemical applications of quantitative ion-microprobe analysis. *Geochim. Cosmochim. Acta* **42**, 1321-1334.

Shu F. H., Shang H. and Lee T. (1996) Toward an astrophysical theory of chondrites. *Science* **271**, 1545-1552.

Shukolyukov A. and Lugmair G. W. (1993a) Live Iron-60 in the early solar system. *Science* **259**, 1138-1142.

Shukolyukov A. and Lugmair G. W. (1993b) ^{60}Fe in eucrites. *Earth Planet. Sci. Lett.* **119**, 159-166.

Slodzian G., Lorin J. C. and Havette A. (1980) Isotopic effect on the ionization probabilities in secondary ion emmision. *J. Phys.* **23**, 555-558.

Sonett C. P. (1969) Fractionation of iron: A cosmogenic sleuthing tool. II. Heating by electrical induction. *Comments on Astrophys. Space Phys.* **1**, 41-48.

Sonett C. P. and Colburn D. S. (1968) The principle of solar wind induced planetary dynomos. *Phys. Earth Planet. Int.* **1**, 326-346.

Srinivasan G., Ulyanov A. A., and Goswami J. N. (1994) ^{41}Ca in the early solar system. *Astrophys. J. Lett.* **431**, L67-L70.

Srinivasan G., Sahijpal S., Ulyanov A. A. and Goswami J. N. (1996) Ion micro-probe studies of Efremovka CAIs: II. Potassium isotope composition and ^{41}Ca in the early solar system. *Geochim. Cosmochim. Acta* **60**, 1823-1835.

Stegmann W. and Specht S. (1983) Investigation of Mg and K isotopic abun-dances in Allende and Leoville Ca-Al-Rich Inclusions. *Meteoritics* **18**, 402.

Sylvester P. J., Simon S. B., and Grossman L. (1993) Refractory inclusions from the Leoville, Efremovka, and Vigarona C3V chondrites: Major element dif-ferences between Types A and B, and extraordinary refractory siderophile element compositions. *Geochim. Cosmochim. Acta* **57**, 3763-3784.

Tera F., Carlson R. W. and Boctor N. Z. (1989) Contrasting Pb-Pb ages of the cumulate and non-cumulate eucrites. *Lunar Planet. Sci.* **XX**, 1111-1112.

Truran J. W. and Cameron A. G. W. (1978) ^{26}Al production in explosive carbon burning. *Astrophys. J.* **219**, 226-229.

Ulyanov A. A. and Kolesov G. M. (1984) REE in CAI's of Efremovka chondrite. *Lunar Planet. Sci.* **XV**, 874-875.

Ulyanov A. A., Korina M. I., Nazarov M. A., and Sherbovsky E. Ya. (1982) Efremovka carbonaceous chondrite. *Lunar Planet. Sci.* **XIII**, 813-814.

Ulyanov A. A., Ustinov V. I., Zagryazhskaya G. D., Gavrilov E. Ya and Shu-lolyukov Yu. A. (1988) Oxygen isotope compositions of refractory inclusions of carbonaceous chondrites. *Geochemistry International* **25** No. 3, 13-20.

Urey H. C. (1955) The cosmic abundances of potassium, uranium and thorium, and the heat balances of the Earth, the Moon, and Mars. In *Proc. Nat. Acad. Sci.*, **41**, 127-144.

Virag A., Zinner E. K., Amari S. and Anders E. (1991) An ion microprobe study of corundum in the Murchison meteorite: Implications for ^{26}Al and ^{16}O in the early solar system. *Geochim. Cosmochim. Acta* **55**, 2045-2062.

Walter F. M. and Barry D. C. (1991) Pre- and main-sequence evolution of solar activity. In *The Sun in Time*, eds. C. P. Sonett et al. (Tucson: The Univ. of Arizona Press), 633-657.

Walter R. and Maeder A. (1989) The synthesis of ^{26}Al in massive stars. *Astron. Astrophys.* **218**, 123-130.

Wark D. A. and Lovering J. F. (1980) More early solar system stratigraphy: coarse-grained CAI's. *Lunar Planet. Sci.* **XI**, 1208-1210.

Wark D. A. and Lovering J. F. (1982) The nature and origin of type B1 and B2 Ca-Al-rich inclusion in the Allende meteorite. *Geochim. Cosmochim. Acta* **46**, 2581-2594.

Wark D. A. and Wasserburg G. J. (1980) Anomalous mineral chemistry of Allende FUN inclusions C1, EK-1-4-1 and EGG3. *Lunar Planet. Sci.* **XI**, 1214-1216.

Wasserburg G. J. (1985) Short-lived nuclei in early solar system. In *Protostars and Planets II* eds. Black D. C. and Matthews M. S. (Tucson, Univ. of Arizona Press), 703-737.

Wasserburg G. J. and Arnould M. (1987) A possible relationship between extinct ^{26}Al and ^{53}Mn in meteorites and early solar system. In *Lecture Notes in Physics 287, 4th workshop on Nuclear Astrophysics*, eds. W. Hillebrandt et al. (Springer-Verlag), 262-276.

Wasserburg G. J., Busso M., Gallino R., and Raiteri C. M. (1994) Asymptotic Giant Branch Stars as a source of short-lived radioactive nuclei in the solar nebula. *Astrophys. J.* **424**, 412-428.

Wasserburg G. J., Gallino R., Busso M., Goswami J. N., and Raiteri C. M. (1995) Injection of freshly synthesized ^{41}Ca in the early solar nebula by an asymptotic giant branch star. *Astrophys. J. Lett.* **440**, L101-L104.

Weaver T. A. and Woosley S. E. (1993) Nucleosynthesis in massive stars and the ^{12}C$(\alpha,\gamma)^{16}$O reaction rate. *Phys. Rep.* **227**, 65-96.

Weidenshilling S. J. (1988) Formation processes and time scales for meteorite parent bodies. In *Meteorites and the early solar system*, eds. Kerridge J. F. and Matthews M. S. (Tucson: The Univ. of Arizona Press), 348-371.

Wiescher M., Gorres J., Thielemann F. -K., and Ritter H. (1986) Explosive hydrogen burning in novae. *Astron. Astrophys.* **160**, 56-72.

Wood J. A. and Morfill G. E. (1988) A review of solar nebula models. In *Meteorites and the early solar system*, eds. Kerridge J. F. and Matthews M. S. (Tucson: The Univ. of Arizona Press), 329-347.

Wood J. A. and Pellas P. (1991) What heated the parent meteorite planets? In *The Sun in Time*, eds. C. P. Sonett et al. (Tucson: The Univ. of Arizona Press), 740-760.

Woolum D. S. (1988) Solar-system abundances and processes of nucleosynthesis. In *Meteorites and the early solar system*, eds. Kerridge J. F. and Matthews M. S. (Tucson: The Univ. of Arizona Press), 995-1020.

Woosley S. E. and Weaver T. A. (1980) Explosive neon burning and ^{26}Al gamma ray astronomy. *Astrophys. J.* **238**, 1017-1025.

Woosley S. E. and Weaver T. A. (1995) The evolution and explosion of massive stars. II. Explosive hydrodynamics and nucleosynthesis. *Astrophys. J.(Suppl.)* **101**, 181-235.

Woosley S. E., Arnett W. D., and Clayton D. D. (1973) The explosive burning of oxygen and silicon. *Astrophys. J. (Suppl.)* **26**, 231-312.

Yin Q., Jagoutz E. and Wänke H. (1992) RE- search for extinct ^{99}Tc and ^{98}Tc in the early solar system. *Meteoritics*, **27**, 310.

Yomogida K. and Matsui T. (1983) Physical properties of ordinary chondrites. *J. Geophys. Res.* **88**, 9513-9533.

Zinner E. and Göpel C. (1992) Evidence for ^{26}Al in feldspars from H4 chondrite Ste. Marguerite. *Meteoritics*, **27**, 311-312.

Zolensky M. and McSween H. Y. (1988) Aqueous alteration. In *Meteorites and the early solar system*, eds. Kerridge J. F. and Matthews M. S. (Tucson: The Univ. of Arizona Press), 114-143.